S T U D I A

UNIVERSITATIS BABEŞ–BOLYAI

CHEMIA

2

CUPRINS – CONTENT – SOMMAIRE – INHALT

Studia Universitatis Babes-Bolyai Chemia has been selected for coverage in Thomson Reuters products and custom information services. Beginning with V. 53 (1) 2008, this publication is indexed and abstracted in the following:

- Science Citation Index Expanded (also known as SciSearch®)
- Chemistry Citation Index®
- Journal Citation Reports/Science Edition

ASPECTS OF IMPROVING CONCRETE DURABILITY

MARIN AMĂREANU[a] AND LARISA MELIȚĂ[a]*

ABSTRACT. Concrete, under certain conditions, may degrade due to corrosion processes. Corrosion protection can be achieved by providing a suitable concrete composition. In this paper the influence of supplements, added to concrete preparation, in the hydration-hydrolysis processes during their setting and hardening, is presented (the evolution of the mechanical strengths). The influence of supplements on the concrete stability in aggressive environments is also studied (two solutions of $(NH_4)_2SO_4$, with the following concentrations: C_1 = 8.25 g/L – corresponding to a high chemical aggressive environment – XA_3 [1], and C_2 = 24.75 g/L, corresponding to an aggressive chemical environment three times as high). Finally, it is noted which supplements can improve concrete durability for use, without serious consequences, in the proposed highly aggressive environments.

Keywords: supplements, concrete, durability, aggressive environments

INTRODUCTION

According to A.C.I. 201.2R-01 [2], concrete durability is defined as its property to resist climatic, chemical and abrasion actions, or any other deterioration processes. So, a durable concrete is a concrete that retains its initial shape, features and functionality in the environments for which it was designed. If we define concrete quality as its ability to meet the users' needs, durability is responsible for maintaining this quality in time.

An important aspect of the study is the fact that the durability of concrete buildings is not regarded as a problem only in the case of aggressive environments, but also in the case of current environments, in which the most buildings with worrying degradation phenomena were found [3].

[a] *Technical University of Civil Engineering of Bucharest, Bdul. Lacul Tei nr: 122-124, Sector 2, cod 020396, Bucharest, Romania, *Corresponding author: larisamelita@gmail.com*

Concrete is designed to be durable under certain in environmental conditions, with the possibility of its use being inadequate under different conditions. For instance, a concrete designed to withstand in aggressive chemical environments will not be suitable for use in environments, characterized by repeated cycles of freeze-thaw and de-icing agents. For this reason it is necessary for the concrete to be designed also regarding composition, depending on the environmental conditions and use. Achieving the projected service time (making only current repairs) in the given environmental conditions and maintaining the original performances can be regarded as synonymous with assuring the required durability.

The modern concepts and the actual trends of durability design [4] can consider two basic strategies against concrete corrosion:

A. Avoiding the chemical reactions of the mineralogical constituents of the cement, with the aggressive external environment which lead to decreased durability.

This strategy can be applied considering the following aspects:

- Eliminating the contact between the concrete and the aggressive environment by applying coatings with protective films on the concrete elements;

- Selecting unreactive materials such as: stainless steel, coated reinforcement steel, unreactive aggregates and sulfate resistant cements;

- Air entrainment in the preparation of fresh concrete to achieve a high resistance to freeze-thaw, reaction inhibition by cathode protection, etc.

B. Selection of the materials, of the optimal composition and of the suitable operating conditions for the concrete to withstand the aggressive action of the environment.

Strategy B may cover a series of categories of intervention, for example: selecting a suitable concrete composition – this being found in main objective proposed by this work – and making an appropriate concrete coating over the reinforcement with its weight determined by environmental conditions. The standards and the European norms for concrete production are based on this strategy.

Thus, concerning the selection of a suitable concrete composition that can ensure its protection against corrosion in highly aggressive environment, this paper aims to study the influence of different additives on the quality of cement concrete, regarding its use in optimal conditions, in the analyzed aggressive environment.

RESULTS AND DISCUSSION

After introducing of the hardened concrete, prepared with cement CEM I 42.5 and additives, in an ammonium sulfate aggressive environment, of different concentrations, the concrete's surface was studied from a visual point of view. It was found that the corroded surface layer, after 60 days but especially after 90 days, was bounded from the uncorroded layer by an quantitatively insignificant area given by the presence of compounds like ferric hydroxide, gypsum and ettringite, but also by compounds resulting from the chemical reactions between the aggressive environments and the substances added as additives in the concrete preparation [5, 6].

The main factors determining the corrosive attack on the concrete are: the chemical composition of the cements, the type of aggressive environment and its concentration, exposure time, but also the water/ cement ratio used. Therefore the analysis of the concrete's stability, in the mentioned corrosive environments, will be made by following these factors.

In table 1 the mass variations values (Δm) in time of the concrete exposed in the aggressive environments: ammonium sulfate $(NH_4)_2SO_4$ with concentration C_1 = 8.25 g/L (corresponding to a high chemical aggressive environment – XA_3 according to SR. EN. 206-1) and concentration C_2 = 24.75g/L (corresponding to an environment with a chemical aggressively three times as high) are presented.

Table 1. The variation in time of the concrete mass (Δm) subjected to $(NH_4)_2SO_4$ aggressive environment action with the following concentrations: C_1 = 8.25g/L and C_2 = 24.75g/L

CONCRETE	$\Delta m = m_{60days\ agrs} - m_0$, g		$\Delta m = m_{90days\ agrs} - m_0$, g	
	C_1	C_2	C_1	C_2
I. Reference sample (no additives)	-2.7	1.5	0.7	5.0
II. With sodium silicate additive	-2.0	3.0	1.2	1.2
III. With sodium soap and AlCl₃ additives	0.0	3.0	4.5	7.6
IV. With sodium carbonate additive	-0.7	1.7	1.4	4.2
V. With FeSO₄ additive	-0.9	0.8	0.2	2.0

where:

m_0 - the mass of the concrete sample hardened in water for up to 28 days;

$m_{60days\ agrs}$ - the mass of the concrete sample hardened in water for up to 28 days and kept in the aggressive environment for up to 60 days;

$m_{90days\ agrs}$ - the mass of the concrete sample hardened in water for up to 28 days and kept in the aggressive environment for up to 90 days.

Table 1 shows an increase in mass of the samples kept in high concentrated aggressive environment, C_2. The explanation may be due to either the formation of new compounds which bind an additional amount of water on the surface of the samples (gypsum type compounds, $NH_4(OH)$ or ettringite, but also compounds resulting from the chemical reactions between the aggressive environment and the additives introduced in the concrete) or, most likely, to the superficial corrosion of the samples so that their porosity increases allowing water absorption in their structure.

The stability of the concrete in aggressive environments is also represented by variation in time of the mechanical strengths (Table 2).

Table 2. The variation in time of the mechanical strengths (compressive, R_c and tensile, R_{ti}) of the concretes subjected to $(NH_4)_2SO_4$ aggressive environment action at different concentrations

CONCRETE	$(NH_4)_2SO_4$ aggressive environment (Conc. g/L)	Compressive strength, MPa			Tensile strength, MPa		
		R_c, 28 days	R_c, 60 days	R_c, 90 days	R_{ti}, 28 days	R_{ti}, 60 days	R_{ti}, 90 days
I. Reference sample (no additives)	$C_0 = 0$	44.53	49.35	51.64	4.96	8.2	11.43
	$C_1 = 8.25$		47.89	44.14		12.32	11.71
	$C_2 = 24.75$		41.79	41.80		11.62	11.64
II. With sodium silicate additive	$C_0 = 0$	24.53	35.71	37.42	3.89	6.31	9.23
	$C_1 = 8.25$		34.53	30.07		11.27	10.07
	$C_2 = 24.75$		27.96	29.76		14.47	10.82
III. With sodium soap and $AlCl_3$ additives	$C_0 = 0$	43.75	44.23	44.84	4.45	8.23	9.60
	$C_1 = 8.25$		41.09	39.84		9.98	8.71
	$C_2 = 24.75$		36.09	25.62		9.09	7.21
IV. With sodium carbonate additive	$C_0 = 0$ g/L	21.09	23.45	27.89	3.32	6.84	7.78
	$C_1 = 8.25$		22.89	26.32		8.39	7.73
	$C_2 = 24.75$		21.87	23.35		8.95	7.54

CONCRETE	$(NH_4)_2SO_4$ aggressive environment (Conc. g/L)	Compressive strength, MPa			Tensile strength, MPa		
		R_c, 28 days	R_c, 60 days	R_c, 90 days	R_{ti}, 28 days	R_{ti}, 60 days	R_{ti}, 90 days
V. With FeSO$_4$ additive	$C_0 = 0$	38.75	43.94	48.35	4.21	7.92	10.03
	$C_1 = 8.25$		42.81	43.79		8.43	13.45
	$C_2 = 24.75$		41.79	46.79		10.68	10.64

From the standpoint of the exposure time over a period up to 90 days in XA$_3$ aggressive environment, with concentrations C_1 and C_2 respectively, the values of the compressive strength fluctuate during the corrosion process, as depicted in table 3.

Table 3. The variation of the concretes compressive strength values (ΔR_c) up to 60 days and up to 90 days respectively (in XA$_3$ aggressive environment with C_1 and C_2 concentrations)

CONCRETE	$\Delta R_c = R_{c\ 60days\ (c1, c2)} - R_{c\ 28days\ (water)}$, MPa		$\Delta R_c = R_{c\ 90days\ (c1, c2)} - R_{c\ 28days\ (water)}$, MPa		$\Delta R_c = R_{c\ 90days} - R_{c\ 60days}$, MPa	
	C_1	C_2	C_1	C_2	C_1	C_2
I. Reference sample (no additives)	3.36	-2.74	-0.39	-2.73	-3.75	0.01
II. With sodium silicate additive	10.00	3.43	5.54	5.24	-4.45	1.80
III. With sodium soap and AlCl$_3$ additives	-2.66	-7.66	-3.91	-18.12	-1.25	-10.47
IV. With sodium carbonate additive	1.8	0.78	5.23	2.3	3.43	1.48
V. With FeSO$_4$ additive	4.06	3.04	5.04	8.05	0.98	5.00

According to tables 2 and 3, from point of view of the aggressive environment concentration, after 60 and 90 days respectively, the mechanical strengths, generally, decrease with the increase of the aggressive environment's concentration. Lower values of the compressive strengths variation (ΔR_c) for the concretes subjected to the corrosion process in

11

$(NH_4)_2SO_4$ aggressive environment with C_2 concentration were found, as against to those subjected to the same environment but with concentration C_1. The same situation not happened with the concrete in whose composition the $FeSO_4$ was introduced. In this case, the strengths values were comparable to the ones of the concretes hardened in water, after 60 and 90 days and used as reference samples. Likewise, for the concrete with $FeSO_4$ additive, mass losses are insignificant (see table 1).

Compared with mechanical strengths (compressive and tensile) increase of the concretes kept in water, against mechanical strengths of the concretes in aggressive environment they vary according with data from table 4.

Loss in of the reference samples compressive strengths with sodium silicate, sodium soap and $AlCl_3$ additives can be observed and, minor variations of samples with sodium carbonate and $FeSO_4$ additives are obtained. There weren't any significant drops of the tensile strength values because the corrosion did not occur in the deepness of the concrete. However, there are increases of the tensile strength for samples with $FeSO_4$.

Table 4. The mechanical strengths variation (compressive and tensile) of the concretes kept in aggressive environments with C_1 and C_2 concentrations, for 90 days, compared with values of the mechanical strengths of the same concretes kept in water for 90 days

| CONCRETE	$\Delta R_c = R_{c\ 90days\ (c1,\ c2)} - R_{c\ 90days\ (water)}$, MPa		$\Delta R_{ti} = R_{ti\ 90days\ (c1,\ c2)} - R_{ti\ 90days\ (water)}$, MPa	
	C_1	C_2	C_1	C_2
I. Reference sample (no additives)	-7.5	-9.87	0.28	0.21
II. With sodium silicate additive	-7.35	-7.65	0.87	1.6
III. With sodium soap and $AlCl_3$ additives	-5	-19.2	-0.89	-2.38
IV. With sodium carbonate additive	-1.57	-4.54	-0.05	-0.23
V. With $FeSO_4$ additive	-4.56	-1.56	3.42	0.61

CONCLUSIONS

The aim of this study was to investigate the behavior of concrete in a highly aggressive environment – XA_3 –according to SR EN 206-1. To create a corrosive environment, the ammonium sulfate solution with concentrations C_1 = 8.25 g/L (corresponding to a high chemical aggressive environment - XA_3) and C_2 = 24.75 g/L (three times C_1) were used. The concrete subjected to these aggressive environments, was prepared with CEM I 42.5 cement and following additives: sodium silicate (8%), sodium soap and $AlCl_3$ (2%), sodium carbonate (8%) and $FeSO_4$ (8%) respectively, mass percentage of cement.

The results led to the following observations, regarding to the stability of concrete in aggressive environments:

- Through increase the concentration of aggressive environment leads to a lower concrete stability, appreciated by reducing the mechanical strengths for the same exposure time;
- In terms of exposure time, after 60 and 90 days, the stability of the concrete, expressed as a variation of the mechanical strengths, shows no constancy in the evolution of the corrosion process, regardless of the acid concentration.

The presented data show a good behavior, in the ammonium sulfate aggressive environment with C_1 = 8.25 g/L and C_2 = 24.75 g/L concentrations, of the concrete in whose composition the $FeSO_4$ was introduced. In this case the obtained values of the mechanical strengths are similar to those of mechanical strengths of the concrete hardened in water and used as a reference sample; the mass losses are insignificant.

The reason underlying the protective effect of the iron compounds ($FeSO_4$) to the concrete in aggressive environments can be explained by the following chemical reaction:

$$FeSO_4 + Ca(OH)_2 = Fe(OH)_2 + CaSO_4$$
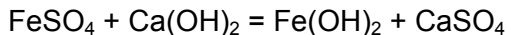
Thus, $Fe(OH)_2$ turns into a colloidal gelatinous precipitate, which has tendency to clog the pores of the concrete thus increasing its resistances to corrosion by elutriation [7, 8].

The $CaSO_4$ formation and any volume increases it may have created, as a result of the combination with tricalcium aluminate in the cement, occurred probably, during the cement binding.

The decreases of mechanical strength for the **sodium silicate concretes** are due by the slow curing of the sodium silicate in air. The hardening process of sodium silicate is due to the silicic acid forming, resulted from hydrolysis of the sodium silicate according to reaction:

$$Na_2O \cdot nSiO_2 + (2n+1)H_2O = 2Na^+ + 2HO^- + nSi(OH)_4$$
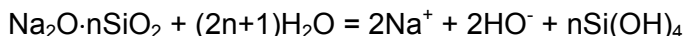
that provides strength of the structure (cementation), by the polycondensation processes with SiO_2 hydrate gel formation with binding properties. In time, the gel is crystallized in a form characterized by mechanical strengths and stability to acids. Through its combination with calcium compounds of the concrete, the gelatinous calcium silicates are obtained, are impermeable to water and by increasing the volume, occlude the concrete capillary pores contributing to increasing of its impermeability [7].

By introducing of Na_2SiF_6 compound, a good acceleration occurs at the silicate strengthening [9], involving the next reactions:

$$Na_2SiO_3 + 3H_2O = 2NaOH + Si(OH)_4$$
$$Na_2SiF_6 + 4H_2O = 2NaF + 4HF + Si(OH)_4$$
$$HF + NaOH = NaF + H_2O$$
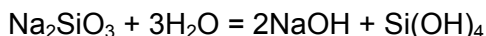
The soluble sodium soaps in combination with AlCl$_3$ turns into insoluble aluminum soaps [7] with hydrophobic action that leads to an improvement in the surfaces resistance to aggressive actions. The $(NH_4)_2SO_4$ aggressive environment, used in this work, did not allow this improvement causing the sulphatic corrosion.
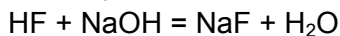
Based on all research, it is recommended that for the concrete exposed to highly corrosive environments, a correlation between the binder types and the aggressive environment characteristics, a key element for assuring the buildings durability.

EXPERIMENTAL SECTION

Experimental conditions and procedures

The researches in this field have suggested the important role of the additives to concrete behavior during the strengthening process and to their properties [7, 8, 10, 11, 12]. Therefore the investigations were performed on concrete containing the following categories of binder systems:

a) cement CEM I 42.5 (reference sample);
b) cement CEM I 42.5 with following additives: sodium silicate (8%), sodium soap and aluminum chloride (2%), sodium carbonate (8%) and $FeSO_4$ (8%), mass percentages in relation to the cement.

The chemical, physical and mechanical characteristics of CEM I 42.5 cement are presented in table 5:

Table 5. The characteristics of CEM I 42.5 cement (cement supplied by HOLCIM)

Chemical Composition (%)												
CaO	SiO_2	SO_3	Al_2O_3	Fe_2O_3	MgO	Na_2O	K_2O	Na_2O eq	Free CaO	P.C.	Inso-luble resi-due	Cl^-
62.79	20.57	2.80	4.45	6.11	1.91	0.18	1.10	0.90	0.61	0.46	0.22	0.018

Physical characteristics		
Specific surface (Blaine) (cm^2/g)	Stability (mm)	Vicat setting time (minutes)
3022	1.0	Initial / Final
		190 / 235

Compressive strength (N/mm^2)		
2 days	7 days	28 days
24.8	35.6	-

On the binder systems listed above, experimental studies have been made regarding their availability to develop strengthened structures, assessed by strength measurements made on the concrete obtained with these binder systems. The water/cement ratio is constant and equal with 0.5, for all obtained concretes. Also the influence of some aggressive environments on the concrete's durability was studied.

The chemical aggressive environments were given by two ammonium sulfate solutions $(NH_4)_2SO_4$ with C_1 = 8.25 g/L (corresponding to a high chemical aggressive environment – XA_3 according to SR EN 206-1), and C_2 = 24.75 g/L (three times C1) concentrations.

In order to emphasize the durability of the obtained concrete with above mentioned binder systems, the influence of the environmental aggression was investigated through:

- The mechanical strengths (tensile and compressive) variations at 28, 60 and 90 days respectively;
- The mass variations of the concrete samples at 28, 60 and 90 days respectively.

The obtained results were compared with those of the similar measurements made on the concrete subjected to a normal environment exposure: water.

The tensile strengths have been carried out on prismatic samples (40x40x60 mm), and the compressive strengths have been carried out on the prism pieces. Were used three samples for each determination; their average was calculated and used for results comments.

REFERENCES

[1] *** Standard SR EN 206-1, „Concrete Part 1: Specification, performance, production and conformity", **2002.**

[2] *** Report of American Concrete Institute Committee ACI 201.2R-08, „Guide to Durable Concrete", **2008.**

[3] D. Georgescu, „Guide to design the concrete durability in conformity with the National Annex application, EN 206-1. Durability classes" (In Roumanian), Ed. Everest, Bucureşti, **2001.**

[4] S. Rostam, "Service Life Design in Practice Today and Tomorrow" *International Conference: Concrete Across Borders*, Copenhaga, **1994.**

[5] I. Biczok, "Corrosion and concrete protection" (In Romanian), Editura Tehnică, Bucureşti, **1965.**

[6] T. Yamaguchi, K. Negishi, S. Hoshino, T. Tanaka, *Cement and Concrete Research*, **2009**, *39*, 1149.

[7] D. Georgescu, A. Apostu, *Romanian Journal of Materials,* **2009***, 39(2),* 119.

[8] I. Neamţu, N. Rujenescu, I. Lazău, D. Becherescu, **"**Using the thermoelectric power station ash in concrete roof tiles production" *The 8th International Conference of Constantin Brâncuşi University*, Târgu Jiu, May 24-26, **2002**.

[9] I. Robu, M. Popescu, "Materiaux de Construction 2 – Liants, mortieres et beton*"*, Editura Conspress, Bucureşti, **2005.**

[10] M. Amăreanu, *Romanian Journal of Materials,* **2010**, *40(3)*, 203.

[11] I. Robu, G. Ilie, I. Pordea, *Romanian Journal of Materials,* **2011***, 41(23)*, 110.

[12] G. Guslicov, C. Ioniţă, D. Mârza, *Romanian Journal of Materials,* **2009***, 39(2), 98.*

COMPUTATIONAL AND EXPERIMENTAL STUDY ON 7-EPICANDICANDIOL ISOLATED FROM *SIDERITIS NIVEOTOMENTOSA* HUBER – MORATHII

CEM BURAK YILDIZ[a,b], ZULEYHA OZER SAGIR[c], TURGUT KILIC[c,d] AND AKIN AZIZOGLU[a,*]

ABSTRACT. 7-epicandicandiol is an *ent*-kaurane diterpenoid isolated from *Sideritis niveotomentosa* Huber – Morathii. The molecular geometry, vibrational frequencies, and gauge including atomic orbital (GIAO) ^{1}H- and ^{13}C-NMR chemical shift values of the title compound in the ground state have been calculated using the Hartree–Fock and Density Functional Theory methods with the 6-31G(d) basis set, and compared with the experimental data. A detailed interpretations of the infrared and NMR spectra of 7-epicandicandiol are also reported. The results of the calculations were applied to unscaled theoretical wavenumbers of the title compound, which show good agreement with observed spectra.

Keywords: terpenes, plants, IR spectrum, DFT, ab-initio

INTRODUCTION

Terpenes are one of the main groups of secondary metabolites in nature showing a great diversity in structure and activity [1]. In industry, they are widely used as building blocks for pharmaceuticals, flavors, fragrances, food supplements and antioxidants [2]. Sideritis species are rich in diterpenes; at least 160 different diterpenes with a remarkable structural variability have been identified and isolated from the aerial parts [3]. 7-epicandicandiol, one of the *ent*-kaurane diterpenoids, can be isolated from the genus Sideritis (Lamiaceae). The Sideritis species are represented by

---

[a] *Department of Chemistry, Faculty of Arts and Sciences, Balikesir University, 10145, Balikesir, Turkey. Corresponding author: azizoglu@balikesir.edu.tr*
[b] *Department of Chemistry, Faculty of Arts and Sciences, Aksaray University, 68100, Aksaray, Turkey*
[c] *Altınoluk Vocational School, Balikesir University, Balikesir, Turkey*
[d] *Department of Science Education, Necatibey Faculty of Education,10145, Balikesir University, Balikesir, Turkey*

more than 150 species, which are distributed mainly in the Mediterranean and the Middle East [4]. 7-epicandicandiol has the antibacterial, antifeedant and toxicity activity [5-7]. Especially, it has been found that 7-epicandicandiol compound inhibits colon cancer moderately [8]. In addition to that, the compounds, 7-epicandicandiol and 7-epicandicandiol diacetate, which are isolated from *Sideritis trojana* have shown good insecticidal activity against to harmful insects [8].
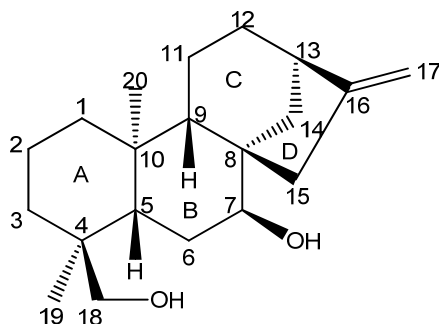
Figure 1. Structure of 7-epicandicandiol

The application of computational predictions, together with experimental methods, is currently limited in the natural products field. However, it has been growing rapidly in the last few years by the successful use of ^{1}H- and ^{13}C-NMR calculated chemical shifts and IR vibrations for structure identification, structure reassignment, and confirmation of natural products. The theoretical methods, such as the density functional theory (DFT), have become the dominant computational tools for dealing with organic molecules, isolated from plants [9-11]. Literature survey reveals that to the best of our knowledge no ab-initio (HF) and DFT calculations of 7-epicandicandiol have been reported so far. It may be due to difficulty in interpreting the results of calculations because of their complexity and low symmetry. Density functional theory (DFT) approaches using hybrid functional are frequently used to study the structural characteristics, vibrational and electronic properties, interactions among different orbitals. Hence, we wish to calculate geometrical parameters, fundamental frequencies and GIAO ^{1}H- and ^{13}C-NMR values of the title compound to distinguish the findings from the experimental ^{1}H- and ^{13}C-NMR values, vibrational frequencies, and geometric parameters, by using the HF and DFT methods with 6-31G(d) basis set. A comparison of the experimental and computational spectra can be very useful in making correct assignments and understanding the basic molecular structure [9-12].

RESULTS AND DISCUSSION

Molecular Structure

In this study, the geometry obtained from X-ray diffractometer was used as input for the full geometry optimization at the HF and DFT methods, together with the 6-31G(d) basis set. The general molecular structure and numbering of the atoms of 7-epicandicandiol is depicted in Figure 1. The optimized geometry calculated by the RB3LYP/6-31G(d) method is visualized in Figure 2.
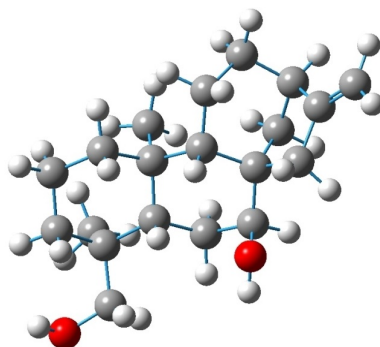
Figure 2. The optimized structure of 7-epicandicandiol achieved by RB3LYP/6-31G(d) method

The theoretically computed structural parameters can be compared with X-ray structure, which have been reported before [13]. The results of optimized parameters (bond lengths, bond angles, and dihedral angles) and experimentally predicted structural data of 7-epicandicandiol are listed in Table 1. As an example, the optimized bond lengths (C4-C5, C7-C8, C16-C17) of 7-epicandicandiol are determined to be 1.564, 1.529 and 1.318 Å for the RHF/6-31G(d) method and 1.568, 1.535 and 1.333 Å for the RB3LYP/6-31G(d) method, which are in much better agreement with that of experimental values 1.563, 1.527 and 1.350 Å, respectively. On the other hand, RHF/6-31G(d) method is insufficient at calculations of C-O bond lengths. For instance, the optimized C7-O7' and C18-O18' bond length by HF method are computed to be 1.414 and 1.405 Å, which are highly shorter than experimental data of 1.444 and 1.432 Å, respectively. Moreover, the theoretical

19

results of C-O bond lengths at RPW91/631G(d) method are much better agreement with experimentally predicted C-O bond lengths than the other theories. In general, all bond lengths and bond angles computed herein show good agreement with experimental findings. For instance, the correlation coefficient values (R^2) between experimental and theoretical bond lengths are found to be 0.9572, 0.9646, 0.965, 0.959, and 0.9517 for RHF, RPW91, RB3LYP, RPBE1PBE, and RLSDA, respectively.

Table 1. Optimized structural parameters (bond length (Å), bond angle (degree), and dihedral angle (degree)) of 7-epicandicandiol

Bond lengths	Exp.	RHF/ 6-31G(d)	RPW91/ 6-31G(d)	RB3LYP/ 6-31G(d)	RPBE1PBE/ 6-31G(d)	RLSDA/ 6-31G(d)
C1-C2	1.526	1.529	1.535	1.534	1.526	1.514
C1-C10	1.547	1.549	1.555	1.555	1.545	1.531
C2-C3	1.521	1.526	1.531	1.531	1.522	1.512
C3-C4	1.544	1.544	1.551	1.551	1.540	1.527
C4-C5	1.563	1.564	1.565	1.568	1.554	1.534
C4-C19	1.539	1.539	1.542	1.542	1.532	1.518
C4-C18	1.538	1.549	1.559	1.558	1.548	1.534
C5-C10	1.561	1.565	1.570	1.571	1.559	1.543
C7-C8	1.527	1.529	1.535	1.535	1.526	1.512
C7-O7'	1.444	1.414	1.441	1.436	1.423	1.414
C8-C14	1.542	1.546	1.554	1.553	1.543	1.531
C8-C15	1.548	1.555	1.563	1.563	1.551	1.538
C9-C10	1.567	1.578	1.583	1.584	1.571	1.553
C10-C20	1.543	1.543	1.545	1.546	1.536	1.523
C13-C16	1.510	1.516	1.521	1.520	1.513	1.504
C15-C16	1.476	1.520	1.523	1.523	1.515	1.503
C16-C17	1.350	1.318	1.341	1.333	1.331	1.332
C18-O18'	1.432	1.405	1.427	1.424	1.412	1.401
Bond angles						
C5-C4-C19	114	115	115	115	115	115
C4-C18-H18'	108	109	109	108	109	110
C7-O7'-(H-O7')	105	109	106	107	107	107
C16-C17-H17'a	119	121	121	121	121	121
C16-C17-H17'b	120	121	121	121	121	121
C15-C16-C17	127	126	126	126	126	126
C13-C16-C17	125	126	125	126	126	125
H7'-C7-O7'	108	108	109	108	109	109
C9-C10-C20	112	112	112	112	112	112
C8-C7-O7'	109	107	107	107	107	106
O18'-C18-H18'a	108	104	104	104	104	105
O18'-C18-H18'b	108	110	110	110	110	111

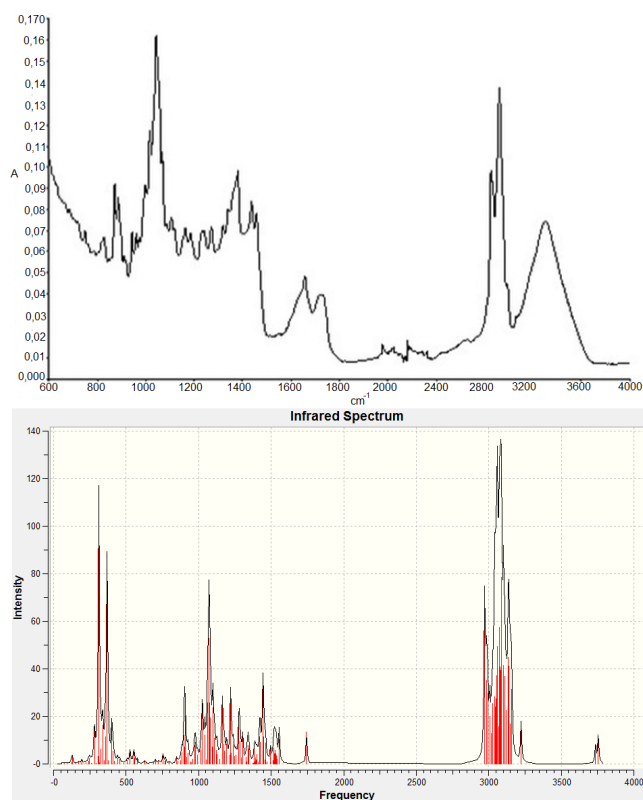| Dihedral angles						
C4-C18-O18'-(H-O18')	-82	-72	-65	-62	-66	-61
(H-O18')-O18'-C18-H18'a	155	166	173	171	172	177
(H-O18')-O18'-C18-H18'b	39	51	58	56	56	61
H7'- C7-O7'-(H-O7')	-41	-57	-65	-62	-64	-71
C15-C16-C17-H17'a	179	178	178	178	178	178
C16-C15-C8-C14	30	30	30	30	30	31
C18-C4-C5-C6	61	60	61	61	61	61
C19-C4-C18-O18'	-60	-65	-63	-63	-64	-63

Vibrational Analysis

Figure 3. Visualization of experimental (above) and theoretical (below at RB3LYP/6-31G(d) level) IR spectra of 7-epicandicandiol

21

The title molecule has 54 atoms which have 156 normal modes from 57 to 4127 cm^{-1} at the RHF/6-31G(d) level, 56 to 3755 cm^{-1} at RB3LYP/6-31G(d) level, 57 to 3818 cm^{-1} at the RPBE1PBE/6-31G(d) level, 56 to 3637 cm^{-1} at the RPW91/6-31G(d) level, and 57 to 3647 cm^{-1} at the RLSDA/6-31G(d) level. It agrees with C1 point group symmetry, all vibrations are active in infrared absorption. In order to facilitate assignment of the observed peaks, we have analyzed vibrational frequencies and compared our calculation with experimental measurements (Table 2). On an absolute scale, it is well known that experimental results of infrared spectroscopy are usually lower than the corresponding computational quantities due to the combination of electron correlation effects and basis set deficiencies [10]. The experimental and theoretical FT-IR spectra are presented in Figure 3. The correlation coefficient (R^2) values between experimental and theoretical FT-IR results are calculated to be 0.9838, 0.9905, 0.9906, 0.9882, and 0.9884 for theories of RHF, RPW91, RB3LYP, RPBE1PBE, and RLSDA, respectively. In total, the RB3LYP/6-31G(d) has higher R^2 (0.9906) value than others. Hence, we have chosen the RB3LYP method as reference theoretical IR spectra for Figure 3. The IR spectra of the title structure are dominated by a broad and intense absorption in the range between 1000-3300 cm^{-1} for O-C and O-H vibrations.

The O–H group vibrations show pronounced shifts in the spectra of the hydrogen-bonded species, so they are most sensitive [14]. The absorption of free O-H group is existed in the region 3700-3580 cm^{-1}, whereas the intermolecular hydrogen bond formation can reduce the O-H stretching frequency to the 3550-3200 cm^{-1} region with increase in intensity [15]. The compound has two O-H groups. For the title compound, the both O-H groups give rise to broad band at about 3303 cm^{-1} for the vibration namely stretching. The stretching vibration have been calculated in the range from 3623.0 to 4127.0 cm^{-1} at the RHF/6-31G(d), RPW91/6-31G(d), RB3LYP/6-31G(d), RPBE1PBE/6-31G(d), and RLSDA/6-31G(d) theory of levels (Table 2). The calculated rocking vibrations of O-H groups are also observed in the range of 272-442 cm^{-1}. The theoretical results depict that the RPW91/6-31G(d) method shows better agreement with the experimental value of 3303.0 cm^{-1} than others for describing of O-H group vibration.

The C-O stretching mode is normally assigned near 1200 cm^{-1} for siderol and its derivatives [10,16]. The molecule has two C-O symmetrical stretching vibrations. In the present study, the stretching vibrations of the C–O are appeared at 1018 cm^{-1} (C18) and 1043 cm^{-1} (C7) in the FT-IR

spectrum. The theoretically predicted wavenumbers were found at 1181 cm^{-1} (C18) and 1205 cm^{-1} (C7) in the RHF/6-31G(d), 1044,1070 cm^{-1} (C18) and 1050 cm^{-1} (C7) in the RPW91/6-31G(d), 1082 cm^{-1} (C18) and 1099 cm^{-1} (C7) in the RB3LYP/6-31G(d), 1107, 1111 cm^{-1} (C18) and 1122 cm^{-1} (C7) in the RPBE1PBE/6-31G(d), 1091 cm^{-1} (C18) and 1099 cm^{-1} (C7) in the RLSDA/6-31G(d). The C-O symmetrical stretching frequencies obtained through the RPW91/6-31G(d) methodology are in excellent agreement with the experimental values reported above.

The ring stretching vibrations are very important due to characteristic nature in the IR spectrum. The C–C stretching vibrations of the ring appear in the range of 1625–1400 cm^{-1} [17]. In this study, experimental C-C bands observed at 1437.0 and 1458.0 cm^{-1}, which are in good agreement with calculated result of 1461.0 cm^{-1} at the RHF/6-31G(d) theory of level. The RHF/6-31G(d), RPW91/6-31G(d), RB3LYP/6-31G(d), RPBE1PBE/6-31G(d), and RLSDA/6-31G(d) theory of levels were performed to analyze the C=C peak absorption, which are 1893.0, 1695.0, 1744.0, and 1767.0, and 1732.0 cm^{-1}, respectively. The RPW91/6-31G(d) level shows better agreement with experimental observation (1660.0 cm^{-1}) than other methods for determination of the C=C signal.

Table 2. Assignment of the observed and calculated FT-IR spectra using RHF/6-31G(d), RPW91/6-31G(d), RB3LYP/6-31G(d), RPBE1PBE/6-31G(d), and RLSDA/6-31G(d) theory of levels for 7-epicandicandiol

Exp. (cm^{-1})	RHF/ 6-31G(d)	RPW91/ 6-31G(d)	RB3LYP/ 6-31G(d)	RPBE1PBE/ 6-31G(d)	RLSDA/ 6-31G(d)	*Approximate description*
	139	128	129	132	132	H-O-CH$_2$ rocking (C18)
	279, 296, 318	273, 301	282, 312	281, 311	272, 299	O-H rocking (C7)
	348, 359, 374, 376, 385	371	338, 369, 402	442, 376, 403	381, 403	O-H rocking (C18)
	406, 546, 596	492, 537	508, 552	509, 555	495	C=C-CH$_2$ rocking
873	753, 785, 909	702, 689	705, 724	694, 714, 729	702, 710	C=CH$_2$ twisting (C18)
	991	896	919	914, 930	904	H-O-CH$_2$ rocking
944	1023, 1024, 1046	859	900, 903, 906	899, 906	848, 854, 863	C=CH$_2$ wagging
1018	1181	1044,1070	1082	1107, 1111	1091	O-C symmetrical stretching C18)
1043	1205	1050	1099	1122	1099	O-C symmetrical stretching (C7)
	1256	1240	1278	1284	1237	H-O-CH$_2$ twisting (C18)
	1419	1250	1294	1293	1330	C=C-CH$_2$ wagging

Exp. (cm^{-1})	RHF/ 6-31G(d)	RPW91/ 6-31G(d)	RB3LYP/ 6-31G(d)	RPBE1PBE/ 6-31G(d)	RLSDA/ 6-31G(d)	Approximate description
	1581, 1587, 1667	1406,1400	1450, 1403	1447, 1403	1338,1374	H-O-CH$_2$ wagging (C18)
	1591	1429	1473	1468, 1470	1401,1404	C=CH$_2$ scissoring
	1624	1443	1495	1486	1416	C=C-CH$_2$ scissoring
	1573	1488	1522,1528, 1532, 1538	1525, 1521, 1533	1456	H-O-CH$_2$ scissoring (C18)
	1165, 1230	1094,1129	1172, 1220	1142, 1155, 1228	1104	C=C-CH$_2$ twisting
1660	1893	1685	1744	1767	1732	C=C symmetrical stretching
2854	3169	2888	2972	3000	2866	H-O-CH symmetrical stretching (C7)
2924	3180	2900	2983	2991	2870	H-O-CH$_2$ symmetrical stretching (C18)
	3241	3013	3072	3104	3015	H$_2$C=C-CH symmetrical stretching
	3222	2980	3048	3069	3087	C=C-CH$_2$ symmetrical stretching
	3276	3036	3222	3128	3170	C=C-CH$_2$ asymmetrical stretching
	3301	3036	3111	3132	3018	H-O-CH$_2$ asymmetrical stretching (C18)
3000	3316	3079	3149	3175	3087	C=CH$_2$ symmetrical stretching
	3388	3166	3222	3255	3170	C=CH$_2$ asymmetrical stretching
3303	4103	3653	3736	3802	3647	O-H symmetrical stretching (C7)
3303	4127	3637	3755	3818	3645	O-H symmetrical stretching (C18)

The vibrations show presence of C-H stretching in the region 3000–3100 cm^{-1}. In this molecule, the symmetrical stretching vibrations of C-H are observed at 2854, 2924 and 3000 cm^{-1} as medium strong band in the IR spectrum of title molecule. The computed wavenumbers for the same mode are assigned in the range of 2972–3149 cm^{-1}. In general, the experimental values agree well with the computed values from all theories used herein.

NMR spectra

The GIAO/DFT (Gauge including atomic orbital/density functional theory) approach is widely used for the NMR calculations [18]. In general, the proton chemical shift of the molecules varies greatly with the electronic environment of the proton. Hydrogen atoms, which are attached the electron-withdrawing atom or group, can decrease the shielding. In this case, the resonance of attached proton is altered towards to a higher frequency, whereas electron-donating atom or group increases the shielding and

moves the resonance towards to a lower frequency [19]. In the present investigation, the calculations of the chemical shift values for carbon atoms were performed by adopting the procedure recommended by Cheeseman et al. [20]. After that, GIAO ^{1}H- and ^{13}C-NMR chemical shift values (with respect to TMS) have been calculated using DFT and HF methods with 6-31G(d) basis set. The findings from theoretical methods were compared to the experimental ^{1}H-NMR and ^{13}C-NMR chemical shift values reported in ppm relative to TMS. The experimental and computed NMR results are tabulated in Table 3 and 4.

Table 3. Experimental and calculated ^{13}C-NMR chemical shifts
(GIAO method) of 7-epicandicandiol

Carbon No	Exp. (ppm)	RB3LYP/ 6-31G(d)	RPBE1PBE/ 6-31G(d)	RSVWN/ 6-31G(d)	RPW91PW91/ 6-31G(d)	RHF/ 6-31G(d)
C1	39	33	27	35	35	32
C2	17	13	7	11	14	15
C3	38	27	22	29	30	28
C4	37	31	23	26	33	29
C5	38	37	30	37	39	34
C6	28	24	18	25	26	25
C7	77	69	62	70	73	65
C8	50	42	33	39	44	37
C9	50	45	37	45	47	41
C10	39	34	25	29	36	30
C11	17	13	7	11	15	14
C12	34	28	22	30	31	27
C13	43	38	32	38	41	35
C14	35	33	27	35	35	31
C15	45	38	33	41	41	38
C16	154	140	136	142	141	147
C17	103	93	91	95	94	101
C18	70	67	61	70	70	64
C19	18	9	5	10	11	14
C20	17	11	7	14	13	15

Table 4. Experimental and calculated ^{1}H-NMR chemical shifts
(GIAO method) of 7-epicandicandiol

Proton No	Exp. (ppm)	RB3LYP/ 6-31G(d)	RPBE1PBE/ 6-31G(d)	RSVWN1/ 6-31G(d)	RPW91PW91/ 6-31G/(d)	RHF/ 6-31G(d)
H(1'a)	-	1,51	1,62	2,66	2,00	1,20
H(1'b)	-	0,64	0,69	1,53	1,07	0,39
H(2'a)	-	1,47	1,54	2,57	1,95	1,11
H(2'b)	-	1,13	1,23	2,11	1,56	0,98
H(3'a)	-	0,61	0,64	1,41	1,02	0,38
H(3'b)	-	1,25	1,31	2,14	1,67	1,04
H(5')	-	1,59	1,66	2,81	2,23	0,90
H(6'a)	-	1,53	1,60	2,75	2,10	0,98
H(6'b)	-	0,73	0,82	1,79	1,22	0,44
H(7')	3,66	3,38	3,35	4,38	3,88	2,80
H(9')	-	1,50	1,53	2,60	2,05	0,92
H(11'a)	-	1,22	1,30	2,29	1,70	0,89
H(11'b)	-	1,38	1,47	2,56	1,88	0,99
H(12'a)	-	1,23	1,30	2,17	1,67	1,00
H(12'b)	-	1,42	1,52	2,60	1,94	1,05
H(13')	2,69	2,25	2,32	3,23	2,73	2,03
H(14'a)	-	1,56	1,68	2,78	2,10	1,12
H(14'b)	-	0,95	1,03	1,97	1,44	0,61
H(15'a)	-	2,24	2,32	3,26	2,70	1,95
H(15'b)	-	2,23	2,29	3,15	2,68	1,92
H(17'a)	4,80	4,51	4,73	5,43	4,33	4,61
H(17'b)	4,80	4,58	4,79	5,45	4,95	4,70
H(18'a)	3,47	3,14	2,74	4,11	3,56	2,98
H(18'b)	2,92	2,74	3,22	3,54	3,18	2,44
H(19'a)	0,69	0,41	0,49	1,29	0,80	0,34
H(19'b)	0,69	0,68	0,76	1,53	1,06	0,59
H(19'c)	0,69	1,11	1,19	2,06	1,50	1,04
H(20'a)	1,05	0,89	0,99	1,94	1,36	0,64
H(20'b)	1,05	0,99	1,09	2,10	1,47	0,69
H(20'c)	1,05	0,56	0,68	1,66	1,00	0,38

As can be seen from Table 3 and 4, the calculated chemical shifts are mostly in agreement with the experimental findings. Comparing theoretical and experimental data, the correlation values of carbon and proton shifts are found to be 0.9909 and 0.9604 for the RHF/6-31G(d), 0.9941 and 0.9798 for the B3LYP/6-31G(d), 0,9944 and 0.9592 for the RPE1PBE/6-31G(d), 0,9889 and 0.9809 for the RSVWN1/6-31G(d), 0,9918 and 0.971 for the RPW91PW91/6-31G(d). However, the predicted chemical shifts from

PBE1PBE theory of level are much lower than experimental values. It seems that we could not obtain correct ^{13}C-NMR values with the PBE1PBE theory of level. The calculated difference is in the range from 8 to 18 ppm. For instance, experimental ^{13}C-NMR chemical shift for C16 is determined to be 154 ppm, whereas that of theoretical value is 136 ppm at PBE1PBE theory of level. The computed difference is found to be very high with 18 ppm. The overall results display that PBE1PBE methodology in the ^{13}C-NMR calculations is not useful for this kind of organic molecules. On the other hand, the chemical shifts at HF and B3LYP methods are in good agreement with experimentally predicted ^{13}C-NMR shifts due to very close values (Table 3). The chemical shifts of C=C of organic molecules are usually observed in the range of 110-150 ppm. Moreover, the carbon atoms (C16 and C17) in the C=C bond are calculated in the range of 93-147 ppm, whereas the experimental ^{13}C-NMR values of C16 and C17 found to be 154 and 103 ppm, respectively. In this case, the HF method shows better agreement with 147 and 101 ppm for C16 and C17, respectively. As can be seen from Table 4, the experimental ^{1}H-NMR chemical shifts are also in good compliance with theoretical findings.

Frontier Molecular Orbitals

The frontier molecular orbitals, which are called HOMO (Highest Occupied Molecular Orbital) and LUMO (Lowest Unoccupied Molecular Orbital) are most important orbitals in molecular systems [21]. The HOMO–LUMO energy gap is an important kinetic stability index and it also reflects the chemical reactivity of a molecule [22-25]. A molecule with a small frontier orbital gap is more polarizable and is generally associated with a high chemical reactivity, low kinetic stability. In the case of 7-epicandicandiol, the calculated energy gap of $\Delta E= 0.257$ eV is identified between the HOMO and LUMO with the help of RB3LYP/6-31G(d) level of theory (Figure 4). This small HOMO-LUMO energy gap explains that the title molecule has low chemical hardness and low excitation energies for corresponding excited states. The title molecule with small energy gap is also more polarizable than hard molecules. The HOMO and LUMO orbitals mainly populate on the C=C bond, which can describe most active sides of the title molecule.
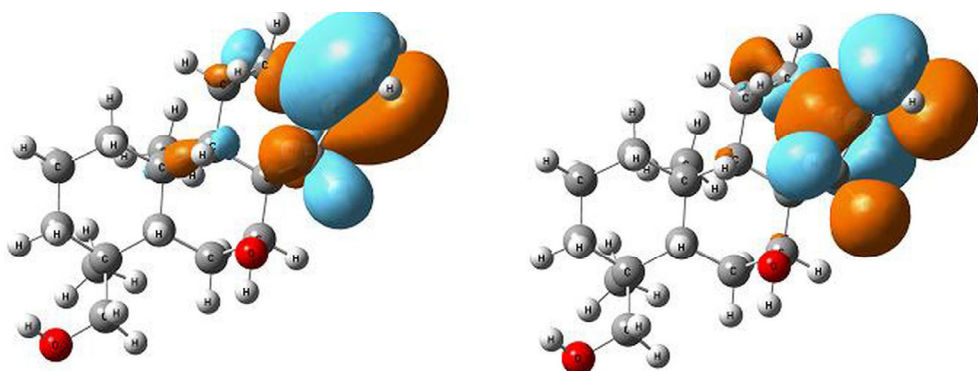
Figure 4. Molecular orbital surfaces and energies (in parentheses, eV) for the HOMO (left, -0.232 eV) and LUMO (right, 0.025 eV) of the 7-epicandicandiol computed at RB3LYP/6-31G(d) level

Molecular electrostatic potential (MEP) maps

The molecular electrostatic potential maps have used for interpreting and predicting for both electrophilic and nucleophilic behaviors in various chemical systems [26-28]. It also provides a visual method to understand the relative polarity of the molecule. In the MEPs, the most suitable atomic site for electrophilic attack is described as red color. On the other hand, the positive electrostatic potentials are appeared as blue surface areas. The MEP was calculated at the RB3LYP/6-31G(d) level for the title optimized geometry as shown in Figure 5. In view of this, we can say that the electron withdrawing hydroxyl substituents are increasing the chemical reactivity of a molecule. As can be seen from Figure 5, the oxygen atoms are covered by a greater surface of red color which describes most negative region of the molecule. The calculated value of mulliken charges on O7 and O18 are determined to be -0.636, and -0.623 at the RB3LYP/6-31G(d) theory of level, respectively. In addition to that, the terminal C atom of C=C bond has a relatively higher electronegative character (-0.440) than the other C atoms. Maximum positive regions are mainly over hydrogen atoms of OH groups with mulliken charges of 0.395 and 0.388. From this calculated results, we can conclude the behaviors of molecule in the electrophilic and nucleophilic reactions depending on its positive and negative sites.
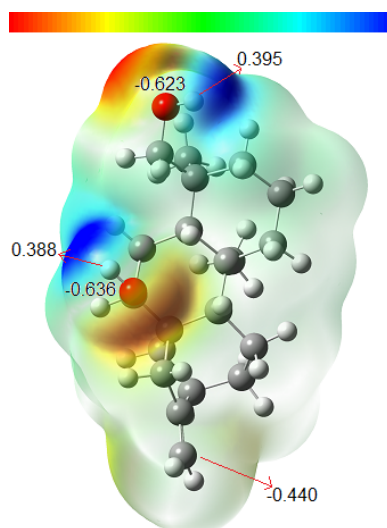
Figure 5. 3D-molecular electrostatic potential map of 7-epicandicandiol calculated at the RB3LYP/6-31G(d) level

CONCLUSIONS

In this study, we have calculated the geometric parameters (bond length, bond angle, dihedral angle), vibrational frequencies, infrared intensities, chemical shifts and thermodynamic parameters of 7-epicandicandiol by using HF and DFT methods with the 6-31G(d) basis set. The calculated vibrational frequencies have been compared with that of obtained experimental IR spectrum. Experimental fundamentals are found to have slightly a better correlation for B3LYP theory than other theories. Moreover, ^{1}H- and ^{13}C-NMR chemical shifts have been compared with experimental values. The computational results at the B3LYP/6-31G(d) method have shown better fit to experimental predictions than others in evaluating ^{1}H-NMR and ^{13}C-NMR chemical shifts. However, there is no sufficient agreement between experimental ^{13}C-NMR chemical shifts and the PBE1PBE method. The calculated structural parameters by B3LYP method closely matches with experimental X-Ray diffraction data. Especially, calculated bond lengths and angels at B3LYP and HF methods show much better agreement than other methods.

EXPERIMENTAL AND COMPUTATIONAL SECTION

The 7-epicandicandiol (ent-7-,18-dihydroxykaur-16-ene) having the ent-kaurene skeleton can be isolated from different species of Sideritis such as *Sideritis sipylea, S. trojana, S. niveotomentosa, S. chamaedrifolia, S. hirsuta, S. lurida, S. argyrea, S. condensata, S. congesta, S. huber-morathii, S. leptoclada, S. ozturkii* [29-32]. In our study, *Sideritis niveotomentosa Huber – Morathii* was collected from Sertuval highway between Mut and Karaman, Turkey at 1600 m altitude. The species were identified by Assoc. Prof. Dr. Tuncay Dirmenci from Balikesir Univ., Turkey. The isolation and experimental measurements on 7-epicandicandiol have been made according to previously reported procedure [10].

In the present work, the electronic structure calculations are performed using Gaussian 03 program suite [33]. The ground state of investigated system was performed using Hartree–Fock (HF) and Density functional theoretical (DFT) levels with using the 6-31G(d) basis set [34,35]. The restricted formalism was used for all calculations. In this study, the geometry was obtained from X-ray diffraction because of the large number of possible conformations for title compound. Firstly, equilibrium geometry was fully optimized without any constraints at RHF/6-31G(d) level. The results of HF/6-31G(d) calculations were repeated with full geometry optimization at higher DFT levels for better description. The optimized structural parameters were used in the vibrational frequency calculations at both HF and DFT levels to characterize all stationary points as minima. The geometry of the title compound, together with that of tetramethylsilane (TMS) is fully optimized. The ^{1}H- and ^{13}C-NMR values are calculated within GIAO approach applying the B3LYP and HF method with the 6-31G(d) basis set. Finally, the frontier molecular orbitals (FMOs) and molecular electrostatic potential map (MEP) were also calculated at the B3LYP/6-31G(d) level. The computed structures were visualized by using the GaussView 3.0 program [36].

REFERENCES

[1]. J. Gershenzon, N. Dudareva, *Nat. Chem. Bio.,* **2007**, *3*, 408.

[2]. I. Khalaf, L. Vlase, B. Ivanescu, D. Lazar, A. Corciova, *Studia UBB Chemia,* **2012**, *57*, 113.

[3]. E. González-Burgos, M.E. Carretero, M.P. Gómez-Serranillos, *J. Ethnopharmacol.* **2011**, *135,* 209.

[4]. E. Kupeli, F.P. Sahin, İ. Çalıs. E. Yeşilada, N. Ezer, *J. Ethnopharmacol.* **2007**, *112,* 356.

[5]. T. Kilic, *Molecules,* **2006**, *11*, 257.

[6]. G. Topcu, A.C. Gören, *Rec.Nat. Prod.*, **2007**, *1*, 1.

[7]. I. Aslan, T. Kilic¸ A.C. Gören, G. Topcu, *Indust. Crops and Prod.*, **2006**, *23*, 171.

[8]. T. Kilic, Y.K. Yıldız, A.C. Gören, G. Tümen, G. Topcu, *Chem. Nat. Comp.*, **2003**, *39,* 453.

[9]. D.S.O. Silva, M.J.C. Corrêa, H.R. Bitencourt, W.R. Monteiro, J. Lameira, L.S. Santos, G.M.S.P. Guilhon, D.S.B. Brasil, *J. Comput. Theor. Nanosci.*, **2012**, *9*, 953.

[10]. A. Azizoglu, Z. Özer, T. Kilic, *Collect. Czech. Chem. Commun.,* **2011**, *76*, 95.

[11]. S.D.O. Silva, R.N.S. Peixoto, J.R.A. Silva, C.N .Alves, *Int. J. Mol. Sci.,* **2011**, *12*, 9389.

[12]. A. Cansız, A. Cetin, C. Orek, M. Karatepe, K. Sarac, A. Kus, P. Kopari, *Spectrochim. Acta Part A*, **2012***, 97*, 606.

[13]. A. Linden, F. P. Şahin, N. Ezer, I. Çalış, *Acta Cryst. Section C*, **2006**, *62*, 253.

[14]. D. Bulgariu, R. Constantin, L. Bulgariu, *Studia UBB Chemia*, **2013**, *58*, 121.

[15]. G. Topçu, A.C. Gören, T. Kiliç, Y.K. Yildız, G. Tümen, *Fitoterapia*, **2001**, *72*, 1.

[16]. S. Çarıkçı, C. Cöl, T. Kılıc, A. Azizoglu, *Rec. Nat. Prod.,* **2007**, *1*, 44.

[17]. D.RH. Olguin, M. Villa, M.L. Senent, M.A.M. Delgado, *J. Mex. Chem. Soc.*, **2008**, *52*, 98.

[18]. O.G. Beltran, J.S. Delgado, P.I. Vasquez, C. Areche, B.K. Cassels, *J. Chil. Chem. Soc.*, **2012**, *57*, 1323.

[19]. E. Kose, A. Atac, M. Karabacak, C. Karaca, M. Eskici, A. Karanfil, *Spectrochim. Acta Part A*, **2012**, *97*, 435.

[20]. J.R. Cheeseman, G.W. Trucks, T.A. Keith, M.J. Frisch, *J. Chem. Phys.*, **1996**, *104*, 5497.

[21]. I. Fleming, "Frontier Orbitals and Org. Chemical Reactions", Wile, London, **1976**.

[22]. B. Cicek, U. Cakir, A. Azizoglu, *J. Incl. Phenom. Macrocycl. Chem.,* **2012**, *72*, 121.

[23]. L. Găină, I. Torje, E. Gal, A. Lupan, C. Bischin, R. Silaghi-Dumitrescu, G. Damian, P. Lönnecke, C. Cristea, L. Silaghi-Dumitrescu, *Dyes Pigm.*, **2014**, *102*, 315.

[24]. V. Bucila, M. Stefu, B. Szefler, *Studia UBB Chemia*, **2013**, *58*, 101.

[25]. C.B. Yildiz, A. Azizoglu, *Struc. Chem.*, **2012**, *23*, 1777.

[26]. C.B. Yildiz, A. Azizoglu, *Comp. Theor. Chem.*, **2013**, *1023*, 24.

[27]. I. Sen, C.B. Yıldız, H. Kara, A. Azizoglu, *Phosphorus, Sulfur, and Silicon*, **2013**, *188*, 1621.

[28]. A. Azizoglu, C. B. Yıldız, *J. Organomet. Chem.*, **2012**, *715*, 19.

[29]. G. Topçu, A.C. Gören, T. Kılıç, Y.K. Yıldız, G. Tümen, *Turk. J. Chem.*, **2002**, *26*, 189.

[30]. G. Topçu, A.C. Gören, T. Kılıç, Y.K. Yıldız, G. Tümen, *Nat. Prod. Lett.*, **2002**, *16*, 33.

[31]. S. Çarıkçi, T. Kılıç, A. Azizoglu, G. Topçu, *Rec. Nat. Prod.*, **2012**, *6*, 101.

[32]. M.F. Braulio, *Phytochemistry*, **2012**, *76*, 7.

[33]. Gaussian 03, Revision C.02, M.J. Frisch, G.W. Trucks, H.B. Schlegel, G.E. Scuseria, M.A. Robb, J.R. Cheeseman, J.A. Montgomery, Jr., T. Vreven, K. N. Kudin, J.C. Burant, J.M. Millam, S.S. Iyengar, J. Tomasi, V. Barone, B. Mennucci, M. Cossi, G. Scalmani, N. Rega, G.A. Petersson, H. Nakatsuji, M. Hada, M. Ehara, K. Toyota, R. Fukuda, J. Hasegawa, M. Ishida, T. Nakajima, Y. Honda, O. Kitao, H. Nakai, M. Klene, X. Li, J.E. Knox, H.P. Hratchian, J.B. Cross, V. Bakken, C. Adamo, J. Jaramillo, R. Gomperts, R.E. Stratmann, O. Yazyev, A.J. Austin, R. Cammi, C. Pomelli, J.W. Ochterski, P. Y. Ayala, K. Morokuma, G.A. Voth, P. Salvador, J.J. Dannenberg, V.G. Zakrzewski, S. Dapprich, A.D. Daniels, M.C. Strain, O. Farkas, D.K. Malick, A.D. Rabuck, K. Raghavachari, J.B. Foresman, J.V. Ortiz, Q. Cui, A.G. Baboul, S. Clifford, J. Cioslowski, B.B. Stefanov, G. Liu, A. Liashenko, P. Piskorz, I. Komaromi, R.L. Martin, D.J. Fox, T. Keith, M.A. Al-Laham, C.Y. Peng, A. Nanayakkara, M. Challacombe, P.M.W. Gill, B. Johnson, W. Chen, M.W. Wong, C. Gonzalez, and J.A. Pople, Gaussian, Inc., Wallingford CT, **2004**.

[34]. W.J. Hehre, L. Radom, P.V.R. Schleyer, J. Pople, "Ab initio molecular orbital theory", Wiley, New York, **1986**.

[35]. F. Jensen, "Introduction to computational chemistry", Wiley, West Sussex, England, **1999**.

[36]. GaussView, Version 3.09, R. Dennington, T. Keith, J. Millam, K. Eppinnett, W.L. Hovell, R. Gilliland, Semichem, Inc., Shawnee Mission, KS, **2003**.

BIOTECHNOLOGICAL PRODUCTION OF SUCCINIC ACID FROM GLYCEROL; THE ROLE OF CO-SUBSTRATES

ZSOLT BODOR[a*], ANDREA FAZAKAS (IUHASZ)[a], ERIKA KOVÁCS[b], SZABOLCS LÁNYI[b], BEÁTA ÁBRAHÁM[b]

ABSTRACT. Our society is merely based on petroleum, however its availability and the impact on environment makes this energy source unsustainable. Hence, search for new renewable energy sources is of major interest. Biodiesel as biofuel is a promising source and intensively studied for the substitution of fossil fuels. However, during the production process glycerol is generated as the main by-product (10% (w/w)). The bio-based conversion of glycerol to valuable chemical such as succinic acid by commonly used microorganisms like *Escherichia coli* is one of possible applications. Succinic acid is used in a number of industries including: polymers, food, it can be converted to biodegradable plastics, etc. Genetically engineered strains can be used to provide a cost-effective, ecologically sustainable alternative to the current petrochemical production process. The main aim of this study was to make predictions and to analyse the production of succinic acid from glycerol if different chemicals (co-substrates) are present in the minimal media. We found that the presence of co-substrate in minimal medium is critical under anaerobic conditions; on the other hand, with genetic modifications the succinic acid production can be significantly influenced. The *in silico* studies presented here may serve as important contribution to the implementation of biorefineries by converting biofuel waste glycerol, into a higher-value chemical, reducing environmental impacts. The new application of glycerol may improve the economic viability of the biodiesel industry.

Keywords: *Glycerol; Succinic acid; Escherichia coli; Metabolic engineering - Modelling;*

[a] *"Politehnica" University of Bucharest, Department of Inorganic Substances Technology and Environment Protection, Splaiul Independenţei, 313, 060042, Romania.*
corresponding author: bodorzsolt@sapientia.siculorum.ro
[b] *Sapientia Hungarian University of Transylvania, Department of Bioengineering, Libertatii square, No. 1, 530104, Miercurea Ciuc, Romania.*

INTRODUCTION

Petroleum is the main fossil energy source utilized worldwide, but the associated environmental impacts; climate change, air pollution, soil degradations, the diminishing of fossil fuel deposits have been raised many concerns, including sustainability [1]. Sustainable development is environment-connected and need to be harmonized to sustain a continuous development and hence, the applications of (bio-based) green technologies is crucial. One of the strong candidates in the conventional diesel engine is the biodiesel production, which is increasing year by year (in 2010 was 1.30 and in 2012 near 3.67 million m^3 in the USA) [1]. Biodiesel production process generates large quantities of glycerol (10% (wt/wt)) which could be an inexpensive carbon source for many microorganisms [1-3] and can be used as un appealing substrate for high value-added biochemicals production [4, 5]. Glycerol is a non-toxic liquid, however, like most organic materials, deplete the oxygen content of water and wetlands very quickly and can suffocate fish and other organisms. Birds can be deadly affected (crude oil spill) and on the other hand the use of rivers for fishing, boating, etc. can be seriously damaged [6].

Glycerol can be converted biologically to succinic acid, what is a dicarboxylic acid with four carbon atoms. It is an important precursor (building-block) for many industrially manufactured chemical commodities and products. For example, it can be hydrogenated into 1,4-Butanediol [7], a potential petroleum alternative, which can be further used to modify succinic acid to form the inexpensive biodegradable plastic polybutylene succinate [8]. A few applications are presented below [9] (Fig. 1).

The U.S. Department of Energy identified succinic acid as one of the 12 top chemical building blocks produced by microorganisms [10]. Today most of the succinic acid derives from the petrochemical industry, and the starting point is the non-renewable fossil fuel butane [11]. One possible way to reduce the "ecological footprint" is to create economically competitive biorefineries to produce fuels (e.g. biodiesel), chemicals (e.g. succinic acid) and different bio-products, reducing the petroleum dependency. The most important challenges is to use renewable resources; e.g. by-products generated by these industries and transform them biologically (using different microorganisms) into valuable chemicals such as succinic acid. To efficiently produce succinic acid biologically various attempts have been made such as, natural succinic acid producers as well as metabolically engineered strains [3, 11, 12].

Is crucial to grow the cell in a low cost medium and the engineered cell should be able to grow and produce the biochemical on the cheapest available raw material (waste-glycerol). The well known *Escherichia coli* could be a strong candidate because it is widely used in biotechnology and the necessary molecular methods are available to carry out genetic and metabolic modifications. The level of succinic acid produced by native strains of *E. coli* in minimal medium is very low [3]. To improve cellular capabilities and the production yield metabolic engineering should be carried out.
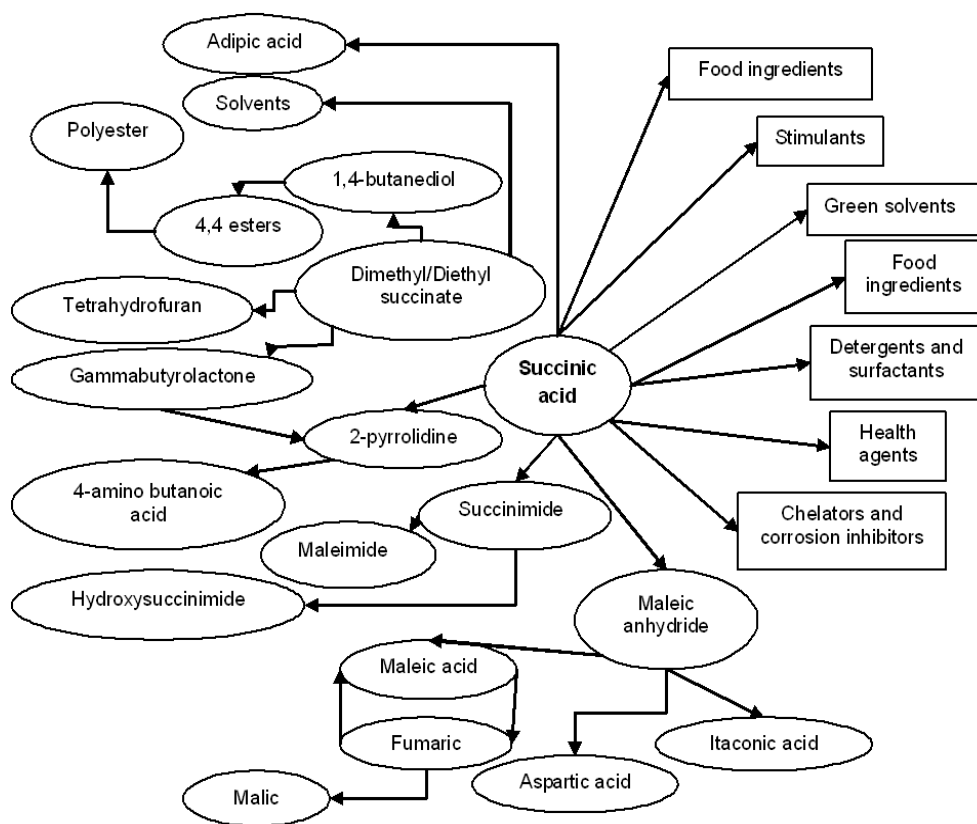

Figure 1. Value-added products that can be derived from succinic acid

Many scientists have described genetic engineering approaches to improve the production in *E. coli* [2,3,13,14] but mediums and applied methods are too complex and complicated. One way could be to block pathways of competing metabolic products such as, formic acid, lactic acid, ethanol and leaving only the succinic acid pathway to achieve redox balance during glycerol utilization [15] in minimal media (M9). Redox balance is not important from glucose, meanwhile it is of central importance in case of glycerol fermentation in *E. coli* [15], will reduce the growth rate or even the biomass production will be inhibited. To overcome these problems different co-substrates need to be used together with glycerol to improve cell viability.

Before *in vivo* tests is mandatory to *in silico* design the new strains, to analyse the behaviour under different genetic and environmental manipulations and to predict the genetic modifications impact on cell metabolism and to the desired flux distribution.

To analyse *in silico* large-scale biological networks, make predictions about cellular behaviours and test the impact or perturbations such as gene deletions, Flux Balance Analysis is an effective tool [16]. The biological models are constructed based on the known stoichiometry of the metabolic reactions, thermodynamic constraints and flux capacities [17]. One of the modelling platforms is COBRA Toolbox [18,19] an open-source and modular platform (widely used in systems biology), incorporating strain optimization tasks, algorithms such as: (FBA), dynamic FBA, phenotypic phase plane analysis, etc.

In this paper we present *in silico* and *in vivo* metabolic engineering studies with the model organism *E. coli* to obtain succinic acid under anaerobic conditions from glycerol. The main aim of the study was the identification of co-substrates necessary to improve the genetically engineered cell viability on glycerol using a complex genome scale metabolic model of *E. coli* [20] and to determine the dynamics of processes. First, we calculated the flux distributions, than we eliminated the three most widely knocked out genes in metabolic engineering (pyruvate formate lyase (*pflB*), lactate dehydrogenase (*ldhA*) and alcohol dehydrogenase (*adhE*)) – from pyruvate metabolism (to improve succinic acid production). The elimination of these genes (pathways) under anaerobic conditions is impossible without co-substrate. We analysed the fitness landscape using dynamic growth simulations, the correlation between genotype and phenotype and phenotypic phase plane analysis was carried out to determine the maximum growth while varying two parameters simultaneously. Wet experiments were carried out, to determine the growth rates and validate the model predictions.

A maximum yield of 0.50 (mol succinic acid mol^{-1} glycerol) can be achieved using glutamic acid or glutamine as co-substrates at an uptake rate of 1 (mM gDW^{-1}h^{-1}) (millimole per gram dry weight of cells per hour) using mutant strain. The change of co-substrate to glucose increased the yield to 0.60 (mol mol^{-1} glycerol).

With complex *in silico* studies we are able to design and genetically engineer industrially important strains, which can be future used in different biotechnological processes to convert renewable feedstocks such as, glycerol from biodiesel industry into a value added biochemical. It is clear that glycerol is a promising abundant carbon source and can improve the economic feasibility of biodiesel industry if will be used biologically, environmental impacts can be reduced and bio-based succinic acid can be obtained without petrochemicals.

RESULTS AND DISCUSSION

The main aim of this study was to redesign *E. coli* strain to create a mutant, being capable to produce succinic acid from renewable resource such glycerol in minimal medium under anaerobic conditions, to understand the succinic acid effect on growth rate and finally to test different co-substrates effect on cellular network. We decided to test co-substrates to enhance the cell viability, such as; aspartic acid, glutamic acid, alanine, glycine, glutamine and glucose (data not shown).

Succinic acid can be produced by *E. coli* under anaerobic conditions but the quantity of the excreted succinic acid is very low. As we know *E. coli* is able to utilize a variety of simple and complex carbohydrate substrate for growth in different environmental conditions.

Under aerobic conditions *E. coli* converts the substrates quantitatively to biomass and CO_2. Changing the environmental conditions (O_2 elimination) reduced biomass formation with 85% on glycerol. In anaerobic conditions the major metabolic by-product was formic acid followed by ethanol and acetic acid (Figure 2).

By-product pathways elimination

Succinic acid production from glycerol involves fixation of CO_2 (greenhouse gas reduction) onto a 3–carbon intermediate, which could be converted to succinic acid. With an uptake rate of 10 mM glycerol the maximal growth rate was 0.56 under aerobic conditions and 0.08 (h^{-1}) under anaerobic conditions (no significant differences were detected with co-substrates).
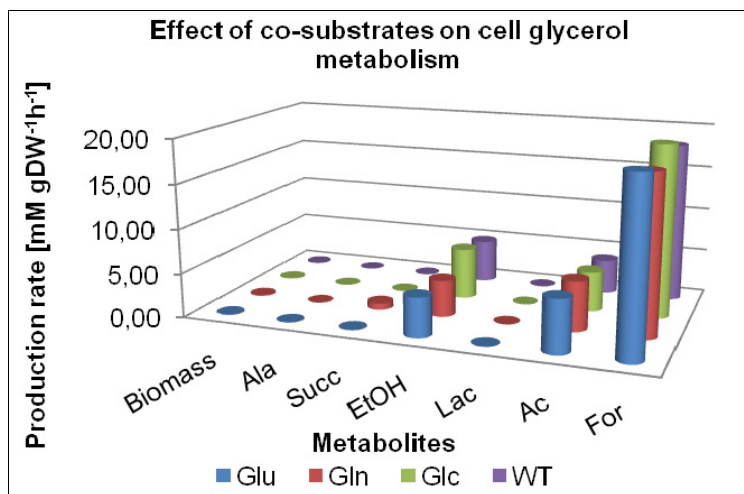
Figure 2. Production rate of different metabolites under anaerobic conditions using glycerol as carbon source and co-substrates; Glu: glutamic acid; Gln: glutamine; Glc: glucose; WT: wild-type without co-substrate; Ala: alanine; Succ: succinic acid; EtOH: ethanol; Lac: lactic acid; Ac: acetic acid; For: formic acid. Fluxes have units of mM gDW^{-1}h^{-1}, except for biomass, which has units of h^{-1}.

To increase the succinic acid production the mentioned genes were eliminated, but the mutant strain failed to grow anaerobically. The explication could be that Acetyl-CoA is an essential metabolite for biosynthesis that is produced primarily by *pflB* during fermentative growth [3]. Three best candidates were detected, two amino acids (glutamic acid, glutamine) and glucose.

As we can observe from (Figure 2) three major fermentation products were predicted in each cases as follows: formic acid, ethanol and acetic acid. It is clear that the elimination of formic acid is necessary because large amounts of carbon are lost. With co-substrates was possible to carry out the genetic modifications. The double mutant showed increased ethanol production. The third eliminated gene was the Δ*adhE* gene to block the synthesis of ethanol as by-product. The double mutant failed to produce succinic acid in a higher rate, but the elimination of the ethanol pathway had a positive effect on succinic acid production.

Using glutamic acid and glutamine as co-substrates at an uptake rate of 1 mM gDW^{-1}h^{-1} and with the Δ*pflB, ΔldhA* and Δ*adhE* eliminations we obtained a succinic acid yield of 0.5 (mol mol^{-1} glycerol). On the other hand, using glucose as co-substrate the triple mutant succinic acid yield increased to 0.6 (mol mol^{-1} glycerol) with 1 mM gDW^{-1}h^{-1} glucose uptake rates, however the cell growth rate was drastically reduced (0.001 h^{-1}) (Fig. 3).
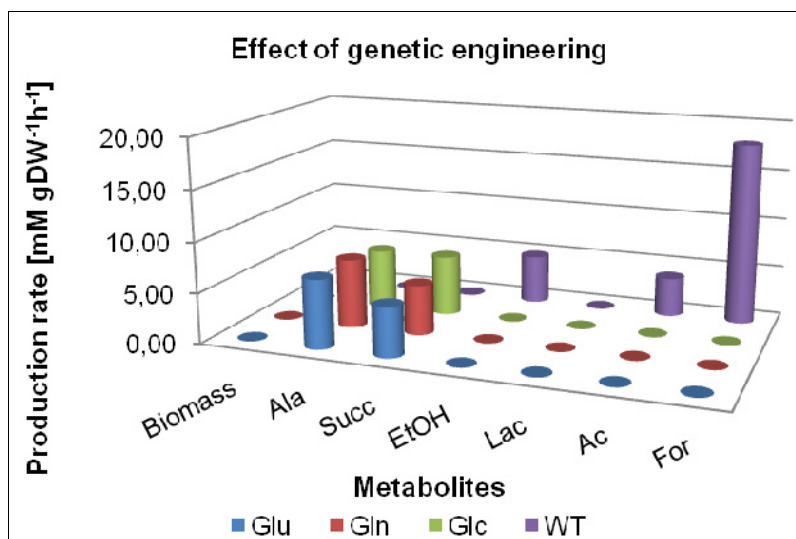
Figure 3. Production rate of different metabolites under anaerobic conditions using glycerol as carbon source and co-substrates after metabolic engineering

In each simulation the biomass production is negatively affected by the succinic acid production. Eliminating the pathways of the metabolites like formic acid, lactic acid and ethanol is considered as an ideal strategy to improve succinic acid yield from glycerol. In each case the production rate of alanine increased significantly compared to wild-type and the acetic acid production was inhibited.

Dynamic FBA of diauxic growth

Although classical static FBA is unable to predict the dynamics of metabolic processes, as the network analysis is based on steady-state solutions, time-dependent processes can be taken into account by extending the classical static FBA to a dynamic FBA (dFBA), as proposed by Schellenberger *et al*. 2011. The dFBA approaches were used to simulate batch growth of wild type and triple mutant (Δ*pflB,* Δ*ldhA,* Δ*adhE*) *E. coli* on glycerol using anaerobic conditions.

Dynamic FBA was performed to simulate batch growth in glycerol minimal media conditions with glycerol as the input and biomass, acetic acid, formic acid, ethanol, lactic acid and succinic acid as the outputs (Figure 4).

The growth rate of mutant strains is extremely low even with co-substrate under anaerobic conditions (Figure 4) without diauxic growth.
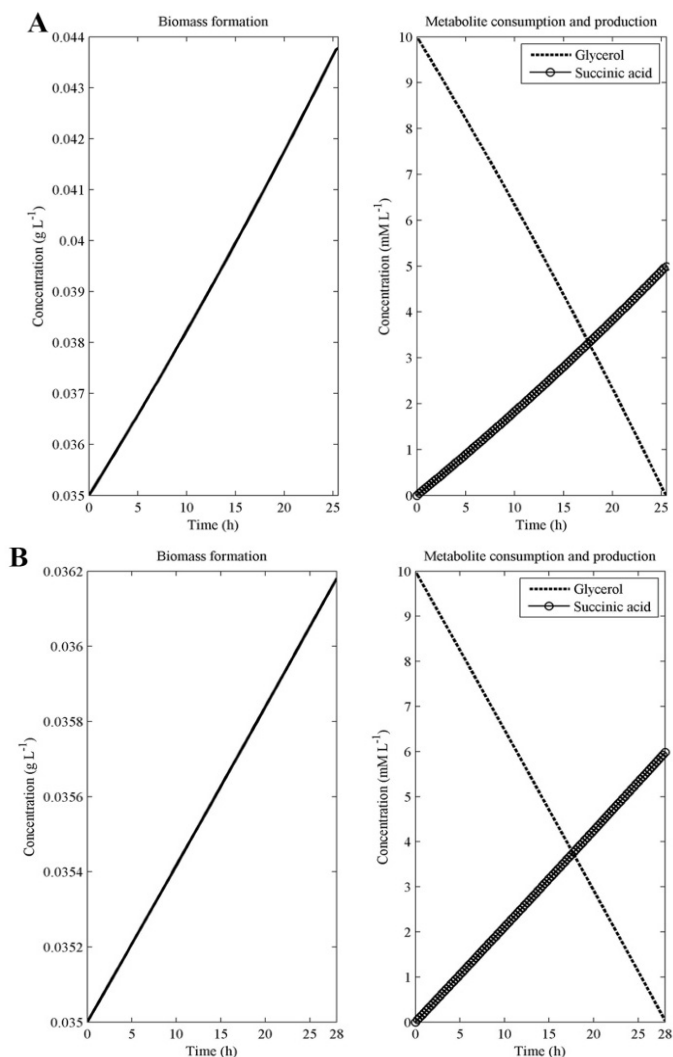
Figure 4. Model predictions using dynamic FBA for the outcomes of mutant strains; Gln (A) and Glc (B)

Phenotypic phase plane analysis (PhPP)

To analyse the optimal utilization of the wild-type and mutant *E. coli* metabolic genotype, phenotypic phase plane analysis was carried out for cellular growth *in silico* on glycerol substrate. We mapped the theoretical optimal metabolic characteristics for biomass production as a function of the environmental variables such as glutamine, glutamic acid and glucose as co-substrates and glycerol together with growth rates (Fig. 5).
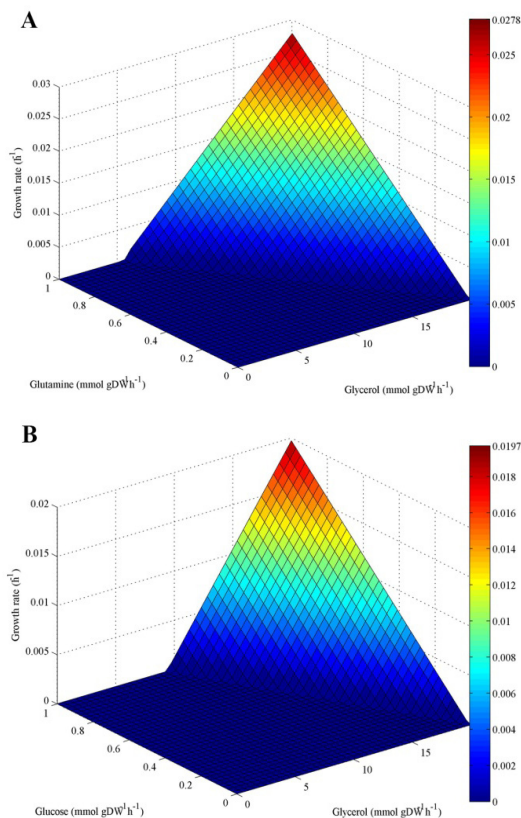
40

Figure 5. Phenotypic phase planes for growth of mutant strains: Gln (A) Glc (B)

It is clear from these plots that each surface has distinct regions, meaning qualitatively distinct phenotypes. The identified phenotypic phase planes are: 5 distinct regions for wild-type (not presented) and 2 for mutant strains with co-substrates (results are for glutamine and glucose co-substrates- there are no differences between glutamine and glutamic acid). Phase 1 (base plane) is characterized by 0 growths. By blocking important reactions in the NADH oxidation pathways the redox potential was significantly affected, led a different optimal metabolic phenotype.

Time-course fermentation experiments were carried out for wild-type and mutant strains (Δ*pflB,* Δ*ldhA,* Δ*adhE*) to follow the changes of metabolites.

Metabolites were identified using GC-MS. Data analysis was carried out with MassLab via comparison with mass spectra obtained from different libraries. The GC chromatograms of the silylated metabolites from the fermentation mixtures are presented in Figure 6.
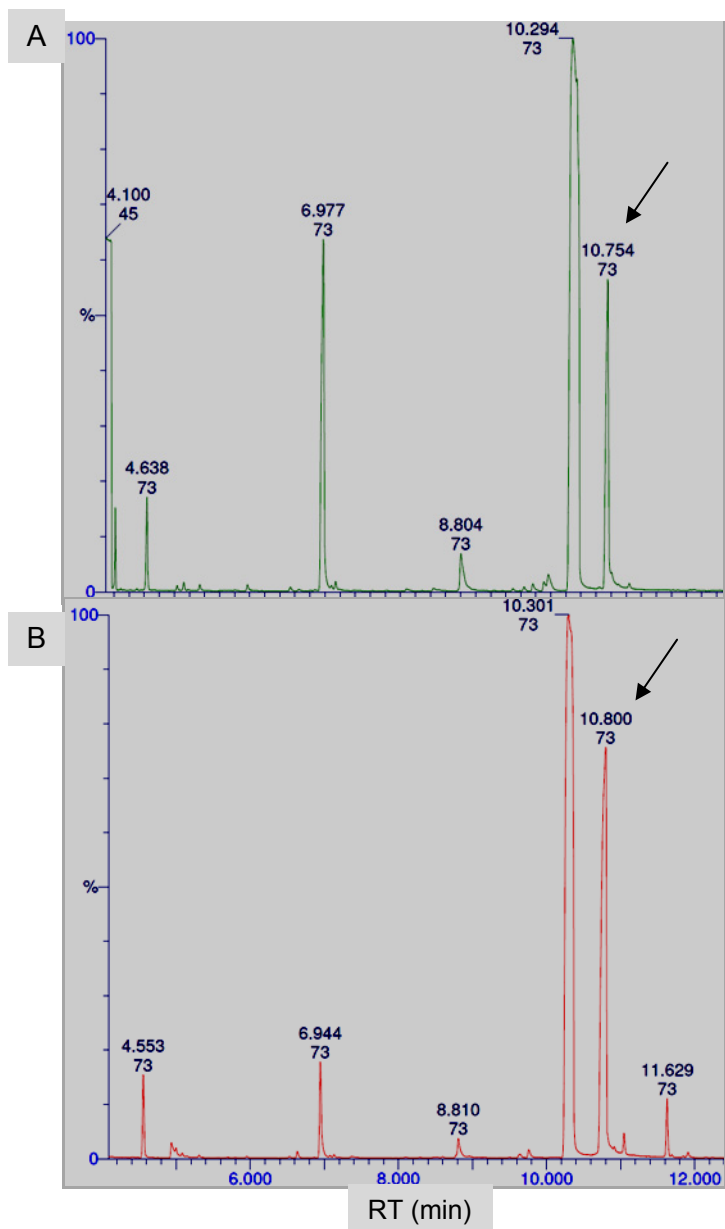
Figure 6. GC-MS analysis of determination of succinic acid from supernatants; wild-type (A), mutant with glucose as co-substrate (B); succinic acid peak was observed at 10' 71". Arrows indicates succinic acid peak.

The heights of the peak indicate the relative concentrations of the metabolites present in the fermentation mixtures. There was a good agreement between simulations and experiments taking into account the growth rates and succinic acid production rates.

CONCLUSIONS

In the long term demands for sustainable development and volatile petroleum prices should favour the use of greener chemicals even if their market price is not cheaper or sometimes even not competitive with the current processes. Increasing awareness of environmental issues and pressures from different public agencies to reduce the pollutions caused by petrochemical industry has led to the development of biomass conversion processes.

On the other hand, the microbiological conversion of by-products (wastes) generated by these methods seems to be the future direction. Important results were obtained in laboratory scale using yeasts and bacteria, especially with efficient selection and construction of recombinant strains based on biochemical and genomic data associated with optimization of fermentation conditions. Most widely considered is the well known *E. coli* with genetically engineered routes.

Biofuels role is critical in reducing green house gas (GHG) emissions and in the transition of the current petroleum-based society towards a more sustainable one. The biodiesel production cost is quite high, hence, the by-product conversion into value-added chemicals with fermentation will improve the net energy, sustainability and profitability of the biodiesel industry. Glycerol may be used as a starting material for large-scale biotechnological processes because it is a good energy and carbon source. Using specific conditions and co-substrates under anaerobic conditions it may be suitable for the biotechnological production of a number of chemicals in fermentative processes. Of course the success depends on strain and condition optimization to achieve the best results. *In silico* analysis are valuable tools to carry out cellular behaviour studies, design industrially important strains by genetic engineering and make predictions. We believe that in the near future the biorefinery concept will gain more attention and will be applied to large-scale processes.

We used the FBA method to investigate the network and global metabolic capability of *Escherichia coli* K12 MG1655. The flux distribution was

estimated under different environmental conditions and genetic modifications. Genome scale models are widely used to reconstruct metabolic networks, to obtain strains with increased capabilities, to produce important products like lycopene, succinic acid, lactic acid, etc. Bio-based succinic acid production has many advantages: raw material cost, increasing market size potential and carbon dioxide fixation.

The production of succinic acid from glycerol offers a green alternative. *E. coli* K12 strain MG1655 can ferment glycerol under anaerobic condition, but the elimination of pathways required a co-substrate to keep the cell viably. Three best candidates were found: glutamine, glutamic acid and glucose. With these genetic modifications the succinic acid yield was ~130 fold higher than in wild-type.

It is clear from these results that the perturbation of redox balance via the deletion of alternative, peripherial redox reactions can drastically affect the central mixed-acid fermentation. The current work demonstrated that the use of minimal medium and the disruption of three genes with co-substrates was sufficient to induce the overproduction of succinic acid from glycerol under anaerobic conditions.

Dynamic FBA was used to simulate batch growth in minimal media conditions to test the effect of co-substrates. Dynamic growth simulations and phenotype phase planes provides a deeper understanding of differences of the metabolic flux distributions between wild-type and genetically engineered strains, especially between genotype and phenotype. We can conclude that the role of co-substrates is crucial, but minimal changes were between them.

Growth rates were consistent during the experimentally measurements, the cultures (on glycerol- wild-type and mutant) were in the different regions on the phase planes; a few primary phenotypes were identified. Strikingly different phenotypes were found for mutant strains 2 PhPP compared to 4 in case of wild-type.

The λ-Red recombineering technology was successfully used for chromosomal modifications in *E. coli*.

The GC-MS was suitable for the identification and quantification of succinic acid.

The *in silico* strains design presented here may serve as important contributions to the implementation of biorefineries. The utilization of crude glycerol from biodiesel industry will improve the economic feasibility and a higher-value chemical (succinic acid) will be obtained reducing dependency on petrochemicals and the same time fixing CO_2 a well known green house gas.

EXPERIMENTAL SECTION

The reconstructed metabolic model of *E. coli* K12 MG1655 iJO1366 [20] was utilized as a basic model throughout the work described herein. The model is the most complex available functionally tested and verified against experimental data to predict correctly the growth rates, metabolites excretion rates and growth phenotypes under different substrate and genetic conditions [21]. The metabolic model is available in SBML format at BioModels online database [http://www.ebi.ac.uk/biomodels-main/]. The model contains 1366 genes, 2251 metabolic reactions and 1136 unique metabolites.

Flux balance analysis (FBA) for wild-type and mutant strains

The most popular constraint-based optimization approach is Flux Balance Analysis (FBA) a direct application of linear programming to biological systems. It was used for computing optimal phenotypes with the objective function of biomass production, using stoichiometric coefficients for each reaction, reversibility and fluxes constraints [22]. The objective function was the rate of biomass synthesis, as follows:

$$\text{Max: } v_{growth} = c^T * v, \tag{1}$$

where *c* denotes the vector defining the weights for each of the fluxes in *v*.

For mathematical representation of the stoichiometric matrix, *S*, is used (each column represents a reaction and each row a metabolite, the numerical elements are the stoichiometric coefficients). Steady-state metabolite flux assumption was performed for FBA calculations described in detail previously [23]. The lower and upper bounds of the fluxes (constraint addition):

- constraints $vl \leq v \leq vu$; *vl* and *vu* are vectors with *n* elements each, which represent the lower and upper bounds on the fluxes, respectively, the constraints for reaction irreversibility or substrate uptake from the environment. In this case the stoichiometric coefficients alone are sufficient for the mathematical maximization of a specific objective function [24].

All computations were performed in MATLAB (mathworks Inc.; Natick, MA, USA) using COBRA Toolbox (version 2.0.5, http://opencobra.sourceforge.net/openCOBRA/Welcome.html) (Becker et al., 2007) software packages with Gurobi optimization solver (Gurobi Optimizer version 5.1.0 Houston, Texas).

Computations

Simulations were carried out using minimal media (M9) containing only inorganic salts and for carbon source we used glycerol. As it is based on constraint based modelling at least one of the reactions must have an experimentally measured value (e.g. substrate uptake rate). One important differences between modelling and analyses of biological systems compared to methods used in physiochemical sciences is that in the former case the network is not stable and may have different states and solutions to reach the optimal value [25]. Consumption rate (substrate uptake rate) in each simulation was set to 10 mM gDW^{-1}h^{-1}- (millimoles dry cell weight per hour). The values are close to that observed experimentally for anaerobic growth in minimal media. To create anaerobic conditions the oxygen uptake rate was set to 0 mM gDW^{-1}h^{-1}.

Three reactions/pathways were eliminated by setting the upper and lower bounds to zero to analyse the cell behaviour. The eliminated reactions were: Δ*pflB*, Δ*ldhA* and Δ*adhE* (Figure 7).
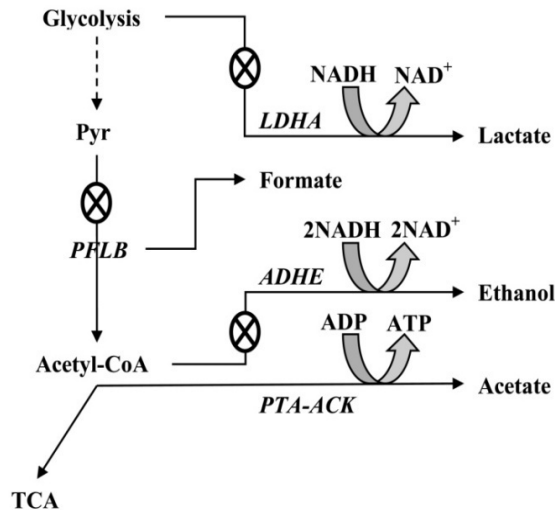

Figure 7. The genetic modifications carried out, crosses represent the reaction knockouts; the following pathways were eliminated: pyruvate formate lyase- Δ*pflB* (formate), lactate dehydrogenase-Δ*ldhA* (lactate), alcohol dehydrogenase-Δ*adhE* (ethanol); Abbreviations: Pyr, Pyruvate; *PFLB, Pyruvate formate lyase; Acetyl-CoA, Acetyl coenzyme A; TCA, Tricarboxylic acid cycle; LDHA, Lactate dehydrogenase; NADH*, nicotinamide adenine dinucleotide; *ADHE*, alcohol dehydrogenase; *ADP*, adenozin difosfat; *ATP*, adenozin trifosfat; *PTA-ACK*, phosphotransacetylase-acetate kinase.

Using the conditions mentioned before the *pflB* mutant failed to grow under anaerobic conditions. Different co-substrates were tested to improve the cell viability including glucose and amino acids.

Combining FBA with an iterative approach based on a quasi-steady-state assumption we are able to analyse dynamic processes e.g. growth rates, metabolites production and consumption rates [18]. The initial substrate concentration was set to 10 mM L^{-1} and the co-substrate uptake to 1 mM $gDW^{-1}h^{-1}$, while the initial biomass concentration was set to 0.035 g L^{-1} (~0.1 optical density (OD)). In order to observe if this diauxic growth is present or not time step was set at a higher value to 25 min and the maximum number of steps to 150 to allow the consumption of metabolites.

Phenotypic phase plane analysis (PhPP) was performed for wild type and mutant strains to identify the robustness of the system under different conditions if two parameters are varied simultaneously. Detailed description of this method can be found elsewhere [16].

Bacterial strain, culture conditions

The strain used in this study was *Escherichia coli* K12 MG1655 from "Deutsche Sammlung von Mikroorganismen und Zellkulturen GmbH" (DSMZ 18039). Fermentation was done at 37°C, in minimal medium under anaerobic conditions with glycerol at a concentration of 0.2% (v/v). Components of M9 medium per liter: Na_2HPO_4*$7H_2O$ (12.8 g), KH_2PO_4 (3 g), NaCl (0.5 g), NH_4Cl (1 g), micronutrients final concentration: $MgSO_4$ (1 mM), $CaCl_2$ (100 µM), $(NH_4)6Mo_7O_{24}$*$4H_2O$ ($3*10^{-9}$ M), H_3BO_3 ($4*10^{-7}$ M), $CoCl_2$*$6H_2O$ ($3*10^{-8}$ M), $CuSO_4$*$5H_2O$ ($1*10^{-8}$ M), $MnSO_4$ ($8*10^{-8}$ M), $ZnCl_2$ ($1*10^{-8}$ M), $FeSO_4$-$7H_2O$ ($1*10^{-6}$ M). Bacterial cells were grown in minimal medium in 5 mL to produce a starter culture and the seed culture was used to inoculate the fermentation medium (OD=0.1). Cells were grown with shaking at 150 rpm (Certomat BS-1 Sartorius) for 24 h in serum bottles (50 mL) with 20 mL M9 medium. Samples were taken in every two hours for the analysis of cell growth. The optical density of the cell cultures was measured at 550 nm (OD_{550}) to quantify cell growth, using a Cary 50 Conc UV-Visible spectrophotometer, as well as dry cell weight determination. To estimate the cell mass we used the following simple assumption (1 OD_{550}=0.36 gDW L^{-1}). 1 mL of the culture supernatant was added in triplicate to pre-weighed Eppendorf tubes, centrifuged, washed with NaCl (0.9%) and dried until constant mass at 105°C.

Chromosomal gene deletion

For gene deletion strategy we used the λ-Red recombineering methods previously described [26]. Plasmids (5 Strain Wanner Lambda Red Gene Disruption Kit) were obtained from the *E. coli* Genetic Stock Center (Yale University).

Analytical procedure

Metabolites were analysed by *Gas chromatography coupled to mass spectrometry (GC-MS)* (6890N/5975 Agilent) based on solid-phase microextraction (SPME) with on-fiber silylation. Silylation was carried out using N, O bis (trimethylsilyl) trifluoroacetamide (BSTFA), following the procedures described elsewhere [27]. The relative % amount of succinnic acid was calculated by comparing its average peak area to the total areas, for chromatograms and spectra analyses we used the MassLab software (ThermoQuest, Manchester, UK). The identification of compounds were identified by comparing the mass spectra obtained with commercially available MS libraries (Wiley, NIST and LIBTX).

ACKNOWLEDGMENTS

REFERENCES

[1].C. Li, K.L. Lesnik, H. Liu, H, *Energies*, **2013**, *6*, 4739.

[2].M.D. Blankschien, J.M. Clomburg, R. Gonzalez**,** *Metabolic Engineering*, **2010**, *12*, 409.

[3]. X. Zhang, K.T. Shanmugam, L.O. Ingram, *Applied and Environmental Microbiology*, **2010**, *76*, 2397.

[4]. X. Fan, R. Burton, Y. Zhou, *The Open Fuels & Energy Science Journal*, **2010**, *3*, 17.

[5]. G. Paulo da Silva, M. Mack, J. Contiero, *Biotechnology Advances*, **2009**, *27*, 30.

[6]. W. Yan, S.K. Hoekman, *Journal of Environmental Protection*, **2012**, *3*, 218.

[7]. H. Yim, R. Haselbeck, W. Niu, C. Pujol-Baxley, A. Burgard, J. Boldt, J. Khandurina, J.D. Trawick, R.E. Osterhout, R. Stephen, J. Estadilla, S. Teisan, H.B. Schreyer, S. Andrae, T.H. Yang, S.Y. Lee, M.J. Burk, S. Van Dien, *Nature Chemical Biology*, **2011**, *7*, 445.

[8]. E. Takiyama, E. Fujimaki, I. Niikura, Y. Hatano, "*Method for producing saturated polyester", US Patent 5*, **1994**, 306, 787.

[9]. G.J. Zeikus, K.M. Jain, P. Elankovan, *Applied Microbiology and Biotechnology*, **1999**, *5*, 545.

[10]. T. Werpy, G. Peterson, *"Top value added chemicals from biomass",* U.S. Department of Energy, Washington DC, **2004**.

[11]. F.V. Wendisch, N.S. Lindner, M.T. Meiswinkel, "*Biodiesel- Quality, Emissions and By-Products",* Dr. Gisela Montero (Ed.), ISBN: 978-953-307- 784-0, InTech, Available from: http://www.intechopen.com/books/biodiesel-quality-emissions-and-byproducts/ use-of-glycerol-in-biotechnological-applications, **2011**.

[12]. S.J. Lee, H. Song, S.Y. Lee, *Applied and Environmental Microbiology*, **2006**, *72*, 1939.

[13]. L. Liang, R. Liu, J. Ma, K. Chen, M. Jiang, P. Wei, *Biotechnology Letters*, **2011**, *33*, 2439.

[14]. W. Wang, Z. Li, J. Xie, Q. Ye, *Bioprocess and Biosystems Engineering*, **2009**, *32*, 737.

[15]. J. Wang, J. Zhu, G.N. Bennett, K.Y. San, *Metabolic Engineering*, **2011**, *13*, 328.

[16]. J.D. Orth, I. Thiele, B. Ø. Palsson, *Nature Biotechnology*, **2010**, *28*, 245.

[17]. P. Vilaça, I. Rocha, M. Rocha, *Biosystems*, **2011**, *103*, 435.

[18]. S.A. Becker, A.M. Feist, M.L. Mo, G. Hannum, B. Ø. Palsson, M. J. Herrgard, *Nature Protocols*, **2007**, *2*, 727.

[19]. J. Schellenberger, R. Que, R.M. Fleming, I. Thiele, J.D. Orth, A.M. Feist, D.C. Zielinski, A. Bordbar, N.E. Lewis, S. Rahmanian, J. Kang, D.R. Hyduke, B.O. Palsson, *Nature Protocols*, **2011**, *4*, 1290.

[20]. J.D. Orth, T.M. Conrad, J. Na, J.A. Lerman, H. Nam, A.M. Feist, B.Ø. Palsson, *Molecular Systems Biology*, **2011**, *7*, 535.

[21]. H.J. Kim, B.K. Hou, S.G. Lee, J.S. Kim, D.W. Lee, S.J. Lee, *Metabolic Engineering*, **2013**, *18*, 44.

[22]. F. Llaneras, J. Picó, *Journal of Bioscience and Bioengineering*, **2008**, *105*, 1.

[23]. N.D. Price, J.L. Reed, B.Ø. Palsson, *Nature Reviews Microbiology*, **2004**, *2*, 886.

[24]. K. Raman, N. Chandra, *Briefings in Bioinformatics*, **2009**, *10*, 435.

[25]. B.Ø. Palsson, "*Systems biology properties of reconstructed networks",* Cambridge university press, Cambridge, New York, **2005**.

[26]. K.A. Datsenko, B.L. Wanner, *Proceedings of the National Academy of Sciences*, **2000**, *97*, 6640.

[27]. T.G. Luan, K.S. Yu, Y. Zhong, H.W. Zhou, C.Y. Lan, N.F. Tam, *Chemosphere*, **2006**, *65*, 2289.

EFFECTS OF ALUMINOSILICATES ON LIPID PEROXIDATION AND ANTIOXIDANTS IN AFLATOXIN B$_1$-INDUCED TISSUE INJURY IN CHICKENS

DEJAN PRVULOVIĆ[a*], MILAN POPOVIĆ[a], DANIJELA KOJIĆ[b], GORDANA GRUBOR-LAJŠIĆ[b]

ABSTRACT. Aflatoxins in poultry cause biochemical changes in major organs, which can assist in the diagnosis of toxication. Producers and researchers have attempted to develop an effective decontamination technology to deal with this feed-borne toxin. Aluminosilicates(clays and zeolites) were preferred because of their high binding capacitiyforaflatoxins and their reducing effect on aflatoxin-absorption from the gastrointestinal tract. The purpose of the present study was to evaluate the toxic effects of aflatoxin B$_1$ (AFB$_1$) by biochemical examination of liver, kidney, spleen, erithrocytes, and pancreas of broiler chickens, and to determine the possible preventive role of ATN-dietary aluminosilicates (mixture of clinoptilolite and bentonite) on the investigated values. In total, 84 broiler chicks were divided into two treatment groups: control-basal diet and basal diet plus 5 g aluminosilicate/kg diet. After 21 days, twelve hours prior to sacrifice, 21 chicks from each group received one dose of AFB$_1$ orally. Lipid peroxidation was significantly increased in the liver and kidney suggesting oxidative stress in these organs. Supplementation withATN decreased these negative effects. No effects due to AFB$_1$ were observed in enzyme activity and lipid peroxidation inthe pancreas, spleen or red blood cells. This data suggest that a single dose of AFB$_1$ could provide a toxin alleviating effect on biochemical indices of liver and kidney in broiler chicken. Therefore, ATN protects broiler chickens against the harmful effects of AFB$_1$.

Keywords: aflatoxin B$_1$, antioxidative enzymes, clay, kidney, liver, zeolite

---

[a] *University of Novi Sad, Faculty of Agriculture, TrgDositejaObradovića, Nr. 8, 21000 Novi Sad, Serbia. * Corresponding author: dejanp@polj.uns.ac.rs*
[b] *University of Novi Sad, Faculty of Science, TrgDositejaObradovića, Nr. 3, 21000 Novi Sad, Serbia*

DEJAN PRVULOVIĆ, MILAN POPOVIĆ, DANIJELA KOJIĆ, GORDANA GRUBOR-LAJŠIĆ

INTRODUCTION

Mycotoxins are secondary metabolites produced by fungi that may be injurious to animals upon ingestion, inhalation, or skin contact. Aflatoxins (AF) are polyketide products (difuranocoumarins) of a number of *Aspergillus* species [1, 2, 3]. They have received greater attention than any other mycotoxins because of their demonstrated potent carcinogenic effects and acute toxicological effects in animals and humans. The biochemical, hematological, immunological and pathological toxic effects of AF have been well described [4, 5, 6, 7, 8]. AF contamination of agricultural products is one of the most important factors determining product quality, and has caused significant financial losses for producing countries [9, 10]. AF are a group of 15-20 closely related compounds. The most common forms in nature are AF B_1, B_2, G_1, and G_2. These abbreviations indicate the colour (blue or green) and relative migration distance, 1 and 2 (higher and lower), of the compounds as seen by thin-layer chromatography under ultraviolet light [1, 8].

Aflatoxin B_1 (AFB$_1$) is considered the most toxic AF. It is metabolized mainly by the liver to AFB$_1$-8, 9-exo-epoxide and 8, 9-endo epoxide. The exo-epoxide binds to DNA to form the predominant 8, 9-dihydro-8-(N_7-guanyl)-9-hydroxy AFB$_1$ (AFB$_1$-N_7-Gua) adduct. Furthermore, AFB$_1$-N_7-Gua may be converted to two secondary forms [3].

Several approaches have been investigated to reduce exposure of animals to AF in contaminated feeds, including: solvent extraction, ammoniation, ozonolysis and other chemical, physical and biological treatments [9, 10, 11, 12]. Binding agents such as activated carbon, clays and zeolites have been added to contaminated feeds in an attempt to reduce or prevent AF exposure in animals. An effective sequestering agent is one that tightly binds the mycotoxin in contaminated feed without disassociating in the gastrointestinal tract of the animal [10, 11, 13, 14].

Clays and zeolites are hydrated and composed mostly of aluminium and silica: belonging to the group of aluminosilicates. Phyllosilicate clays are hydrated, crystalline aluminosilicateswith a layered structure. Montmorillonite, the main constituent of the phyllosilicate ore bentonite, is a trimorphicphyllosilicate formed by 2:1 condensation of layers with aluminium sandwiched between two layers of silica. Montmorillonite possesses exchangeable sodium or calcium cations and has expandable sheets [15]. Natural zeolites are hydrated aluminosilicate minerals characterized by cage-like structures, with high internal and external surface areas, and high cation-

exchange capacities. The basic building blocks of natural zeolites are electrostatically charged tetrahedra of silica and aluminium, with the negative charge balanced by alkaline or alkaline earth cations. The stacking of these tetrahedral gives rise to various three-dimensional honeycomb structures containing tunnels or channels of uniform diameter [16, 17].

The objective of the present study is to explore the possibile use of feed additives based on natural occurring hydrated aluminosilicates (Antitoxic nutrient-ATN) in preventing or minimizing the oxidative stress induced by acute administration of AFB$_1$ in broiler chickens.

RESULTS AND DISCUSSION

The liver is considered to be the main target organ for AF. The hepatotoxic effects of AFB$_1$ have been well-documented in a variety of animal species [18, 19, 20]. AFB$_1$-induced free radical production has been referred to as a possible contributing factorin hepatotoxicity [21, 22, 23, 24, 25]. Table 1 shows the effect of ATN on AFB$_1$-induced LP and antioxidant status in the liver of broiler chickens. The significant increase in LP seen in the AFB$_1$ group was maintained at normal levels by ATN treatment. A significant decrease in the activity of glutathione S-transferase (GST) was observed in the liver of AFB$_1$ treated chickens. Oral intake of AFB$_1$ and ATN alone or in combination did not cause inhibition of the other selected enzyme activities: superoxide dismutase (SOD-1), catalase (CAT), pyrogallol peroxidase (PPx), and guaiacol peroxidase (GPx) in the liver of broiler chickens. ATN alone did not induce any significant changesin the activities of these measured enzymes, and did not induce lipid peroxidation in liver tissue.

Table 1. Effect of aflatoxin B$_1$ (AFB$_1$)exposure alone and in combination with ATN on the activities of endogenous antioxidant enzymes and lipid peroxidation in the liver of broiler chickens

	Experimental group			
	Control	ATN	AFB$_1$	ATN + AFB$_1$
SOD-1 [IU/mg protein]	18.37 ± 0.52[a]	19.41 ± 0.87[a]	18.05 ± 0.55[a]	19.11 ± 0.74[a]
CAT [IU/mg protein]	22.75 ± 0.95[a]	23.87 ± 2.12[a]	22.00 ± 0.80[a]	25.07 ± 0.57[a]
GPx [IU/mg protein]	2.11 ± 0.08[a]	2.09 ± 0.06[a]	1.95 ± 0.06[a]	1.96 ± 0.06[a]

	Experimental group			
	Control	ATN	AFB$_1$	ATN + AFB$_1$
PPx [IU/mg protein]	64.02 ± 2.88[a]	59.21 ± 1.68[a]	57.18 ± 1.87[a]	56.92 ± 2.07[a]
GST [IU/mg protein]	393.14 ± 11.36[a]	378.84 ± 13.21[a]	298.17 ± 7.32[b]	354.68 ± 9.98[a]
Lipid peroxidation [nmol MDA/mg protein]	2.01 ± 0.11[a]	1.94 ± 0.06[a]	2.58 ± 0.05[b]	1.77 ± 0.05[a]

The data are mean values ± standard error

[a, b] values without the same superscript within each row differ significantly (*P*< 0.05)

SOD-1, superoxid dismutase; CAT, catalase; GPx, guaiacol peroxidase; PPx, pyrogallol peroxidase; GST, glutathion S-transferase

LP is one of the main manifestations of oxidative damage initiated by ROS and has been linked with altered membrane structure and enzyme inactivation. It is initiated by the abstraction of a hydrogen atom from the side chain of polyunsaturated fatty acids in the membrane [26]. The present data reveals that AFB$_1$ administration produces a marked oxidative impact as evidenced from the significant increase in LP (Table 1). This increase in lipid peroxides might result from increased production of free radicals and a decrease in antioxidant status. The oxidative stress observed in our study is in agreement with other reports, where it has been implicated in AFB$_1$-induced hepatotoxicity in various animal species: broiler chickens [23, 27], ducklings [28], laying hens [29], mice [22, 25, 30] and rats [20, 21, 24]. In this study, ATN treatment significantly reduced AFB$_1$-induced LP, presumably by its ability to scavenge molecules of AFB$_1$ in the gastrointestinal tract.

GST plays a critical role in the protection of tissues from the deleterious effects of activated AFB$_1$. GST catalyzes the conjugation of AFB$_1$-8, 9-epoxides with glutathione (GSH) to form AFB$_1$-epoxide-GSH conjugates, thereby decreasing intracellular glutathione content [31]. This observation supports our findings, where we observed a significant decline in the activity of GST in AFB$_1$-induced chickens (Table 1). This agrees with other reports on experimental AF in mice[30], and rats [20, 31]. There was no significant difference in liver GST activityin controlsorin animals treated with ATN or ATN along with AFB$_1$. This result indicates that ATN provides full protection

tothe liver of broiler chickens exposed to harmful AFB$_1$ treatment. Our previous study also demonstrates that oral intake of ATN does not provoke inhibition or stimulation of liver GST in broiler chickens[32].

Unlike other authors [20, 21, 25, 30, 31], we did not observe any change in the activity of other measured antioxidative enzymes in the liver following AFB$_1$ intoxication (Table 1). A single dose of AFB$_1$ is not enough to induce a shift in CAT, SOD-1 or peroxidase activities in the liver of broiler chickens.

Table 2 shows the effects of AFB$_1$, ATN, and AFB$_1$ plus ATN on lipid peroxidation and the activities of CAT, SOD-1, PGx, and GPx in the kidney of broiler chickens. No significant alterations between the control and ATN group were observed. The level of lipid peroxidation was significantly higher vs. the control group in AFB$_1$ treated chickens. Oral administration of ATN along with AFB$_1$ ameliorates AFB$_1$-induced lipid peroxidation. Oral administration of AFB$_1$ or ATN did not induce CAT or GPx activity in the kidneys. SOD-1 activity is an indicator of ROS production. In the kidneys of broiler chickens treated with AFB$_1$, SOD-1 and PPx activities were significantly decreased.

Table 2. Effect of aflatoxin B$_1$ (AFB$_1$)exposure alone and in combination with ATN on the activity of endogenous antioxidant enzymes and lipid peroxidation in the kidney of broiler chickens

	Experimental group			
	Control	ATN	AFB$_1$	ATN + AFB$_1$
SOD-1 [IU/mg protein]	10.68 ± 0.42^a	11.10 ± 0.34^a	6.89 ± 0.45^b	9.89 ± 0.31^a
CAT [IU/mg protein]	64.08 ± 4.20^a	62.42 ± 3.21^a	69.25 ± 6.92^a	67.96 ± 6.05^a
GPx [IU/mg protein]	15.10 ± 1.00^a	16.56 ± 1.18^a	7.64 ± 1.66^a	15.10 ± 1.76^a
PPx [IU/mg protein]	49.84 ± 2.15^a	47.22 ± 2.44^a	38.09 ± 2.81^b	37.18 ± 2.02^b
Lipid peroxidation [nmol MDA/mg protein]	2.31 ± 0.10^a	2.58 ± 0.08^a	3.33 ± 0.06^b	2.95 ± 0.16$^{a, b}$
The data are mean values ± standard error [a, b]values without the same superscript within each row differ significantly (*P*< 0.05) SOD-1, superoxide dismutase; CAT, catalase; GPx, guaiacol peroxidase; PPx, pyrogallol peroxidase				

Under oxidative stress, SOD can behave in two different ways: initially and when stress is moderated, cells act by suppressing SOD-1; but if the stress lasts for a long time and favors increased production of ROS, the enzyme is exhausted and its concentration falls. The low activity of SOD could also be due to inactivation of the enzyme by crosslinking or DNA damage [33]. In our case, the decreased SOD-1 activity observed could be explained by the massive production of superoxide anions, which override enzymatic activity and lead to a fall in its concentration in kidneys. These results are in agreement with the results of other authors, in studies mostly performed on rats [20, 21] and mice [22, 25]. ATN successfully restored SOD-1 activity to control levels, but did not restore PPxactivity.

Table 3 shows the activity of measured antioxidant enzymes, hemoglobin (Hb) concentration and MDA levels in the erythrocytes of broiler chickens. Activities of protective antioxidative enzymes and MDA levels in the pancreatic tissue of broiler chickensare presented in Table 4. It was observed that oral intake of ATNand AFB_1alone or in combination did not cause impairment of the selected enzyme activities or the level of lipid peroxidation in the red blood cells and pancreas of broiler chickens. Although chronic exposure of mice to AF could provoke oxidative stress in erythrocytes [24], a single oral dose of AFB_1 does not induce that effect in broiler chickens.

Table 3. Effect of aflatoxin B_1 (AFB_1) exposure alone and in combination with ATN on hemoglobin concentration, activity of endogenous antioxidant enzymes and lipid peroxidation in the erythrocytes of broiler chickens

	Experimental group			
	Control	ATN	AFB_1	ATN + AFB_1
Hb [g/l]	144.95 ± 3.71	145.05 ± 3.24	145.44 ± 4.32	147.23 ± 5.11
SOD-1 [IU/mg Hb]	467.16 ± 13.23	485.57 ± 14.55	470.16 ± 14.22	482.38 ± 11.87
CAT [IU/mg Hb]	8.14 ± 0.53	8.22 ± 0.59	7.31 ± 0.56	7.04 ± 0.62
GPx [IU/mg Hb]	6.47 ± 0.21	6.85 ± 0.19	6.50 ± 0.20	6.82 ± 0.32
PPx [IU/mg Hb]	14.44 ± 0.50	14.96 ± 0.48	14.35 ± 0.43	14.20 ± 0.55
GST [IU/mg Hb]	124.04 ± 2.81	131.08 ± 2.95	116.12 ± 2.71	114.30 ± 2.66

Lipid peroxidation [nmol MDA/mg Hb]	1.17 ± 0.10	1.39 ± 0.06	1.07 ± 0.12	1.29 ± 0.12

The data are mean values ± standard error

There were no statistically significant differences among values within the same row

Hb, hemoglobin; SOD-1, superoxide dismutase; CAT, catalase; GPx, guaiacol peroxidase; PPx, pyrogallol peroxidase; GST, glutathione S-transferase

Table 4. Effect of aflatoxin B$_1$ (AFB$_1$) exposure alone and in combination with ATN on the activity of endogenous antioxidant enzymes and lipid peroxidation in the pancreas of broiler chickens

	Experimental group			
	Control	ATN	AFB$_1$	ATN + AFB$_1$
SOD-1 [IU/mg protein]	4.14 ± 0.13	4.25 ± 0.21	4.02 ± 0.09	4.26 ± 0.10
CAT [IU/mg protein]	7.67 ± 0.45	7.40 ± 0.34	8.71 ± 0.34	7.80 ± 0.32
GPx [IU/mg protein]	0.35 ± 0.02	0.39 ± 0.03	0.36 ± 0.01	0.36 ± 0.01
PPx [IU/mg protein]	2.51 ± 0.22	2.15 ± 0.14	2.13 ± 0.27	2.46 ± 0.15
Lipid peroxidation [nmol MDA/mg protein]	3.21 ± 0.35	2, 96 ± 0.08	2.88 ± 0.11	2.78 ± 0.11

The data are mean values ± standard error

There were no statistically significant differences among values within the same row

SOD-1, superoxide dismutase; CAT, catalase; GPx, guaiacol peroxidase; PPx, pyrogallol peroxidase

The activities of enzymatic antioxidants, such as SOD-1, CAT, GPx, and PPx, and levels of lipid peroxidation in the spleen are presented in Table 5. The spleen is the principal peripheral lymphoid organ and plays an important role in protective immune reactions. It is involved in humoral and cellular immune responses through its role in the generation, maturation and storage of lymphocytes. Dietary intake of AF can increase apoptotic percentages of splenocytes, which may relate to DNA damage and

mitochondrial lesions caused by increased oxidative stress [25, 34, 35, 36]. We found that a single oral dose of AFB_1 is not capable of disturbing the normal activity of SOD-1 and peroxidases or inducing oxidative stress in the spleen.

Table 5. Effect of aflatoxin B_1 (AFB_1)exposure alone and in combination with ATN on the activity of endogenous antioxidant enzymes and lipid peroxidation in the spleen of broiler chickens

	Experimental group			
	Control	ATN	AFB_1	ATN + AFB_1
SOD-1 [IU/mg protein]	3.82 ± 0.14[a]	3.71 ± 0.19[a]	3.85 ± 0.15[a]	4.00 ± 0.15[a]
CAT [IU/mg protein]	5.63 ± 0.15[a]	5.14 ± 0.14[a]	6.85 ± 0.21[b]	6.52 ± 0.31[a, b]
GPx [IU/mg protein]	0.58 ± 0.03[a]	0.62 ± 0.03[a]	0.59 ± 0.03[a]	0.61 ± 0.02[a]
PPx [IU/mg protein]	16.23 ± 1.05[a]	14.36 ± 0.71[a]	14.75 ± 0.97[a]	16.39 ± 2.35[a]
Lipid peroxidation [nmol MDA/mg protein]	2.62 ± 0.06[a]	2.61 ± 0.08[a]	2.75 ± 0.12[a]	2.31 ± 0.15[a]
The data are mean values ± standard error SOD-1, superoxide dismutase; CAT, catalase; GPx, guaiacol peroxidase; PPx, pyrogallol peroxidase				

CONCLUSIONS

In conclusion, co-administration of naturally occurring aluminosilicates (ATN) offers significant protection against AFB_1-induced oxidative stress in the liver and kidney tissue of broiler chickens. A single dose of AFB_1 did not induce any adverse effectsin the pancreas, spleen or erythrocytes. ATN has the ability to absorb AFB_1 in the lumen of the digestive tract, and thus could be used as a supplementary agent in animal feeds.

EXPERIMENTAL SECTION

Chickens and diet

Eighty-four 1-day-old, unvaccinated broiler chicks of both sexes were obtained from a commercial hatchery. Individually weighed chicks were divided at random into four groups. There were seven replicates of three broiler chicks for each dietary treatment. The chicks were housed in electrically heated batteries under fluorescent lighting and received a commercial basal diet (maize and soybean meal diet 220 g protein, 13.00 MJ ME kg^{-1}) formulated to contain National research Council (1994) requirements. Food and water were available *ad libitum* and lighting was continuous.

Experimental design

The experimental design consisted of two dietary treatments: 1. Control: basal diet; 2. ATN: basal diet plus 5.0 g ATN kg^{-1} diet. ATN (Antitoxic nutrient) is a fine powder containing mostly zeolitic ore (with > 90% of clinoptilolite) and bentonite (with > 83% of montmorillonite), together with small amounts of activated charcoal (ratio 60:20:1/zeolite:bentonite:charcoal). After 21 days, twelve hours prior to sacrifice, 21 broiler chickens from each group received one dose of AFB$_1$ from *Aspergillusflavus*(Sigma, Germany)orally (AFB$_1$ and AFB$_1$ + ATN groups).AFB$_1$ was dissolved in distilled waterand every chicken received 1 mg of AFB$_1$/kg body weight.

Blood sampling and slaughter

Twelve hours after intoxication, the feeding trial was terminated and all broiler chickens were bled by cardiac puncture. Heparin was used as an anticoagulant and non-coagulated blood was used for separation of erythrocytes. Hemoglobin (Hb) concentration in red blood cells was determined by the cyanomethemoglobin procedure [37]. All 84 broiler chickens were sacrificed by cervical dislocation and liver, kidney, spleen, and pancreas were removed. Homogenates of these organs with phosphate buffer (pH=7.0) were used for further biochemical analysis.

Biochemical analysis

Activity of antioxidant enzymes: superoxide dismutase (SOD-1), catalase (CAT), guaiacol peroxidase (GPx), pyrogallol peroxidase (PPx), and lipid peroxidation were measured in erythrocytes, liver, kidney, spleen and pancreas. Glutathione S-transferase (GST) activity was evaluated in erythrocytes and liver homogenates. Protein content in homogenates of liver, spleen, and pancreas were determined according to the method of Bradford

[38], using bovine serum albumin as a protein standard. SOD-1 activity was determined in samples according to McCord and Fridovich[39]. The CAT activity was assayed by the method of Clairborne[40]. Utilization of hydrogen peroxide by CAT in the samples was measured spectrophotometrically as the decrease in optical density at 240 nm. GPx activity was measured by following the H_2O_2 dependent oxidation of guaiacol at 470 nm Agrawal and Laloraya[41]. The activity of PPx was measured using pyrogallol as the substrate according to Chance and Maehly[42]. The formation of purpurogallin was followed at 430 nm. GST activity in samples was evaluated using 1-chloro-2, 4-dinitrobenzene (CDNB) as the substrate as previously described by Habig*et al.* [43]. The formation of the adduct of GSH-CDNB (2, 4-dinitrophenyl glutathione) was monitored by measuring the increase in absorbance at 340 nm against a blank with a spectrophotometer. MDA levels were analyzed with 2-thiobarbituric acid, monitoring the change in absorbance at 532 nm with a spectrophotometer [44].

Statistical analysis

Results are expressed as the mean of determinations of 3 independent samples made in triplicates. Statistical significance was tested by analysis of variance followed by comparison by Duncan's multiple range test ($P< 0.05$) calculated using STATISTICA for Windows version 9.0 (StatSoft, Tulsa, OK, USA).

ACKNOWLEDGEMENTS

REFERENCES

[1]. M.A. Klich, *Mycoscience*, **2007**, *48*, 71.
[2]. D.R. Georgianna, G.A. Payne, *Fungal Genetics and Biology*, **2009**, *46*, 113.
[3]. S. Marin, A.J. Ramos, G. Cano-Sancho, V. Sanchis, *Food and Chemical* Toxicology, **2013**, *60*, 218.

[4]. H. Oğuz, F. Kurtoğlu, V. Kurtoğlu, Y.O. Birdane, *Research in Veterinary Science*, **2002**, *73*, 101.

[5]. G. Eraslan, D. Eşsiz, M. Akdoğan, F. Şahindokuyucu, L. Altintaş, *Turkish Journal of Veterinary and Animal Sciences*, **2005**, *29*, 601.

[6]. G. Eraslan, M. Akdoğan, B.C. Liman, M. Kanbur, N. Delibaş, *Turkish Journal of Veterinary and Animal Sciences*, **2006**, *30*, 41.

[7]. M. Denli, F. Okan, *South African Journal of Animal Science*, **2006**, *36*, 222.

[8]. S. Rawal, J.E. Kim, R. Coulombe Jr., *Research in Veterinary Science*, **2010**, *89*, 325.

[9]. M. Arab Abousadi, E. Rowghani, M. EbrahimiHonarmand, *Iranian Journal of Veterinary Research*, **2007**, *8*, 144.

[10]. H. Oguz, *Eurasian Journal of Veterinary Sciences*, **2011**, *27*, 1.

[11]. D.E. Diaz, W.M. Hagler Jr., B.A. Hopkins, L.W. Whitlow, *Mycopathologia*, **2002**, *156*, 223.

[12]. E. Diao, H. Hou, H. Dong, *Trends in Food Science and Technology*, **2013**, *33*, 21.

[13]. T.S. Edrington, A.B. Sarr, L.F. Kubena, R.B. Harvey, T.D. Phillips, *Toxicology Letters*, **1996**, *89*, 115.

[14]. T.D. Phillips, *Toxicological Sciences*, **1999**, *52*, 118.

[15]. E.M. Serwicka, K. Bahranovski, *Catalysis Today*, **2004**, *90*, 85.

[16]. J. Lemić, S. Milošević, M. Vukašinović, A. Radosavljević-Mihajlović, D. Kovačević, *Journal of Serbian Chemical Society*, **2006**, *71*, 1161.

[17]. S. Matijašević, A. Daković, M. Tomašević-Čanović, M. Stojanović, D. Ileš, *Journal of Serbian Chemical Society*, **2006**, *71*, 1323.

[18]. M. Ortatatli, H. Oğuz, *Research in Veterinary Science*, **2001**, *71*, 59.

[19]. C.A. Bailey, G.W. Latimer, A.C. Barr, W.L. Wigle, A.U. Haq, J.E. Balthrop, L.F. Kubena, *Journal of Applied Poultry Research*, **2006**, *15*, 198.

[20]. G. Devendran, U. Balasubramanian, *Asian Journal of Plant Science and Research*, **2011**, *1*, 61.

[21]. M.A. Abdel-Wahhab, S.E. Aly, *Journal of Agricultural and Food Chemistry*, **2003**, *51*, 2409.

[22]. R.J. Verma, N. Mathuria, *ActaPoloniaePharmaceutica-Drug Research*, **2008**, *65*, 195.

[23]. N.K.S. Gowda, D.R. Ledoux, G.E. Rottinghaus, A.J. Bermudez, Y.C. Chen, *British Journal of Nutrition*, **2009**, *102*, 1629.

[24]. Z. Yener, I. Celik, F. Ilhan, R. Bal, *Food and Chemical Toxicology*, **2009**, *47*, 418.

[25]. M. Kanbur, G. Eraslan, Z.S. Sarica, Ö. Aslan, *Food and Chemical Toxicology*, **2011**, *49*, 1960.

[26]. N. Gahalain, J. Chaudhary, A. Kumar, S. Sharma, A. Jain, *International Journal of Pharmaceutical Sciences and Research*, **2011**, *2*, 2757.

[27]. N.K.S. Gowda, D.R. Ledoux, G.E. Rottinghaus, A.J. Bermudez, Y.C. Chen, *Poultry Science*, **2008**, *87*, 1125.
[28]. Y. Li, Y.H. Liu, Z.B. Yang, X.L. Wan, F. Chi, *Journal of Applied Poultry Research*, **2012**, *21*, 806.
[29]. Q.G. Ma, X. Gao, T. Zhou, L.H. Zhao, Y, Fan, X.Y. Li, Y.P. Lei, C. Ji, J.Y. Zhang, *Poultry Science*, **2012**, *91*, 2852.
[30]. F. Naaz, S. Javed, M. Z. Abdin, *Journal of Ethnopharmacology*, **2007**, *113*, 503.
[31]. S.P. Preetha, M. Kanniappan, E. Selvakumar, M. Nagaraj, P. Varalakshmi, *Comparative Biochemistry and Physiology, Part C*, **2006**, *143*, 333.
[32]. D. Prvulović, D. Kojić, G. Grubor-Lajšić, S. Košarčić, *Turkish Journal of Veterinary and Animal Scinces*, **2008**, *32*, 183.
[33]. S.A. Levine, P.M. Kidd, "Antioxidant adaptation: its role in free radical pathology", Biocurrents Division, Allergy research Group, San Leonardo, **1996**.
[34]. J. Chen, K. Chen, S. Yuan, X. Peng, J. Fang, F. Wang, H. Cui, Z. Chen, J. Yuan, Y. Geng, *Toxicology and Industrial Health*, **2013**, *October*, 1.
[35]. F. Wang, G. Shu, X. Peng, J. Fang, K. Chen, H. Cui, Z. Chen, Z. Zuo, J. Deng, Y. Geng, W. Lai, *International Journal of Environmental Research and Public Health*, **2013**, *10*, 2834.
[36]. K. Kanchana, S.S. Kumar, P. Shanthi, P. Sachdanandam, *International Journal of Biological and Pharmaceutical Research*, **2013**, *4*, 568.
[37]. W.I. Leong, C.L. Bowlus, J. Tallkvist, B. Lonnerdal, *American Journal of Physiology Gastrointestinal and Liver Physiology*, **2003**, *285*, 1153.
[38]. M.M. Bradford, *Analytical Biochemistry*, **1976**, *72*, 248.
[39]. J.M. McCord, I. Fridovich, *Journal of Biological Chemistry*, **1968**, *243*, 5753.
[40]. A. Clairborne, "Handbook for methods for oxygen radical research", CRC Press Inc, Boca Raton, **1986**, 283.
[41]. P. Agrawal, M.M. Laloraya, *Biochemical Journal*, **1977**, *166*, 205.
[42]. B. Chance, A.C. Maehly, „Methods in enzymology", Academic Press, New York, **1955**, 764.
[43]. W.H. Habig, M.J. Pabst, W.B. Jakoby, *Journal of Biological Chemistry*, **1974**, *249*, 7130.
[44]. Z.A. Placer, L.L. Cushman, B.C. Johnson, *Analytical Biochemistry*, **1966**, *16*, 359.

INDOLE-3-ACETIC ACID PRODUCING BACTERIA AND THEIR EFFECT ON THE GROWTH OF *PISUM SATIVUM*

SAROLTA SZENTES[a*], ÉVA LASLO[a], SZABOLCS LÁNYI[b], GABRIEL-LUCIAN RADU[a], GYÖNGYVÉR MARA[b]

ABSTRACT. Indole-3-acetic acid (auxin) is a well known phytohormone which is involved in the regulation of plant growth and development. A high number of plant growth promoting rhizobacteria (PGPR) produce auxin, thus play major role in plant development. In this study we characterized 25 bacterial strains by their auxin producing ability. The growth promoting effect of two selected bacterial strains on pea (*Pisum sativum*) was studied.

Keywords: *indole-3-acetic acid, phytohormones, plant-growth promoting rhizobacteria*

INTRODUCTION

Plant growth promoting bacteria enhance and regulate plant growth by different mechanisms such as solubilisation of phosphorous, production of phytohormones, stimulation of certain metabolic pathways (nitrogen fixation or control the pathogenic microorganisms) [1, 2, 3].

Plants regulate and control their development by using chemical signals, such as hormones. Among these hormones auxin (represented by indole-3-acetic acid - IAA) is the most active. It is responsible for the division, expansion and differentiation of plant cells and tissues [4].

Attachment of bacteria to the roots is beneficial for plant growth and productivity. In their interaction with plants, these microorganisms interfere with plant development by disturbing the auxin balance in plants. Two major pathways for auxin biosynthesis have been proposed: the indole-3-acetamide and the indole-3-pyruvate pathway [3, 5, 8]. The ability of auxin production has been found among various microorganisms, representatives of the

[a] *Universitatea POLITEHNICA, Facultatea de Chimie Aplicată şi Ştiinţa Materialelor, Splaiul Independenţei 313, RO-060042 Bucureşti, Romania.*
corresponding author szentessarolta@sapientia.sciulorum.ro
[b] *Universitatea Sapientia, Facultatea de Ştiinţe, Piaţa Libertăţii nr. 1, RO-530104 Miercurea Ciuc, Romania*

genera *Pseudomonas*, *Agrobacterium*, *Azospirillum*, *Azotobacter*, *Bacillus*, *Flavobacterium*, *Micrococcus*, *Rhizobium*, *Bradyrhizobium* etc. [3, 7, 8, 9].

The increasing interest in PGPR microorganisms led to an extensive use of different biofertilizers. These products represent an alternative for chemical fertilizers [10]

The aim of the current study is to determine the auxin production ability of selected bacterial strains using a colorimetric method. It is well known that one of the main mechanisms of plant growth regulation is production of different phytohormones; thus we studied the effect on the growth of pea (*Pisum sativum)* of two selected bacterial strains, which proved to be the best auxin producers.

RESULTS AND DISCUSSION

In this study the beneficial properties of 25 bacterial strains was assayed; bacteria were isolated from the rhizosphere of *Sphagnum* plants. The ability of auxin production was analyzed. Auxin is a phytohormone which plays crucial role in plant growth and development. During our work we examined the effect of two selected bacterial strain on the growth and development of pea (*Pisum sativum)*.

In Table 1 are presented the auxin concentrations, produced by the studied bacterial strains. The amount of auxin produced is between 2.29 – 17.79 µg ml^{-1}; the highest amount of auxin was produced by *Pseudomonas fluorescens E8*. *Serratia nematodiphila P17* found to produce auxin in the less concentration.

Table 1. The values of auxin concentration produced by the examined bacterial strains

Bacterial strain	Absorbance (530 nm)	Auxin concentration (µg ml^{-1})
Bacillus cereus P2	0.172	6.79
Bacillus mycoides B6	0.073	2.66
Bacillus thuringiensis B11	0.159	6.25
Lysinibacillus fusiformis P24	0.317	12.83
Viridibacillus arenosi P13	0.214	8.54
Pseudomonas fluorescens E8	0.436	17.79
Pseudomonas fluorescens B14	0.285	11.5

Pseudomonas jessenii E20	0.264	10.62
Pseudomonas koreensis P8	0.313	12.66
Pseudomonas koreensis P15	0.316	12.79
Pseudomonas lurida P20	0.166	6.54
Pseudomonas stutzeri P23	0.294	11.87
Serratia fonticola P5	0.106	4.04
Serratia fonticola B17	0.327	13.25
Serratia marcescens E11	0.066	2.375
Serratia nematodiphila P17	0.064	2.29
Serratia plymuthica B19	0.209	8.33
Serratia plymuthica E5	0.15	5.87
Stenotrophomonas rhizophila B21	0.317	12.83
Stenotrophomonas rhizophila E3	0.265	10.66
Paracoccus yeei P3	0.072	2.62
Cedecea neteri P4	0.072	2.62
Delftia acidovorans P12	0.326	13.20
Microbacterium hydrocarbonoxydans P21	0.133	5.16
Enterobacter sp.E6	0.295	11.91

Inoculation of *P. sativum* plants with *S. fonticola B17* and *P. fluorescens E8* stimulated plant growth. A significant increase ($p < 0.001$) in shoot length was observed between treated plants and control sample (Figure 1.).
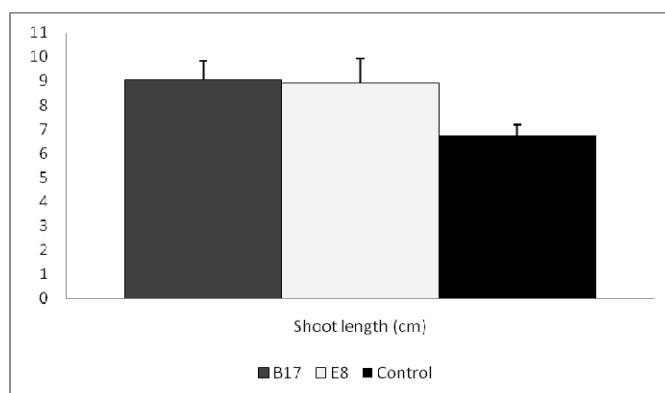
Figure 1. The mean values of shoot length

In case of pea plants a significant difference were obtained for the shoot and root fresh weight between plants treated with *P. fluorescens E8* and *S. fonticola B17* and control plants (Figure 2.); no differences were observed between the shoot and root dry weights of the control and treated plants.
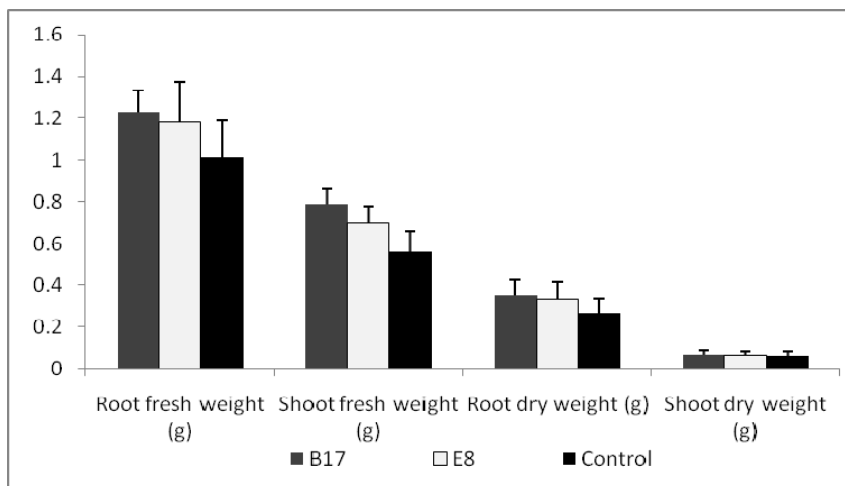

Figure 2. Mean values of root and shoot fresh and dry weight

CONCLUSIONS

During our study the auxin production ability was examined. The best auxin producers proved to be strains belonging to *Pseudomonas* genera: *P. fluorescens*, *P. koreensis*, *P. stutzeri*, *P. jessenii*.

Bacterial strains belonging to *Delftia*, *Serratia*, *Stenotrophomonas* and *Lysinibacillus* were also good auxin producers. Our results are in correlation with results found in the scientific literature. Ali et al. (2009) [11] studied the auxin production property of different bacterial strains belonging to *Bacillus*, *Pseudomonas*, *Escherichia*, *Micrococcus* and *Staphylococcus* genera; these strains were demonstrated having potential to increase the growth of wheat (*Triticum aestivum*). It is known that auxin producing *Enterobacterium sp.* and *Bacillus sp.* promoted the growth of orchids (*Cattelya walkeriana*) [12]. Husen et al. [8] studied bacteria isolated from rhizosphere and plant roots in Bohol and Tarlac, Philippines, which showed high IAA and siderophore producing ability.

Sphagnum associated bacteria found in raised bogs from Germany and Norway, are known as good antagonists of plant pathogens like Verticillium or Ralstonia, according to Opelt and Berg (2004) and Opelt et al (2007), but none of them showed auxin producing properties [13, 14]. Our data indicates that bacterial strains isolated and identified as *Pseudomonas fluorescens E8* and *Serratia fonticola B17* were able to develop plant growth promoting effects in laboratory conditions.

EXPERIMENTAL SECTION

Bacterial strains

25 bacterial strains, isolated from rhizosphere of Sphagnum plants in Borsáros raised bog natural reserve (Harghita County, Romania) were examined. Bacterial strains were grouped using RFLP (restriction fragment length polymorphism) method, by digesting the 16S ribosomal DNA fragments with *MspI* and *HaeIII* restriction enzymes. Identification of 16S rDNA fragments were realized by sequencing. To identify similar sequences that are available in the NCBI GenBank, sequences were compared with BLAST algorithm. The sequences obtained are deposited in the European Molecular Biology Laboratory – European Bioinformatics Laboratory (EMBL-EBI) European Nucleotide Archive (ENA) database (data not shown).

Auxin production

Production of the well known plant hormone indole acetic acid was determined through colorimetric analysis using Salkowsky reagent [15]. Bacterial strains were grown in Triptone-Soy Broth (triptone 15 g, peptone from soy-meal 5 g, sodium chloride 5 g, distilled water 1000 ml) supplemented with tryptophan (10 mg/ml final concentration), for 3 days at 28 °C, shaken at 150 rpm. After incubation 1.5 ml from each bacterial suspension was centrifuged at 5000 rpm, for 15 minutes. The amount of indolic compounds was estimated adding 1 ml of culture supernatant to 2 ml of Salkowsky reagent (concentrated sulfuric acid 300 ml, 0.5 M $FeCl_3$ 15 ml, distilled water 500 ml). The mixture was incubated in dark, at room temperature for 30 minutes (during this period the mixture color become red, darker red indicated a higher amount of indole compounds). The color intensity was measured at an absorbance of 530 nm. The auxin concentration was estimated using a standard curve prepared with known amounts (5, 10, 15, 20, 25 and 35 µg/ml) of auxin solutions, that generated the equation y=0.024x + 0.01, with an R^2 = 0.993.

Plant growth experiment

Beneficial properties of two selected bacterial strains, identified as *Pseudomonas fluorescens E8* and *Serratia fonticola B17* was examined on pea (*Pisum sativum*) plants.

Seeds were surface steriliesed and germinated for three days at 28 °C. Soil samples were sterilised at 105 °C, for 60 minutes, for three times, with a 24 h interval. Bacterial strains were grown in liquid Nutirent medium (peptone 5 g, sodium chloride 5 g, yeast extract 2 g, meat extract 1 g), for 1 day and concentration was adjusted to 10^7 colony forming units (CFU) in every ml of suspension.

20-20 germinated seeds were sown in the sterile soil and 1 ml of bacterial suspension was added to every seed. Plants were grown for 10 days in a growth chamber 16 h light at 25 °C and 8 h dark at 20 °C, 70% relative humidity.

As a control germinated seeds were sown in soil samples, without bacterial inoculation.

Shoot length, root and shoot fresh and dry weight was measured after incubation. Statistical analyses were conducted using F and T test (p<0.001) of Past statistic software package.

ACKNOWLEDGMENTS

REFERENCES

[1]. É. Laslo, É. György, Gy. Mara, É. Tamás, B. Ábrahám, Sz. Lányi, *Crop Protection*, **2012**, *40*, 43.
[2]. P. Hariprasad, S. T. Divakara, S. R. Niranjana, *Crop Protection,* **2011**, *30*, 1606.
[3]. X. Zhuang, J. Chen, H. Shim, Z. Bai*, Environment International*, **2007**, *33*, 406.
[4]. A. Ahmed, S. Hashnain, *Pure Appl. Chem*, **2010**, *82(1)*, 313.
[5]. S. Spaepen, J. Vanderleyden, *Cold Spring Harbor Perspectives in Biology*, **2010**, 1.
[6]. D.K. Maheshwari, "Plant Growth and Health Promoting Bacteria", Springer, Münster, **2010**.
[7]. E.A. Tsavkelova, T.A. Cherdyntseva, A.I. Netrusov, *Microbiology*, **2005**, *74*(1), 55.
[8]. E. Husen, *Indonesian Journal of Agricultural Science*, **2003**, *4*(1), 27.
[9]. L.E. de-Bashan, H. Antoun, Y. Bashan, *J. Phycol*., **2008**, *44*, 938.
[10]. G.V. Bloemberg, B.J.J. Lugtenberg, *Current Opinion in Plant Biology*, **2001**, *4*, 343.
[11]. B. Ali, A.N. Sabri, K. Ljung, S. Hasnain, *Letters in applied Microbiology*, **2008**, *48*, 542.
[12]. R.F. Galdiano Junior, E. Aparecida, N. Pedrinho, T.C.L. Castellane, E.G.M. Lemos, *R. Bras. Ci. Solo,* **2011**, *35*, 729.
[13]. K. Opelt, G. Berg, *Applied and Environmental Microbiology*, **2004**, *70*(11), 6569.
[14]. K. Opelt, C. Berg, G. Berg, *FEMS Microbiol Ecol*, **2007**, *61*, 38.
[15]. S.A. Gordon, R.P. Weber, *Plant Physiol*., **1951**, *26*, 192.

OMEGA POLYNOMIAL OF A BENZENOID SYSTEM

MOHAMMAD R. FARAHANI[a*], MIRANDA P. VLAD[b]

ABSTRACT. The Omega polynomial $\Omega(G,x)$ is defined as the collection of the equidistant, topologically parallel opposite edge stripes in the molecular graph. This polynomial was introduced by *Diudea* in 2006. In this paper, we compute the Omega polynomial of an important class of benzenoid system.

Keywords: *Molecular graph, Omega polynomial, Opposite edge strip, Benzenoid systems.*

INTRODUCTION

Let *G* be a simple connected graph in the Chemical Graph Theory. The vertex set and edge set of the molecular graph G are denoted by *V(G)* and *E(G)* respectively and its vertices correspond to the atoms while the edges correspond to the covalent bonds [1,2].

A topological index of *G* is a numeric quantity, derived following certain rules, which can be used to characterize the property of molecules and is invariant under the automorphism of the graph. Usage of topological indices in chemistry began in 1947 when *Harold Wiener* developed the most widely known topological descriptor, *Wiener index* [3], defined as

$$W(G) = \frac{1}{2} \sum_{u \in V(G)} \sum_{v \in V(G)} d(u,v)$$

where the topological distance *d(u,v)* between two vertices *u* and *v* is the number of edges in the shortest path connecting them.

---

[a] *Department of Applied Mathematics, Iran University of Science and Technology (IUST) Narmak, Tehran 16844, Iran. * corresponding author: Mr_Farahani@Mathdep.iust.ac.ir*
[b] *Faculty of Economic Sciences Cluj, Dimitrie Cantemir University, Bucharest*

Let $G(V,E)$, be a molecular graph; two edges $e=uv$ and $f=xy$ of G are called co-distant (briefly: e co f) if they obey the topologically parallel edges relation. For some edges of a connected graph G there are the following relations satisfied [4-7]

$$e \, co \, e$$
$$e \, co \, f \leftrightarrow f \, co \, e$$
$$e \, co \, f \, \& \, f \, co \, h \rightarrow f \, co \, h$$

though the last relation is not always valid.

Set $C(e):=\{f \in E(G)| \, e \, co \, f\}$. If the relation "co" is transitive on $C(e)$ then C(e) is called an *orthogonal cut "oc"* of the graph G. The graph G is called co-graph if and only if the edge set $E(G)$ is the union of disjoint orthogonal cuts.

$$E(G) = C_1 \cup C_2 \cup ... \cup C_{k-1} \cup C_k \text{ and } C_i \cap C_j = \varnothing,$$

for $i \neq j$ and $i, j=1, 2, …, k$.

The Omega polynomial $\Omega(G,x)$ counts the "quasi-orthogonal cut' strips, qoc strips (because the relation is not always transitive, see above) in G and was defined by *M.V. Diudea* (2006) as

$$\Omega(G,x) = \sum_c m(G,c) x^c$$

where $m(G,c)$ is the number of *qoc* strips of length c. The summation runs up to the maximum length of *qoc* strips in G.

The first derivative of Omega polynomial (in $x=1$), equals the number of edges in G (see also the papers [8-16]):

$$\Omega'(G,1) = \sum_c m(G,c) \times c = |E(G)|$$

Herein, our notations are standard and taken from the standard books of Graph Theory [1,2]. The aim of this study is to compute the Omega polynomial of an important class of benzenoid system called hexagonal system $B_{m,n}$ (Figure1).

RESULTS AND DISCUSSION

The Omega polynomial of an infinite family of benzenoid system was computed as described above.

Shui Ling-Ling et al.[17] defined a new hexagonal system named jagged-rectangle. An $a \times b$ hexagonal jagged-rectangle whose shape forms a rectangle and the number of hexagonal cells in each chain alternate a

and $a-1$. For two independent positive integer numbers $a \geq 2$ & $b \geq 1$, the vertex set of $B_{a,b}$ is defined as (see Figure1 and [17, 18]).

$$V(B_{a,b}) = \{(x,y) \mid 0 \leq x \leq 2a, 0 \leq y \leq 2b-1\}$$

$$\cup \{(x,-1) \mid 0 \leq x \leq 2a-1\} \cup \{(x,2b) \mid 1 \leq x \leq 2a-1\}$$

This graph has $4ab+4a+2b-2$ vertices, since $|V(B_{a,b})|=2b(2a+1)+(2a-1)+(2a-1)$. It is easy to see that $\forall a \in \square -\{1\}$, $B_{a,a}$ has exactly $4a^2+6a-2$ vertices and $6a^2+6a-4$ edges. A general representation of this hexagonal system is shown in Figure 1.
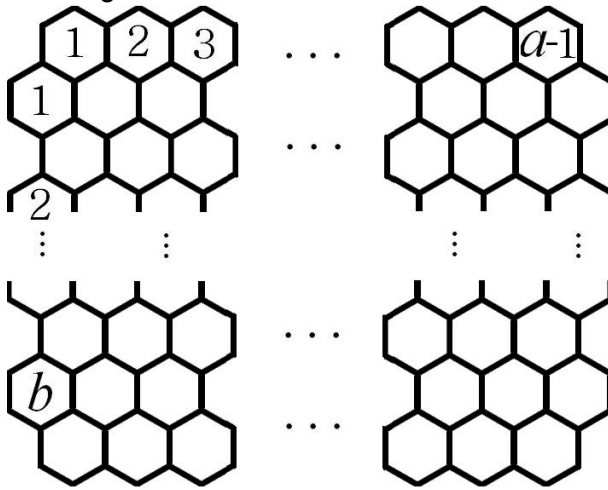

Figure 1. A general representation of the Benzenoid system $B_{a,b}$ ($\forall a,b \geq 1$).

Theorem 1. The Omega polynomial of the hexagonal system $B_{a,b}$ $\forall a,b \in \square$, is as follows:

If $a \geq b+2$: $\qquad \Omega(B_{a,b}, \text{x}) = (b+1)x^a + bx^{a+1} + \sum_{i=1}^{b}\left(4\text{x}^{2i+1}\right) + 2(a-b-1)x^{2b+2}$

If $a \leq b+1$: $\qquad \Omega(B_{a,b}, \text{x}) = (b+1)x^a + bx^{a+1} + \sum_{i=1}^{a-1}\left(4\text{x}^{2i+1}\right) + 2(b-a+1)x^{2a}$

Proof. Let $G=B_{a,b}$ be the hexagonal system, with $4ab+4a+2b-2$ vertices. To compute the Omega polynomial of G it is enough to calculate $C(e)$ for every e in $E(G)$. Now, by using the *Cut Method,* and by using the Tables 1

and 2 and Figure 2, the proof is easily. The *Cut Method* in its general form was studied by *S. Klavžar* [19] and used in paper series [20-30].

So, from Table 1 we have

$$\Omega\left(B_{a,b}, \mathrm{x}\right) = \sum_c \mathrm{m}\left(B_{a,b}, c\right) \mathrm{x}^c$$

$$= (b+1)x^a + bx^{a+1} + \sum_{i=1}^{b}\left(4\mathrm{x}^{2i+1}\right) + 2\left(a-b-1\right)x^{2b+2}$$

Table 1. The number of co-distant edges, when *a≥b+2*

quasi-orthogonal cuts	Number of co-distant edges	No
C_{2i+1} ∀ *i=0,…,b*	1	*a*
C_{2i} ∀ *i=1,…,b*	1	*a+1*
$\mathcal{C}_i$ ∀ *i=1,…,b*	4	*2i+1*
$\mathcal{C}_{b+1}$	*2(a-b-1)*	*2b+2*

On other hands, from Table 2, ∀*a≤b+1*:

$$\Omega\left(B_{a,b}, \mathrm{x}\right) = (b+1)x^a + bx^{a+1} + \sum_{i=1}^{a-1}\left(4\mathrm{x}^{2i+1}\right) + 2(b-a+1)x^{2a}$$

Table 2. The number of co-distant edges, when *a≤b+1*

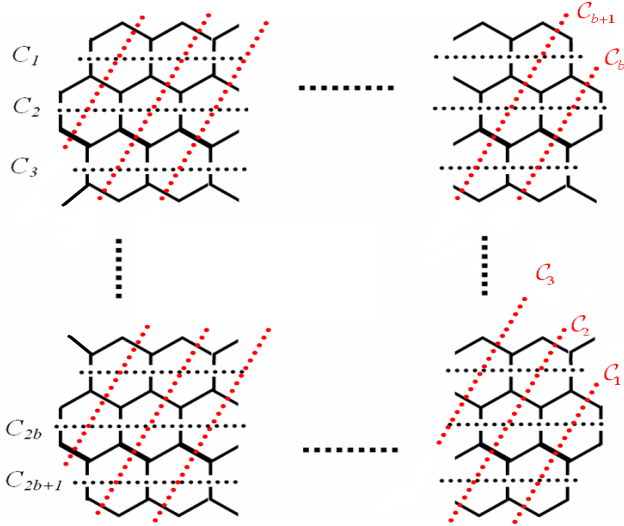| quasi-orthogonal cuts	Number of co-distant edges	No
C_{2i+1} ∀ *i=0,…,b*	1	*a*
C_{2i} ∀ *i=1,…,b*	1	*a+1*
$\mathcal{C}_i$ ∀ *i=1,…,a-1*	4	*2i+1*
$\mathcal{C}_a$	*2(b-a+1)*	*2a*

and this completes the proof.

Figure 2. The presentation of quasi-orthogonal cuts (qoc strips) of $B_{a,b}$.

From Theorem 1, one can to see that the number of edges in G is equal to

$$\left|E\left(B_{a,b}\right)\right|=\Omega'\left(B_{a,b},\mathrm{x}\right)\big|_{x=1}$$

$$=\frac{\partial\left((b+1)x^a+bx^{a+1}+\sum_{i=1}^{b}\left(4\mathrm{x}^{2i+1}\right)+2(a-b-1)x^{2b+2}\right)}{\partial x}\Bigg|_{x=1}$$

$$=a(b+1)+b(a+1)+4\sum_{i=1}^{b}(2i+1)+2(a-b-1)(2b+2)$$

$$=ab+a+ab+b+4\left(\frac{2b(b+1)}{2}+b\right)+4ab-4b^2+4a-8b-4$$

=6ab+5a+b-4.

And also $\left|E\left(B_{a,b}\right)\right|=\dfrac{\partial\left((b+1)x^a+bx^{a+1}+\sum_{i=1}^{a-1}\left(4\mathrm{x}^{2i+1}\right)+2(b-a+1)x^{2a}\right)}{\partial x}\Bigg|_{x=1}$

$$=a(b+1)+b(a+1)+4\sum_{i=1}^{a-1}(2i+1)+2(b-a+1)(2a)$$

$$=2ab+a+b+4\left(\frac{2a(a-1)}{2}+a-1\right)+4ab-4a^2+4a$$
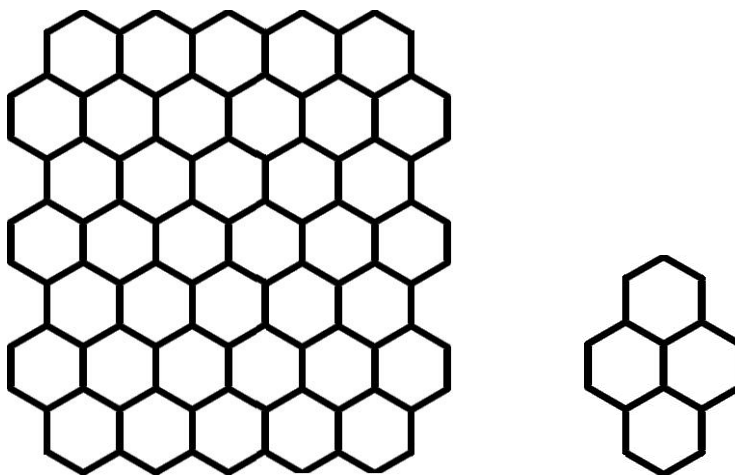
=6ab+5a+b-4.

75

Figure 3. The hexagonal systems $B_{6,3}$ and $B_{2,1}$ (the first member of this hexagonal systems).

Example 1. By using Theorem 1, the Omega polynomial of the hexagonal system $B_{6,3}$ (Figure 3) is equal to $\Omega(B_{6,3},x)=4x^3+4x^5+4x^6+7x^7+4x^8$.

Example 2. From the second equation in Theorem 1, it's easy to see that the Omega polynomial of $B_{2,1}$ (Figure 3) is $\Omega(B_{6,3},x)=2x^2+5x^3$.

Example 3. By using Theorem 1 one can see that the Omega polynomial of the hexagonal system $B_{3,1}$ or the coronene H_2 (Figure 4) is equal to $\Omega(B_{6,3},x)=2x^3+x^4+4x^3+2x^4=6x^3+3x^4=\Omega(H_2,x)$.
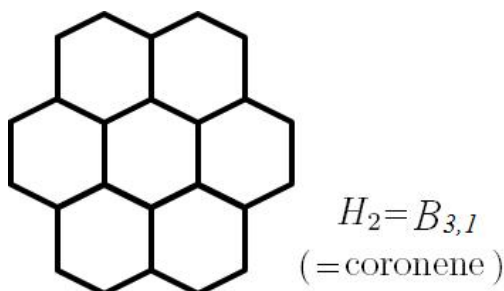

$$H_2 = B_{3,1}$$
$$(= \text{coronene})$$

Figure 4. The hexagonal system $B_{3,1}$ ("coronene H_2" the second member of the circumcoronene series of benzenoid).

Theorem 2. The Omega polynomial of the hexagonal system $B_{a,a}$ $\forall a \in \square$, is equal to

$$\Omega\left(B_{a,a}, \mathrm{x}\right) = (a+1)x^a + ax^{a+1} + \sum_{i=1}^{a-1}\left(4\mathrm{x}^{2i+1}\right) + 2x^{2a}$$
$$= ax^3 + 4x^5 + ... + (a+1)x^a + ax^{a+1} + ... + 4x^{2a-1} + 2x^{2a}$$

REFERENCES

[1]. N. Trinajstić, Chemical Graph Theory, CRC Press, Boca Raton, FL, **1992**.

[2]. M.V. Diudea, I. Gutman, L. Jäntschi, *Molecular Topology*, NOVA, New York, **2002**.

[3]. H. Wiener, Structural determination of paraffin boiling points, *J. Am. Chem. Soc.* **1947**, *69,* 17.

[4]. M.V. Diudea, S. Cigher, A.E. Vizitiu, O. Ursu and P.E. John. *Croat. Chem. Acta*, **2006**, *79,* 445.

[5]. M.V. Diudea, Omega Polynomial. *Carpath. J. Math.* **2006**, *22,* 43.

[6]. P.E. John, A.E. Vizitiu, S. Cigher, and M.V. Diudea, *MATCH Commun. Math. Comput. Chem.* **2007**, *57,* 479.

[7]. M.V. Diudea, S. Cigher and P.E. John. *MATCH Commun. Math. Comput. Chem,* **2008**, *60,* 237.

[8]. A.E. Vizitiu, S. Cigher, M.V. Diudea and M.S. Florescu, *MATCH Commun. Math. Comput. Chem,* **2007**, *57,* 457.

[9]. M. Saheli, M. Neamati, A. Ilić and M.V. Diudea. *Croat. Chem. Acta.* **2010**, *83(4),* 395.

[10]. A. Bahrani and J. Yazdani. *Digest. J. Nanomater. Bios.* **2008**, *3(4),* 309.

[11]. A.R. Ashrafi, M. Ghorbani and M. Jalili. *Digest. J. Nanomater. Bios.* **2009**, *4(3),* 403.

[12]. M. Ghorbani. *Digest. J. Nanomater. Bios.* **2011**, *6(2),* 599.

[13]. M. Ghorbani and M. Ghazi. *Digest. J. Nanomater. Bios.* **2010**, *5(4),* 843.

[14]. M. Ghorbani and M. Jalili. *Digest. J. Nanomater. Bios.* **2009**, *4(1),* 177.

[15]. J. Yazdani and A. Bahrani. *Digest. J. Nanomater. Bios.* **2009**, *4(3),* 507.

[16]. M.V. Diudea, S. Cigher, A.E. Vizitiu, M.S. Florescu and P.E. John*, J. Math. Chem.* **2009**, *45*, 316.

[17]. S. Ling-Ling, W. Zhi-Ning and Z. Li-Qiang, *Chinese J. Chem.* **2005**, *23(3)*, 245.

[18]. Z. Bagheri, A. Mahmiani and O. Khormali. *Iran. J. Math. Sci. Informat.* **2008**, *3(1)*, 31.

[19]. S. Klavžar. *MATCH Commun. Math. Comput. Chem.* **2008**, *60,* 255.

[20]. P.E. John, P.V. Khadikar and J. Singh. *J. Math. Chem.* **2007**, *42(1),* 27.

[21]. M.V. Diudea, *MATCH Commun. Math. Comput. Chem.* **2010**, *64*, 569.

[22]. M.V. Diudea, Nanomolecules and Nanostructures - Polynomials and Indices, MCM series, No. 10**,** Univ. Kragujevac, Serbia, **2010**.

[23]. M.R. Farahani, K. Kato and M.P. Vlad*. Studia Univ. Babes-Bolyai. Chemia* **2012**, *57(3),* 177.

[24]. M.R. Farahani, *Acta Chim. Slov.* **2012**, *59,* 965.

[25]. M.R. Farahani, *Int. J. Comput. Theoret. Chem.* **2013**, *1*(2), 7.

[26]. M.R. Farahani, *Int. J. Comput.Sci. Appl.* **2013**, *3*(5), 1.

[27]. M.R. Farahani, *J. Chem. Acta*. **2013**, *2*, 43.

[28]. M.R. Farahani, *Int. J. Theoret. Chem.* **2013**, *1*(1), 1.

[29]. M.R. Farahani, *World J. Sci. Technol. Res.* **2013**, *1*(7), 135.

[30]. M.R. Farahani, *World Appl. Sci. J*. **2012**, *20*(9), 1248.

OMEGA POLYNOMIAL IN TWO APPEARANCESOF THE CRYSTAL NETWORK *DIU15*, SPACE GROUP *IM-3M*

MAHBOUBEH SAHELI[a], MOHAMMAD A. IRANMANESH[a], MIRCEA V. DIUDEA[b]*

ABSTRACT. Omega polynomial$\Omega(G,x)$ is defined on opposite edge strips ops in a graph. The first and second derivatives, in X = 1, of Omega polynomial provide the Cluj-Ilmenau CI index. Design of a new crystal network, called diu15, by means of the Medial map operation is presented. The topology of this network, in two different appearances, is described in terms of Omega polynomial, function of the net parameters. Close formulas for the polynomial are given and examples tabulated.

Keywords: Omega polynomial**,** CI index, map operation, diu15 crystal network

INTRODUCTION

Mathematical calculations are absolutely necessary to explore important concepts in Chemistry. Mathematical Chemistry is a branch of Theoretical Chemistry developed for discussion and prediction of molecular structures using mathematical methods without necessarily referring to quantum mechanics. Chemical Graph Theory is an important tool for studying molecular structures. This theory had an important effect on the development of the chemical sciences.

Numbers reflecting certain structural features of organic molecules, obtained from their associate molecular graphs are usually called graph invariants or more commonly topological indices. The oldest and most

[a] *Department of Mathematics, Yazd University, 89175-741, Yazd, Iran.*
[b] *Faculty of Chemistry and Chemical Engineering, "Babes-Bolyai" University, 400028 Cluj, Romania, *Corresponding author: diudea@chem.ubbcluj.ro*

thoroughly examined topological index in Chemistry was proposed and used by Wiener [1] in the study of paraffin thermodynamic properties and this topological index was called the Wiener index.

A finite sequence of some graph-theoretical categories/properties, such as the distance degree sequence or the sequence of the number of k-independent edge sets, can be described by so-called counting polynomials:

$$P(G,x) = \sum_k p(G,k) \cdot x^k \tag{1}$$

where $p(G,k)$ is the frequency of occurrence of the property partitions of G, of length k, and x is simply a parameter to hold k.

Counting polynomials were introduced, in the Mathematical Chemistry literature, by Hosoya with his Z-counting (independent edgesets) and the distance degree polynomials, initially called Wiener and later Hosoya polynomial [2]. Their coefficients are used for the characterization of the topological nature of hydrocarbons.

The present work describes the design and topology (in terms of Omegapolynomial) of two appearances of Diudea'sdiu15 3-periodic lattice.

LATTICE BUILDING

The repeating unit of diu15 network is designed by using a map operation, named medial Med (or subdivision). This operation is achieved by putting new vertices in the middle of the original edges of a map M (i.e. a discretized closed surface)); next join two such vertices if the corresponding edges span an angle (and are consecutive within a rotation path around their common vertex in M). The transform Med(M) is a 4-valent graph and Med(M)=Med(Du(M)). The transformed map parameters are:

$v = e_0$; $e = 2e_0$; $f = f_0 + v_0$.(the subscript zero denoted the original map parameters). The medial of Cube and Octahedron is the Cuboctahedron CO (Figure 1).The medial operation rotates parent s-gonal faces by π/s. Points in the medial map represent the original edges; this property can be used in topological analysis of edges in the parent polyhedron. Similarly, the points in the dual map give information on the topology of parent faces.

Figure 1. The Cuboctahedron CO=Med(C)

The unit **CO@(CO$_8$)_60** (Figure 2, top left) is composed of eight CO disposed around an empty hollow having also the geometry of CO; it can be obtained as**Med(Oct@Oct$_8$_18)**by applying the Med operation on**Oct@Oct$_8$_18** (Figure 2, top right) that is a hyperstructure of the Octahedron Oct. Note, the last number in the above object names is the number of points/atoms.

The lattice diu15 is built by translating the unit **CO@(CO$_8$)_60**, with the identification of the superposed hyper-faces; this results in two appearances diu15X (Figure 2, bottom left) and diu15 (Figure 2, bottom right). This is a new 2-nodal network (by TOPOS database), belonging to the space group *Im-3m*and having the point symbol for net: (33.46.56)2(34.410.512.62)6,8-c net with stoichiometry (6-c)2(8-c).
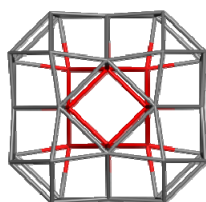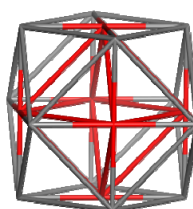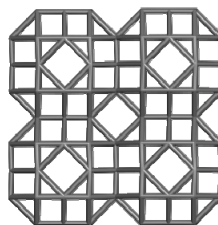

CO@(CO$_8$)_60   **Oct@Oct$_8$_18**
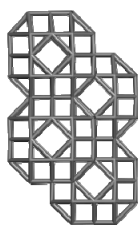
diu15X_222_342   **diu15_222_384**

Figure 2. Top row: a spongy unit **CO@(CO$_8$)_60** consisting of cuboctahedra CO, designed by Medial (i.e., Subdivision) map operation applied on**Oct@Oct$_8$_18**; Bottom row: two apearances of the crystal network**diu15**, space group *Im-3m*.

OMEGA POLYNOMIAL

The Omega polynomial is a counting polynomial introduced by Diudea. In the recent years, several papers on methods for computing Omega polynomial in molecular graphs and nanostructures have been published [11 – 17].

Let G(V,E) be a connected graph, with the vertex set V(G) and edge set E(G). Two edges e = uv and f = xy of G are called *codistant*, ***e co f***, if they obey the following relation [3]:

$$d(v,x) = d(v,y) + 1 = d(u,x) + 1 = d(u,y) \tag{2}$$

which is reflexive, that is, e co e holds for any edge e of G, and symmetric, if e co f then f co e. In general, relation co is not transitive; an example showing this fact is the complete bipartite graph $K_{2,n}$. If "*co*" is also transitive, thus it is an equivalence relation, then G is called a co-graph and the set of edges $C(e) := \{f \in E(G);\ f\ co\ e\}$ is called an orthogonal cut oc of G, E(G) being the union of disjoint orthogonal cuts:

$$E(G) = C_1 \cup C_2 \cup ... \cup C_k,\ \ C_i \cap C_j = \varnothing, i \neq j\ .$$

Klavžar [4] has shown that relation co is a theta Djoković-Winkler relation[5,6].

We say that edges e and f of a plane graph G are in relation opposite, e op f, if they are opposite edges of an inner face of G. Note that the relation co is defined in the whole graph while op is defined only infaces. Using the relation op we can partition the edge set of G into opposite edge strips, ops. An ops is a quasi-orthogonal cut qoc, since ops is not transitive.

Let G be a connected graph and $S_1, S_2, ..., S_k$ be the ops strips of G. Then the ops strips form a partition of E(G). The length of ops is taken as maximum. It depends on the size of the maximum fold face/ringF_{max}/R_{max} considered, so that any result on Omega polynomial will have this specification.

Denote by m(G,s) the number of ops of length s and define the Omega polynomial as[7-9]:

$$\Omega(G,x) = \sum_{s} m(G,s) \cdot x^s \tag{3}$$

Its first derivative (in x=1) equals the number of edges in the graph:

$$\Omega'(G,1) = \sum_{s} m(G,s) \cdot s = e = \left| E(G) \right| \tag{4}$$

On Omega polynomial, the Cluj-Ilmenau index, *CI=CI(G)*, was defined:

$$CI(G) = \left\{ [\Omega'(G,1)]^2 - [\Omega'(G,1) + \Omega''(G,1)] \right\} \tag{5}$$

MAIN RESULTS

Within this paper, the Omega polynomial and derived Cluj-Ilmenau CI index refer toF_{max}(4).Data were calculated by software program Nano Studio [10], developed at the TOPO Group Cluj. Formulas for the infinite networks of the two series were derived by numerical analysis, function of k that is the number of repeating units in a row of a cubic domain (k,k,k), and are listed in Tables 1 and 2; examples are given at the bottom of these tables.

Table1. Omega polynomials in **diu15X** Network

Formulas
$\Omega(G,x) = 2\left(4k^2 + 9k - 1\right)x^2 + 2\left(14k^2 - 5k - 3\right)x^3 + 2\left(3k^3 + 3k^2 + 5k - 2\right)x^4$ $+ 2\left(8k^2 - 13k + 5\right)x^5 + 2\left(3k^3 - 4k^2 + k\right)x^6$
$\lvert V(G)\rvert = 18k^3 + 58k^2 - 18k + 2$
$\lvert E(G)\rvert = 60k^3 + 156k^2 - 72k + 12$
$CI(G) = 3600k^6 + 18720k^5 + 15696k^4 - 21336k^3 + 8436k^2 - 1292k + 20$

k	Omega polynomial: examples	*V(G)*	*E(G)*	*CI(G)*
1	$24x^2 + 12x^3 + 18x^4$	60	156	23844
2	$66x^2 + 86x^3 + 88x^4 + 22x^5 + 20x^6$	342	972	941068
3	$124x^2 + 216x^3 + 242x^4 + 76x^5 + 96x^6$	956	2820	7940732
4	$198x^2 + 402x^3 + 516x^4 + 162x^5 + 264x^6$	2010	6060	36697380
5	$288x^2 + 644x^3 + 946x^4 + 280x^5 + 560x^6$	3612	11052	122097460
6	$394x^2 + 942x^3 + 1513x^4 + 430x^5 + 1020x^6$	5870	18156	329557724
7	$516x^2 + 1296x^3 + 2418x^4 + 612x^5 + 1680x^6$	8892	27732	768935628

Table 2. Omega polynomials in **diu15** Network

Formulas

$$\Omega(G,x) = 24k\,x^2 + 12k\left(4k-3\right)x^3 + 6k\left(2k^2+1\right)x^4 + 6k\left(2k^2-3k+1\right)x^6$$

$$|V(G)| = 12k^2(3k+2)$$

$$|E(G)| = 120k^3 + 36k^2$$

$$CI(G) = 14400k^6 + 8640k^5 + 12966k^4 - 624k^3 + 216k^2 - 84k$$

k	Omega polynomial: examples	V(G)	E(G)	CI(G)
1	$24\,x^2 + 12\,x^3 + 18\,x^4$	60	156	23844
2	$48\,x^2 + 120\,x^3 + 108\,x^4 + 36\,x^6$	384	1104	1214520
3	$72\,x^2 + 324\,x^3 + 342\,x^4 + 180\,x^6$	1188	3564	12686940
4	$96\,x^2 + 624\,x^3 + 792\,x^4 + 504\,x^6$	2688	8256	68124720
5	$120\,x^2 + 1020\,x^3 + 1530\,x^4 + 1080\,x^6$	5100	15900	252736980
6	$144\,x^2 + 1512\,x^3 + 2628\,x^4 + 1980\,x^6$	8640	27216	740583144
7	$168\,x^2 + 2100\,x^3 + 4158\,x^4 + 3276\,x^6$	13524	42924	1842265740

CONCLUSION

Omega polynomial description proved to be a simple and efficient method in topological characterization of some new designed nano-structures.

REFERENCES

[1]. H. Wiener, *J. Am.Chem. Soc.***1947**, *69*, 17.

[2]. H. Hosoya, *Bull. Chem. Soc.Japan*., **1971**, *44*, 23.

[3]. P.E. John, A. E.Vizitiu, S. Cigher and M.V. Diudea,*MATCH Commun. Math. Comput. Chem.,* **2007**, *57*, 479.

[4]. S. Klavžar, *MATCH Commun. Math. Comput. Chem.*, **2008**, *59*, 217.

[5]. D.Ž. Djoković, *J. Combin. Theory Ser.*, **1973**, *14*, 263.

[6]. P.M. Winkler, *Discrete Appl. Math.*, **1984**, *8*, 209.

[7]. M.V. Diudea, *Carpath. J. Math.*, **2006**, *22*, 43.

[8]. M.V. Diudea, S. Cigher and P.E. John, *MATCH Commun. Math. Comput. Chem.* **2008**, *60*, 237.

[9]. M.V. Diudea, S. Cigher, A.E. Vizitiu, M.S. Florescu and P.E. John, *J. Math. Chem.* **2009**, *45*, 316.

[10]. Cs.L. Nagy and M.V. Diudea, "Nano Studio software", Babes-Bolyai Univ., **2009**.

[11]. M.V. Diudea, M. Ghorbani and M.A. Hosseinzadeh, *Util. Math.*, **2011**, *84*, 165.

[12]. A.R. Ashrafi, M. Jalali, M. GhorbaniandM. V. Diudea, *MATCH Commun. Math. Comput. Chem.*, **2008**, *60*, 905.

[13]. M. Saheli, A.R. Ashrafi and M.V. Diudea, *Studia UBB Chemia,* **2010**, *4*, 233.

[14]. M. Saheli and M.V. Diudea, *Studia UBB Chemia,* **2010**, *4*, 215.

[15]. M. Saheli, M. Ghorbani, M.L. Pop andM. V. Diudea, *Studia UBB Chemia,* **2010**, *4*, 241.

[16]. M. Saheli, O. Pop,L. Pop and M.V. Diudea, *Studia UBB Chemia,* **2010**, *4*, 215.

[17]. A.R. Ashrafi, M. Ghorbani and M. Jalali, *Ind. J. Chem.*, **2008**, *47*, 535.

RHEOLOGICAL CHARACTERISTICS OF BEEF FILLING MIXTURE WITH VEGETABLE OILS

CRISTIAN TUDOSE[a], LIVIA PATRASCU[a]*, PETRU ALEXE[a]

ABSTRACT. In this study, two vegetable oils have been characterized from the rheological point of view (olive and palm). The resulting emulsion from these two oils and also a meat mixture obtained by replacing animal fat with vegetable fats were rheologically analysed in order to observe structure changes caused by totally replacing animal fat with vegetable ones. Experimental data have shown that an emulsion from these two oils could be appropriate for using in meat industry but at a higher rate of olive oil. The emulsified mixture from beef and oils behaved rheologically as a solid material, temperature ramp test demonstrating that it could be used on a large scale in meat industry in order to obtain a dietetic product.

Key words: beef; emulsion; olive oil, palm oil, rheology, viscosity.

INTRODUCTION

During this period researchers are seeking an ideal formula resulting from the combination of fats with superior nutritional characteristics, formula that will lead to the development of new types of foods which are balanced in nutritional and biological values [1-3].

Vegetable oil fats in comparison to animal fats are better in terms of nutrition composition due to the presence of unsaturated fatty acids, but may affect product organoleptic properties, when referring to meat and products manufactured from chopped or restructured meat. However there is considered that meat industry is the branch of the food industry where animal fat can be successfully replaced with vegetable oils without changing quality properties. JIMENEZ-COLMENERO et al., [4] have replaced pork back fat with vegetable oils, especially olive oil, in frankfurters and they obtained a new meat product

---

[a] *Department of Biochemistry, Faculty of Food Science and Engineering, Dunarea de Jos University, 111 Domneasca Street, 800201 Galati, Romania.*
Corresponding author: Tel:+40743261889; e-mail: livia.mantoc@ugal.ro

which had a reasonable level of flavour and juicy and overall the product was very close to a standard one, without changes in terms of organoleptic characteristics. Also, according to BABJI et al., [5] and TAN et al., [6] palm oil in meat products enhances the sensory qualities of the product.

It should be also recalled the key role which plays antioxidants, compounds that protect against degradation due to free radical reactions. The most important nutritional antioxidants mention vitamin E, carotenoids, tocopherols, polyphenols and vitamin C [9, 10].

Biological value of fats depends on the fatty acids they contain, the number and position of double bonds and stereochemical configuration of the molecule ("cis" and "trans" isomers) [11]. Fatty acids composition in foods is important, but must be in connection with the role of phospholipids, sterols and fat-soluble vitamins which contributes substantially to the biological action of fat [12]. From nutritional point of view the optimal ratio for fatty acids is: 33 % of saturated and unsaturated fats, 34 % of oleic acid (Omega-9), 27.5 % of linoleic acid (Omega-6) and 5.5 % of linolenic acid (Omega-3) [13, 14]. Because in animal fats there are no unsaturated fatty acids Omega-3 and Omega-6, in order to ensure optimal ratio mentioned above we need to replace these animal fats with vegetable fats partially containing these PUFAs [15]. A dietary product must have selected qualities in order to be suitable for human health. To obtain a dietetic product animal fat (which has a high content of saturated fatty acids and cholesterol) can be replaced with vegetable fats rich in unsaturated fatty acids (Omega-3 and Omega-6), antioxidants and cholesterol [19, 20].

According to a recent research addition of palm oil in meat products enhanced its sensory qualities [19]. However vegetable oils from various sources have been reported to differ significantly from physical point of view, thus when added to meat products, some quality characteristics could be affected [21, 22]. When incorporating fats that are difficult to stabilize, pre-emulsion is generally used (oil in- water emulsion with an emulsifier, typically a protein of non-meat origin) [1]. Taking into account that there are many factors that can affect stability of such a product knowing rheological characteristics in different conditions is a requisite. CHOI et al., [22] concluded that the replacement of up to 50% pork backfat with pre-emulsified vegetable oil in meat batter formulations significantly affected rheological and composition of unheated meat batters.

Given the increasing demand for meat products with improved nutritional qualities and because fats play a very important role in the organoleptic qualities of meat products we aimed to substitute all animal fat from a meat based foodstuff with a pre-emulsion obtained from vegetable oils. Concerning

88

utilization of olive and palm oils in meat industry most of the existed studies focused on single oil types. Olive oil was investigated as a possible animal fat replacement by LURNENA-MARTINEZ et al., [3], VUARL et al., [4], PAPPA et al., [22]. Regarding palm oil, there are also many researches [18, 23, 24, 25]. However, given the structure difference between olive and palm oils, no study investigated the possibility of coupling these two oils in order to obtain a stable pre-emulsion. Thus, the aim of this study was to identify a suitable vegetable oil emulsion from rheological standpoint that could be suitable for replacing animal fat in meat products based on minced meat.

RESULTS AND DISCUSSION

Physico-chemical characteristics of extra virgin olive oil and palm oil

Physico-chemical analysis results showed that both oils had very good characteristics and complied with the regulations (Table 1).

Table 1. Physico-chemical characteristics of studied oils

Quality characteristics	Extra virgin olive oil		Palm oil	
	Bulletin	Test	Bulletin	Test
Acidity value (mg NaOH /g)	0.43	0.56±0.02	0.10	0.23±0.02
Peroxide value (ml sodium thiosulfate 0.01n /g)	12.60	11.78±0.02	9.20	10.10±0.02
TBA value (mg malon aldehyde /kg)	-	1.085±0.01	-	0.235±0.02
Humidity (%)	-	0.02±0.04	-	0.01±0.04

Values represent means of three replicates± Standard Deviation

Rheological behaviour of olive oil

Figure 1 presents results obtained for oscillatory and flow tests describing olive oil rheological characteristics. Regarding oscillatory tests it can be seen the existence of the viscous or terminal region until 4 Hz were G`` predominates and the viscous (flow) behaviour prevails [26]. The crossover frequency at which G` = G`` (a measure of the longest relaxation time), was registered at 5 Hz (G`= 1.289 Pa and G`` = 1.065 Pa), after which elastic behaviour dominated. This means that when applying low strain values (0.5%) for longer times tested oil will respond as a viscous

material and will begin to flow. Shift angle (δ) values confirmed that at longer times olive oil will behave as a perfect liquid (90°), heading to solid (elastic) behaviour at short times, higher frequencies respectively.

When subjected to flow, over the range of 0.1-100 s^{-1} olive oil presented a Newtonian behaviour, like the majority of edible oils [27]. The rate index determined by applying Power Low equation was 0.99 when increasing shear rate and 1.00 when decreasing shear rate and the overall viscosity was 0.03805 Pa*s. At a constant temperature of 25 °C the resulted shear stress values formed a line whose slope was a measure of viscosity not showing any thixotropy phenomenon, and viscosity values remaining constant throughout experiment.
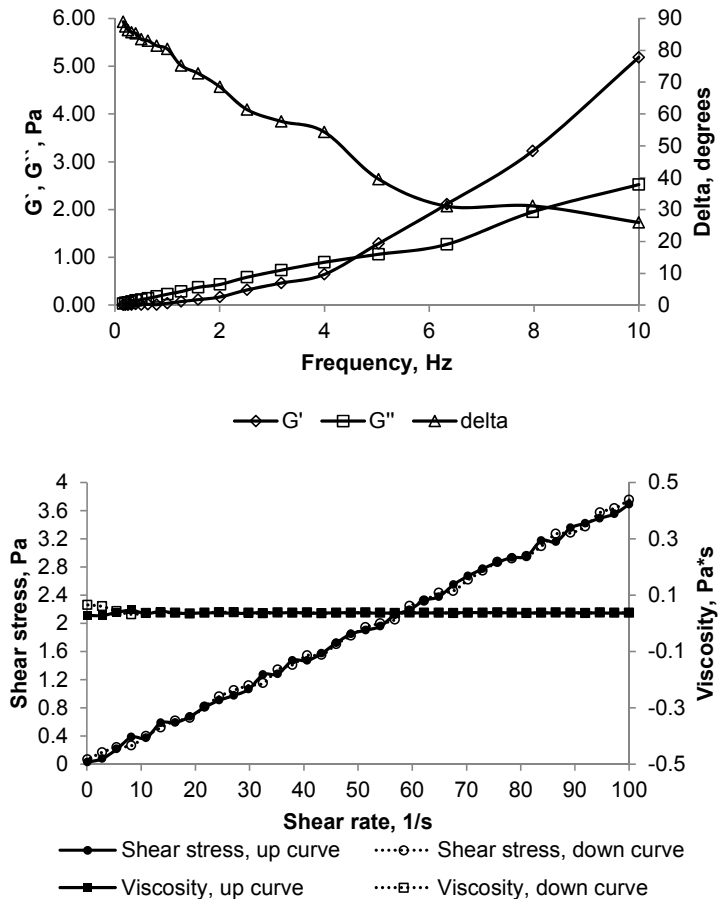

Figure 1. Rheological behaviour of extra virgin olive oil under frequency sweep and flow tests

Rheological behaviour of palm oil

Palm oil rheological characteristics are presented in figure 2. It can be seen that unlike olive oil, at longer times (lower frequency) it presented an elastic behaviour.

The cross over point (G` = G``) was registered similar to olive oil at the same frequency domain. Also higher values for both G` and G`` were recorded for palm oil comparing to olive one (278 Pa at crossover point). Delta values confirmed the elastic (solid) behaviour of palm oil, rising from 30° to 50° throughout the experiment. KALOGIANNI et al., [27] had investigated different oils for rheological characterisation and identified palm oil to have a Newtonian behaviour, however their analysis had been performed at a higher temperature of 50°C.
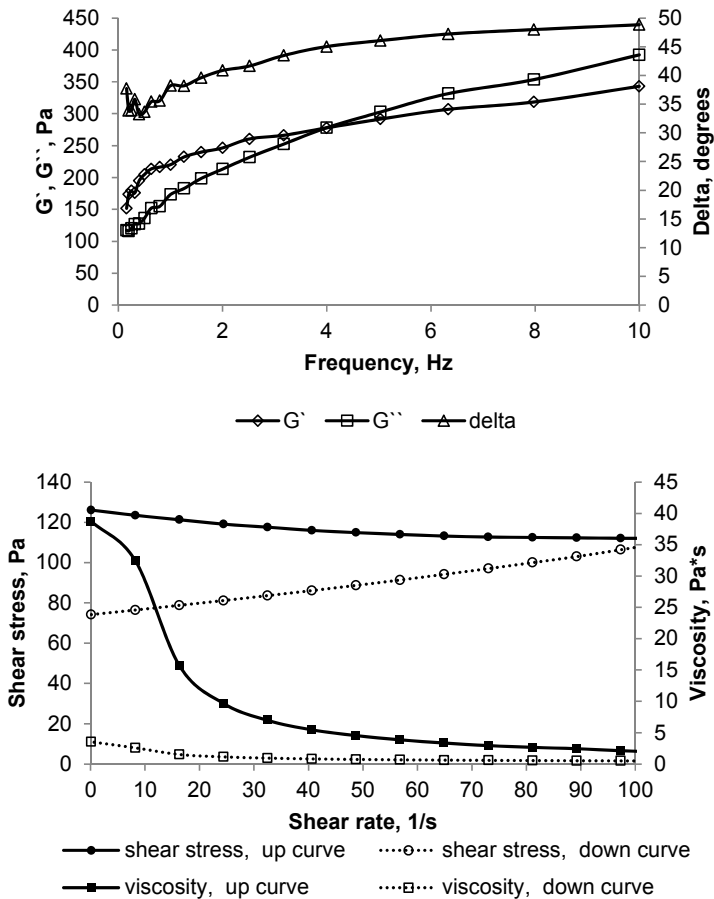

Figure 2. Rheological behaviour of palm oil under frequency sweep and flow tests

Besides shear thinning behaviour (decreasing viscosity when subjected to increasing shear rates), data recorded for flow conditions reported an unstable structure, it being unable to recover when shear rate was decreased to initial $0.1s^{-1}$. By applying Power Low equation, a hysteresis area of 31930 Pa/s was calculated. More, rate index for the up curve was 4.83×10^{-8} increasing till 0.6243 for the down curve, so according to rate index values we can conclude that palm oil in tested conditions presented a shear thinning behaviour. Viscosity values for tested palm oil presented significantly different values ($p<0.05$) for up and down curves, as shown by Power Low equation, namely 170.9 Pa*s versus 2.88 Pa*s. The beginning of flow required a rather high yield stress which resulted to be 235.9 Pa, calculated with Bingham equation.

Rheological behaviour of pork backfat

In order to compare oils rheological behaviour to usually used animal fat in meat technology, minced pork backfat (80μm particle size) was subjected to same conditions of testing. From figure 3 it can be seen that despite vegetable oils, animal fat did not present a crossover point, material being more elastic like.

G` values overcome those of vegetable oils, beginning from 2386 Pa till 6527 Pa at the end of the experiment.

A shear thinning behaviour was observed when subjected to flow (rate index = 1.86×10^{-8} for the up curve and 0.037 for the down curve). However, despite palm oil, animal fat had a more stable structure, viscosity values having a reversible tendency when decreasing shear rate, with a lower hysteresis area (12410 Pa/s). As indicated by the Power Low equation, viscosity value was 227.8 Pa*s for the up curve and 90.80 Pa*s for the down curve. The beginning of flow in case of animal fat required a yield stress of 227.3 Pa, calculated with Bingham equation. Viscosity Similar to our findings ALVAREZ et al., [28] also reported for frankfurters made with backfat a higher consistency and lower resistance to structure failure than vegetable oil emulsions.
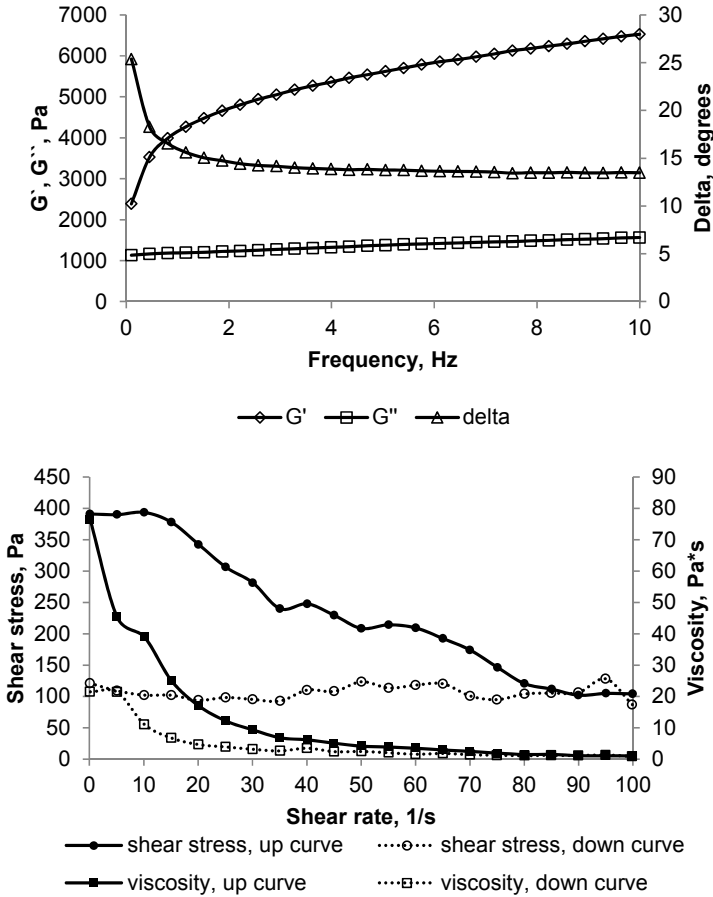
Figure 3. Rheological behaviour of pork backfat under frequency sweep and flow tests

Rheological behaviour of olive-palm oil pre-emulsion

The ideal combination between extra virgin olive oil and palm oil for a more stabilized emulsion was observed to be at a higher percentage of extra virgin olive oil (70/30). Because palm oil present solid characteristics up to a temperature of over 20 $^{\circ}$C it can give instability to emulsion, therefore palm oil must be added carefully as the last piece. Rheological characteristics during flow and oscillatory tests were represented in figure4.
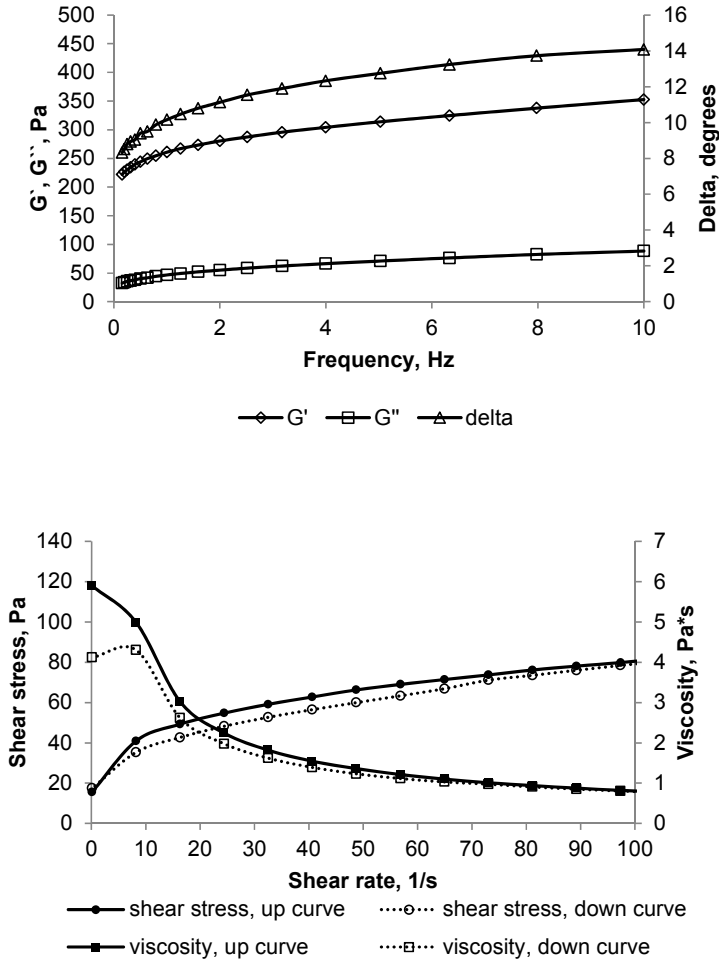
Figure 4. Rheological behaviour of the olive - palm oil pre-emulsion under frequency sweep and flow test

Oscillatory test of frequency sweep presented a solid like behaviour for the analysed emulsion similar to pork backfat. Shift angle had an increasing tendency over the tested frequency range similar to palm oil, with values ranging from 8 to 14°. Besides a higher G` modulus for the entire test, values were lower than those registered for animal fat, being closer to those of palm oil.

The stability of the obtained pre-emulsion could be observed during flow test. The hysteresis loop of shear stress had a rather low value, of only 320.0 Pa/s and the yield stress, given by Bingham equation, at which the emulsion began to flow had the value of only 50.88 Pa. Viscosity values for the up and down curves given by Power Low equation had much closer values in comparison with pork backfat or palm oil, namely 20.71 versus 16.01 Pa*s. Given the results we could appreciate that this pre-emulsion would have the adequate stability in a meat matrix in order to resist a technological process.

Rheological characteristics of meat - oil matrix

The most important objective of the experiment was to maintain the main properties of the meat emulsion by replacing pork backfat with a vegetable oil pre-emulsion. In order to do that, meat–oil rheological characteristics (Figure 6) were compared with a standard meat–animal fat mixture (Figure 5). Similar to olive–palm oil pre-emulsion, meat composition obtained with pork backfat showed elastic behaviour when subjected to frequency sweep test with G` > G`` for the entire tested frequency range.

Rheological tests of temperature sweep are usually used for observing material behaviour during heat treatment, one being able to determine proteins` nature without destroying the colloidal system [29]. The inflection point, were there is supposed myosin denaturation occurs was recorded near 46 °C, at G` = 1018 Pa, after which, the elasticity continued to rise progressively until the end of the heat treatment. For both moduli (G` and G``) the shoulder peak was recorded around 60 °C, after which elastic modulus increased rapidly highlighting the transformation from a viscous sol to an elastic gel network. Samples` solid like structure was confirmed also by delta values, which decreased from 15 to 9° at the end of the temperature ramp test. PATRASCU et al., [30] stated that meat emulsified systems containing animal fat and carrageenan showed a solid like behaviour and when subjected to temperature ramp test, inflexion point of protein denaturation started just after 40 °C till 60 °C. ÁLVAREZ, et al., [28] stated that the exact magnitude of G′ rheograms, especially at around 60 °C and at the end of heating, was influenced by the fat type and the specific ingredient added.
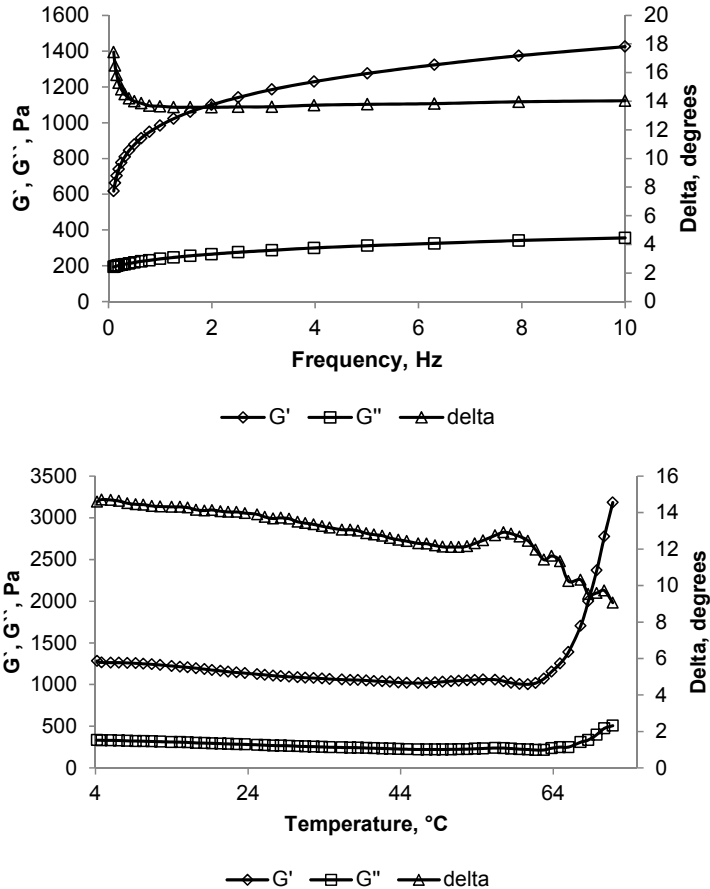
Figure 5. Rheological characteristics of control (meat-pork backfat) emulsified system

As one can see from figure 5 and 6 there are a lot of similarities between behaviour of beef mixture with pork backfat and beef mixture with vegetable oils pre-emulsion, the only difference being viscoelasticity values, much lower than in first case.

Although for G` were recorded values under 150 Pa, shift angle (δ), fitted under 30° for frequency sweep test and beneath 20° for temperature ramp test confirming that our mixture had a solid like behaviour. Thus there must be mentioned that during temperature rising beef composition with vegetable oil did not expel technological water added to the system, mixture remained stable and formed a nice slice of frankfurter at the end of the test.
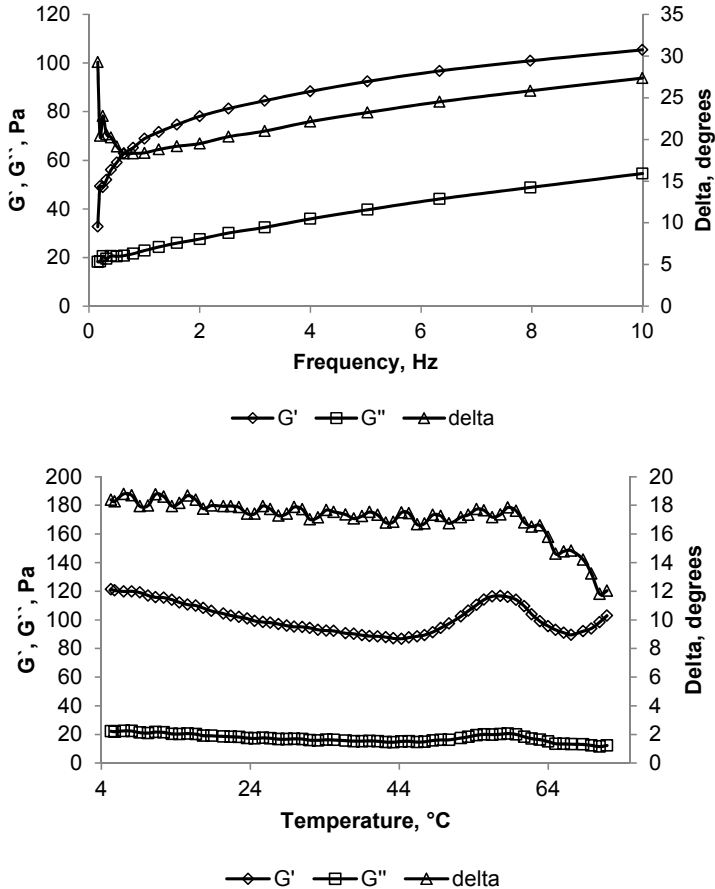
Figure 6. Rheological characteristics of meat–oil emulsified system

CONCLUSIONS

Our objective was to investigate the possibility of obtaining new meat products with improved nutritional qualities by using new advanced technologies with standard organoleptic properties.

After analysing both oils rheological parameters, we could conclude that the selected pre-emulsion of two vegetable oils (70/30 olive and palm) have features that are appropriate for partial or total replacement of animal fat in meat products and obtaining a meat product with superior nutritional

qualities. Results demonstrated that the new meat matrix had similar rheological properties to a standard product (meat emulsion with animal fat) even after the heat treatment. Thus, a meat product (frankfurter like) with total replacement of animal fat can be a possible dietetic one produced on large scale (meat industry).

Further analyses are however needed in order to observe final product stability and sensorial characteristics.

EXPERIMENTAL SECTION

Frozen beef (a mixture of *Adductor*, *Biceps femoris* and *Gracilis* muscles) was taken from a local meat distributor. Beef was slowly thawed in refrigerated conditions at +4 ^{o}C for 24 hours. Two types of oil were used in this study: palm oil (Indochina) and extra virgin olive oil (Emilio Vallejo, Spain). Extra virgin olive oil and palm oil were tested in order to confirm the analysis bulletins results.

Preparation of oil-in-water emulsion

In this study five different proportions of oil/palm oils were considered for obtaining a stable pre-emulsion at the following ratios of extra virgin olive oil and palm oil: 30/70; 40/60; 50/50; 60/40 and 70/30. For stabilizing the composition 15% of soy protein isolate was added to each sample (91% protein concentration) (Supro EX37–Solae Europe Belgium).

Pre-emulsions stability was observed over a period of 4 hours at +4°C in resting conditions. Thus, only one version presented emulsion stability at the end of the resting period, namely the pre-emulsion obtained from 70% of extra virgin olive oil with 30% olive oil. It`s rheological characteristics were further analysed and discussed in the results section. Also the mentioned oils ratio was incorporated in meat system in order to investigate the possibility of obtaining a functional product.

Experiment design and mixture preparation

For technological samples, thawed beef (Dry matter = 25.7%) was coarse chopped in a mincing devise (Wolf) up to 3 mm particle size than mixed with sodium chloride (1.8 kg/100 kg meat), sodium nitrate (15 g/100 kg meat) and ice (10 kg/100 kg meat), after which the composition was let to age for 24 hours at +5 ^{o}C.

After 24 hours the composition was further chopped in a cutter (3000 rot/min) for 4 minutes. In the same time progressively were added sodium tripolyphosphate (0.4 kg/100 kg meat) and the oil pre-emulsion (70/30 ratio of extra virgin olive oil and palm oil) at +2 $^{\circ}$C, in proportion of 30%). The temperature was maintained by adding ice (10 kg/100 kg composition). At last spices were added (pepper, nutmeg, garlic). The final proximate composition of the recipe per 100 kg was: 58.33 kg beef; 25 kg oil pre-emulsion; 16.66 kg water.

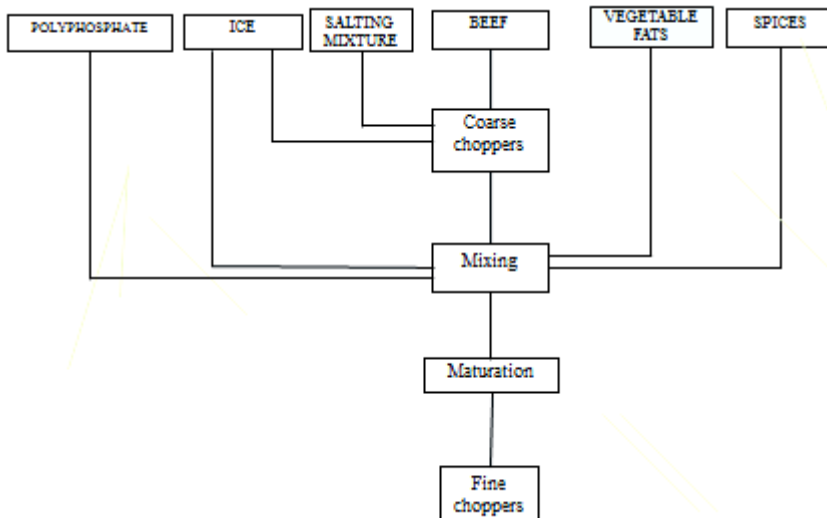The technological scheme applied is shown in figure 7:

Figure 7. Technological scheme for obtaining a meat mixture with vegetable fats

Rheological analysis

Rheological characteristics were determined with an AR2000ex rheometer (TA Instruments, Ltd). Analyses were performed using a cone - plate geometry with 40 mm in diameter and 2° cone angle. A gap of 1500 μm was used. Oscillatory tests were used for analysing samples rheological characteristics. First a strain sweep test was used in order to determine the viscoelastic domain, after which all following tests were performed at a controlled strain of 0.5%. Then, a frequency sweep step was applied, increasing oscillation frequency from 0.1 to 10 Hz in order to observe the behaviour of viscoelastic modulus G` and G``, together with shift angle (δ).

When the material is completely elastic the phase angle δ will be close to 0° and when is completely viscous the phase angle δ will be 90 ^{o}C. A good emulsion must have a proportional change of G' and G" moduli [5].

Structure changes of meat-oil mixture during technological heat treatment was studied by applying a temperature ramp test were temperature was increased from 10 to 72 ^{o}C controlled with a Peltier plate system.

In order to observe flow behaviour of tested oils, pork backfat and oil emulsions, a stepped flow step was applied and shear rate was increased from 0.1 to $100s^{-1}$, and then decreased back to $0.1s^{-1}$. Temperature was set to +25 ^{o}C observed to be the lowest temperature at which palm oil had a suitable consistency in order to be able to flow, more it is commonly considered for product utilization as a foodstuff [1]. Tests were performed in triplicate and mean values were represented in graphs. After every test a new sample was used. Data were analysed using TA Rheology Advantage Data Analysis Software V 4.8.3 and the mathematical models of Power Low and Bingham equations were used when necessary.

ACKNOWLEDGEMENTS

REFERENCES

[1]. F. Jimenez-Colmenero, *Trends in Food Science and Technology*, **2007**, *18*, 567.
[2]. J.G. Bloukas, E. D. Paneras, *Meat Science*, **1997**, *45*, 133.
[3]. I. López-López, S. Cofrades, C. Ruiz-Capillas, F. Jiménez-Colmenero, *Meat Science*, **2009**, *83*(2), 255.
[4]. F. Jimenez-Colmenero, A. Herrero, T. Pintado, M.T. Solas, C. Ruiz-Capillas, *Food Research International*, **2010**, *43*, 2068.

[5]. A.S. Babji, A.R. Alina, M.S.A. Yusoff, W.I. Wan Sulaiman, *Meat International*, **2001**, *11*(2), 26.

[6]. S.S. Tan, A. Aminah, X. G. Zhang, S. B. Abdul, *Meat Science*, **2006**, *72*(3), 387.

[7]. P. Howe, B. Meyer, S. Record, K. Baghurst, *Nutrition*, **2006**, *22*(1), 47.

[8]. E.D. Paneras, J.G. Bloukas, D.G. Filis, *Journal of Muscle Foods*, **1998**, *9*(2), 111.

[9]. S. Lee, C. Faustman, D. Djordjevic, H. Faraji, Decker, *Meat Science*, **2006**, *72*(1), 18.

[10]. K. Arhiara, *Meat Science*, **2006**, *74*, 219.

[11]. O. Tokusoglu, M. Kemal Unal, *Pakistan Journal of Nutrition*, **2003**, *2*(3), 196.

[12]. I. López-López, S. Cofrades, F. Jiménez-Colmenero, *Meat Science*, **2008**, *83*(1), 148.

[13]. F. Jiménez Colmenero, J. Carballo, S. Cofrades, *Meat Science*, **2001**, *59* (1), 5.

[14]. G. Delgado-Pando, S. Cofrades, C. Capillas, M. T. Solas, J. Colmenero, *European Journal of Lipid Science and Technology*, **2010**, *112*(7), 791.

[15]. J.G. Bloukas, E.D. Paneras, *Journal of Food Science*, **1993**, *58*(4), 705.

[16]. C. Yun-Sang, C. Ji-Hun, H. Doo-Jeong, K. Hack-Youn, L. Mi-Ai, K. Hyun-Wook, J-Y. Jeong, K. Cheon-Jei, *Meat Science*, **2009**, *82*(2), 266.

[17]. J. Ambrosiadis, K.P. Vareltzis, S.A. Georgakis, *International Journal of Food and Technology*, **1996**, *31*(2), 189.

[18]. A.S. Babji, A.R. Alina, M.Y.S. Chempaka, T. Sharmini, R. Basker, S.L. Yap, *International Journal of Food Science and Nutrition*, **1998**, *49*(5), 327.

[19]. E. Muguerza, D. Ansorena, I. Astiasaran, *Journal of the Science of Food and Agriculture*, **2004**, *84*(9), 1061.

[20]. E.J. Margues, E.M. Ahmed, R.L. West, D.D. Johnson, *Journal of Food Science*, **1998**, *54*(4), 867.

[21]. Paneras, E.D. & Bloukas, J.G., Journal of Food Science, **1994**, *59*, 725.

[22]. Choi, Y.S., Choi, J.H., Han, D.J., Kim, H.Y., Lee, M.A., Kim, H.W. & Kim, C.J., *Meat Science*, **2009**, *82*(2), 266.

[23]. Wan Rosli, A.S. Babji, A. Aminah, S.P. Foo, O. Abd Malik, *Journal of Food Lipids*, **2006**, *13*(2), 186.

[24]. S.S. Tan, A. Aminah, X.G. Zhang, S. B. Abdul, <u>*Meat Sci.*</u> **2006**, *72*(3):387.

[25]. A.S. Alina, A. Siti Mashitoh, A.S. Babji, I. Maznah, K.M.W. Syamsul and Y. Muhyiddin, *World Applied Sciences Journal*, **2012**, *17*, 62.

[26]. H.A. Barnes, "A Handbook of Elementary Rheology". Institute of Non-Newtonian Fluid Mechanics, *University of Wales*, **2000**, chapter 13.

[27]. Kalogianni, E.P., Karapantsios, T.D. & Miller, R., *Journal of Food Engineering*, **2011**, *105*(1), 169.

[28]. Álvarez, D., Xiong, Y.L., Castillo, M., Payne, F.A. & Garrido, M.D., *Meat science*, **2012**, *92*(1), 8.

[29]. M.H. Tunick, *Journal of Agricultural and Food Chemistry*, **2011**, *59*, 1481.

[30]. L. Patrascu, I. Dobre, P. Alexe, S*tudia UBB. Chemia*, **2010**, *LV*, 3.

[31]. Babji, A.S. Alina, A.R., Yusoff, M.S.A. & Wan Sulaiman, W.I., *Meat International*, **2001**, *11*(2), 26.

INDOOR AIR BTEX MEASUREMENTS

DIANA FLORESCU[a], MONICA CULEA[a], PAULA PODEA[b*]

ABSTRACT. An improved quantitative method was used for measuring benzene, toluene, ethyl benzene, *m/p*-xylene and *o*-xylene (BTEX)] by preconcentration on active charcoal followed by gas chromatography-mass spectrometry (GC/MS) analysis. The selected ion monitoring (SIM) mode was used for the quantitative GC/MS analysis. The internal standard used was stable isotopically labeled benzene. The compounds of interest were eluted in 7.5 min. The method is simple, rapid and shows good validation parameters (linearity, precision and accuracy) for the studied compounds. The method was tested for the investigation of the indoor emissions from different materials and furniture. The results showed that attention should be paid to the new furniture and to the inflating indoor of the new vacuum packed mattresses.

Keywords: GC/MS, BTEX, isotopic dilution, SIM

INTRODUCTION

Benzene, toluene, ethyl benzene and xylene (BTEX) are widespread pollutants having as main sources the vehicle traffic in the outside environment and the cigarette smoke in the indoor environment. They are also present in small quantities in drinking water and food, in painting substances or adhesives. The high toxicity of aromatic hydrocarbons, especially of BTEX, present in gasoline, paint thinner, glue and adhesive products and used as solvent, is well known. The chronic exposure to benzene and other aromatics, followed by their vapor inhalation, could cause disorders in the central nervous system and gastrointestinal tract, but the most relevant consequences of chronic poisoning are anemia and leukemia [1, 2]. The effects of indoor air pollution on human health are of high concern. The minimal risk level (MRL) is estimated for the human exposure/day to a hazardous substance that is without appreciable risk of adverse non-cancer health effects over a specified

[a] *Babes-Bolyai University, Faculty of Physics*
[b] *Babes-Bolyai University, Faculty of Chemistry and Chemical Engineering, Kogalniceanu str. No. 1, RO-400084 Cluj-Napoca, Romania,* *Corresponding author: mpaula@chem.ubbcluj.ro*

duration of exposure [3]. Environmental Protection Agency estimated that 13 - 45 µg m^{-3} BTEX in air may be responsible for developing cancer [4, 5]. The outdoor maximum limit recommended for benzene by the European Community is 10 µg·m^{-3} [6]. Occupational maximum exposure limit is 16 mg·m^{-3} [7]. A major class of contaminants of indoor air, the volatile organic compounds (VOCs), may be up to 10 times higher indoors than outdoors. This indicates contributions from indoor sources such as furniture wax, smoking, paints, glues, carpets and also breathing or body odor. These chemical mixtures are recognized as causative agents of "building-related illness" or "sick-building syndrome" [8]. The methods used for volatile organic compounds sampling presume preconcentration of samples on adsorbents. All the methods vary from each other according to the sampling technique, type of sorbent, method of extraction and detection technique [9, 10]. BTEX have been considered as hazardous by the amendments of 1990 in the Clean Air Act (USEPA 1990). Benzene was classified as human carcinogen of Group A [11]. Since most people spend almost 90% of their time inside a building, indoor air pollution is a significant concern. Recent data indicate that asthma and allergies in children are most pronounced in the developed countries [12].

Gas chromatography (GC) and gas chromatography-mass spectrometry (GC/MS) are the most used quantitative methods for VOCs levels determination in the air [1-30].

The aim of the present work was to improve and apply a GC/MS method to evaluate the toxic aromatic ambient pollutants. The internal standard used was stable isotopically labelled benzene. The GC/MS method was used in the selected ion monitoring (SIM) mode for determining the levels of indoor air BTEX concentrations.

RESULTS AND DISCUSSION

The GC/MS method developed for BTEX determinations in indoor air is simple and rapid. The mass spectrometer operating in the SIM mode gave a high selectivity and specificity to the method developed, which allowed the peak deconvolution of benzene and its deuterated analogue internal standard, as they were co-eluting in the total ion chromatogram. Also SIM mode offers higher sensitivity than the scan mode. The validation of the method gave good values for precision, R.S.D. of 3.02 – 18.75 % and accuracy, between 0.59 - 17.8% in the case of deuterated benzene used as internal standard in comparison with the case of using pyridine as internal standard, when precision was lower than 25.8%, and accuracy was lower than 24.9% [24]. The limit of detection for BTEX was of 0.01µg. By using active charcoal cartridges for BTEX determination, the extraction method is rapid and inexpensive.

The linearity parameters obtained for BTEX in the range 0 – 80 µg by using deuterated benzene as internal standard are presented in Table 1 and Fig.1 in comparison with BTEX linearity parameters obtained for BTEX in the range 1-100 µg by using pyridine as internal standard. Very good coefficients of regression were obtained for deuterated benzene internal standard (r > 0.99) in comparison with those obtained with pyridine as internal standard (r>0.90). Precision, calculated by using deuterated benzene as internal standard for the aliquot samples of 40 and 80 µg, showed R.S.D. values between 13.13 – 18.75 % and respectively between 3.02 - 6.41%. The accuracy R.S.D. calculated values were between 2.5 - 17.7 % for the sample of 40 µg and between 0.59 - 17.8 % for the sample of 80 µg. In the case of using pyridine as internal standard, precision and accuracy were lower than 25.8%, respectively 24.9% [24].

Table1. Linearity for BTEX

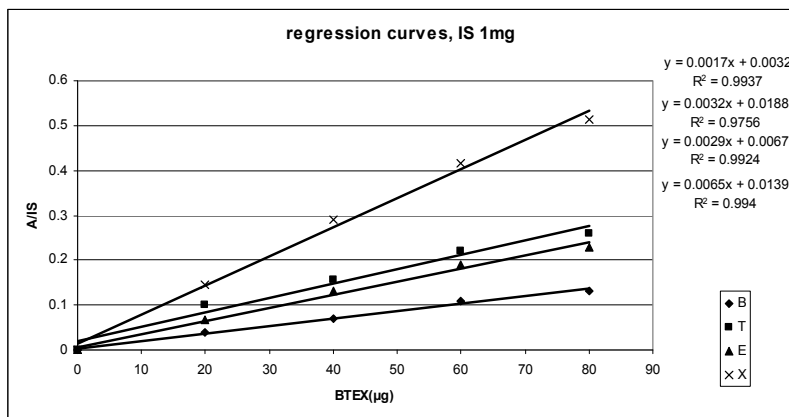| Range: 0-80µg (IS: 1mg deuterated benzene)		
Compound	Regression curve	r
B	y=0.0017x+0.0032	0.997
T	y=0.0032x+0.0188	0.988
E	y=0.0029x+0.0067	0.996
X	y=0.0065x+0.0139	0.997
Range: 0- 100µg (IS: 1mg pyridine)		
B	y=0.0016x+0.0067	0.998
T	y=0.005x+0.8572	0.908
E	y=0.0137x+0.7655	0.962
X	y=0.0266x+1.6832	0.966

Fig.1. Regression curves for BTEX by using deuterated benzene as the internal standard

105

Table 2 presents the results obtained for precision and accuracy. A limit of detection of 0.01 μg was obtained for the studied VOCs.

Table 2. Precision and accuracy of the method for indoor air BTEX

Compound n	Added	Concentration(μg)	Measured		Comp/IS SD	Precision RSD(%)	Accuracy (%)
B	4	40	45.18	0.08	0.01	12.50	12.94
T	4	40	41.00	0.15	0.02	13.33	2.50
E	4	40	42.05	0.13	0.02	15.38	6.29
X	4	40	47.09	0.32	0.06	18.75	17.73
B	3	80	80.47	0.14	0.009	6.43	0.59
T	3	80	91.00	0.31	0.01	3.22	13.75
E	3	80	94.24	0.28	0.02	7.14	17.80
X	3	80	74.28	0.50	0.02	4.0	6.52
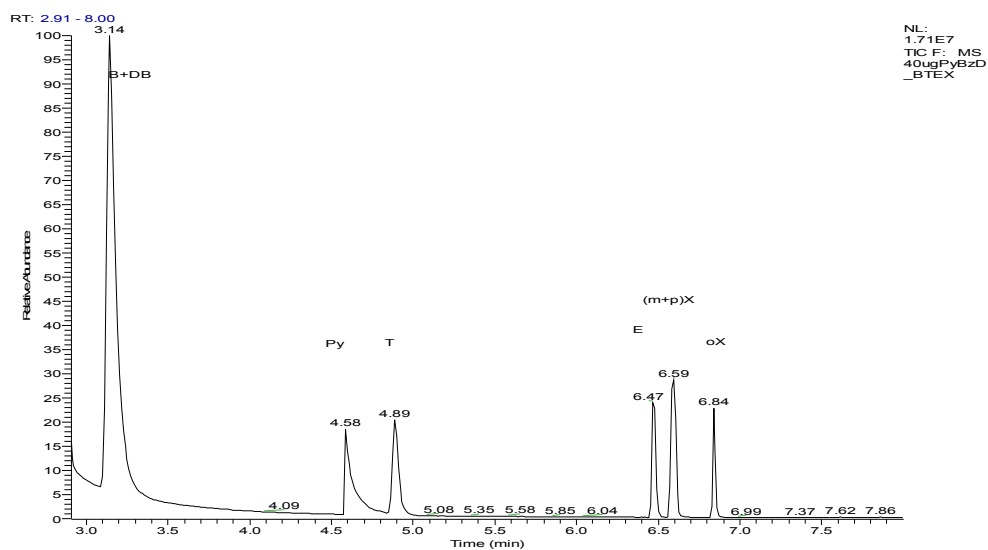
Fig. 2. Chromatographic separation of BTEX and the internal standards, deuterated benzene (DB) and pyridine(Py). The temperature program, 7.5 min: $33^{o}C$ (2 min), $10^{o}C/min$ to 70 ^{o} C then $50^{o}C/min$ to $200^{o}C$, SIM mode.

The separation chromatogram for BTEX in the SIM mode, with the both internal standards added, is presented in Fig. 2. A 7.5 minutes temperature program was used. Fig. 3 presents the chromatograms of BTEX (SIM mode, the both internal standards added) found in the air samples collected from

indoor environment, more precisely: close to an opened new furniture box, in a room with new furniture (1 year old, where a vacuum packed mattress was also placed with the new furniture, one year ago) and a bathroom cabinet (one year old).

Table 3 shows the BTEX levels measured in the air contaminated when new furniture (one year old) is brought into a room of the apartment, as well as the indoor pollutants found in the case of a vacuum packed mattress placed in the same room with the new furniture. The indoor air contaminated in the first days, when the furniture was placed in the room, has been kept into the mattress. By jumping on the mattress, the second column in Table 3, similar BTEX values were obtained as in a new furniture box, first column. Without jumping on the mattress, the indoor air BTEX values extracted are smaller in the room with the furniture bought one year ago, as shown in the third column. In the last column, the levels for indoor air were obtained when the cartridge was placed into a bathroom cabinet, one year old.

Table 3. BTEX ($\mu g\ m^{-3}$) determination in some indoor air measurements (n=2)

Compound	new box	room (mattress)	room	bathroom cabinet
B	2021.8	1314.4	4.9	1017.5
T	938.5	659.7	36.5	546.5
E	14.5	15.7	6.5	7.3
X	54.0	48.7	12.6	35.3

Table 4 compares some indoor air values for BTEX measured inside a parked car (4 years old) under sunlight conditions, with their engines turned on and air conditioner opened (first column) and after ten minutes of ventilation (opened windows). The plastic posters of a laboratory, kept in two poster boxes, gave the BTEX values in the last two columns.

Table 4. BTEX ($\mu g\ m^{-3}$) determination in indoor air extracts, n=2)

Compound	car	vent car	poster box 1	poster box 2
B	13.3	15.9	13.9	15.3
T	101.4	114.0	102.9	135.6
E	22.0	24.4	22.4	33.0
X	31.1	37.4	39.2	51.1

Fig. 3 presents the separation chromatograms of BTEX from indoor air extracts near a new box furniture, the indoor air of an apartment room of 15 m^2 with new furniture (one year old, but jumping on the mattress) and into a bathroom cabinet (one year old).

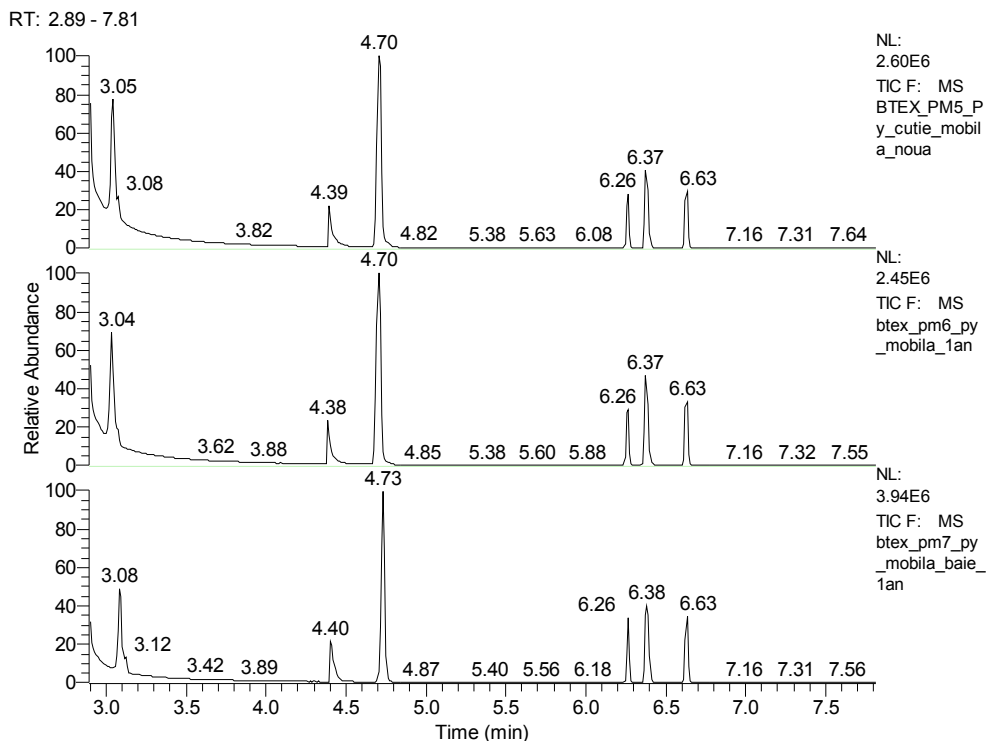**Fig. 3.** Separation chromatograms of BTEX from indoor air extracts near a new box furniture, from the indoor air of a small apartment room of 15 m^2 with new furniture (one year old) and into a bathroom cabinet (SIM mode)

The BTEX values presented in Table 3 and 4 are compared in Fig. 4, especially in order to underline the necessity of marking on the vacuum mattress, when inflate, to be fresh air or an empty room, without any contaminants. It is very important to ventilate the rooms with new furniture, especially in the case of small children rooms.

The BTEX levels in the above applications were also calculated by using pyridine as internal standard and similar results have been obtained.
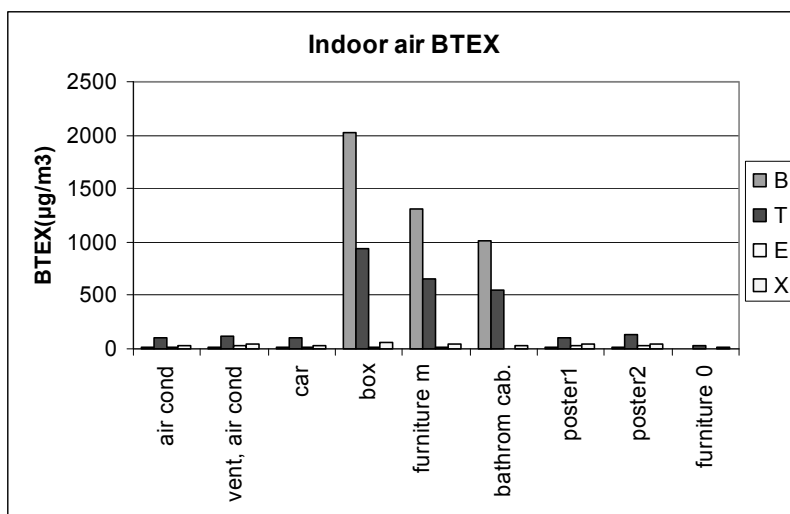
Fig. 4. Comparison of BTEX values (car indoor air, room indoor air, poster boxes; furniture m: jumping on the mattress; furniture 0: no jumping)

The mass spectrometer operating in the SIM mode gave a high selectivity and specificity to the method developed, which allowed the peak deconvolution of benzene and its deuterated analogue internal standard, as they were co-eluting in the total ion chromatogram. Also SIM mode offers higher sensitivity than the scan mode. The validation of the method gave good values for precision, R.S.D. of 3.02 – 18.75 % and accuracy, between 0.59 - 17.8%

The SIM-GC/MS method gave selectivity and specificity allowing the peak deconvolution of benzene and its isotopically labeled analogue. The validation of the method gave good values for precision, R.S.D. lower than 18.75 % and accuracy, lower than 17.8%. The limit of detection for BTEX was of 0.01µg. By using active charcoal cartridges for BTEX determination, the extraction method is rapid and inexpensive.

The method tested for some applications showed BTEX indoor values (µg m^{-3}) in a room and bathroom near new furniture or in the indoor air of a car or boxes containing posters of plastic (Table 3 and 4). Application measurements for precision (R.S.D.) gave lower values than 14 %. The results obtained were higher than BTEX measured in the ambient air in the vicinity of industrial area, where in addition to the traffic emissions, industrial activity enhanced the concentration levels of VOCs [11,15,17,19-21]. The precision of the repeated measurements gave R.S.D. lower than 10 %.

Linearity and precision gave good results in the case of deuterated benzene as internal standard compared with pyridine as internal standard [24]. Similar results for applications were obtained with both internal standards. When the internal standard was deuterated benzene, the intercept values were smaller, consequently we obtained better regression curves.

The BTEX levels inside a parked car, a used vehicle under simulated hot-sunlight conditions, with their engines turned on, showed no apparent health hazard of indoor air of the vehicle. A total of 10.9 mg per cubic meter of VOCs in the new car and 1.2 mg per cubic meter in the old car have been reported [27].

CONCLUSIONS

The GC/MS method developed for BTEX determinations in indoor air is simple, rapid, with high sensitivity, selectivity and specificity. Better linearity was obtained by using deuterated benzene as internal standard than pyridine [24]. The values for BTEX measured close to the new furniture showed higher values than outdoor maximum limit recommended by the European Community, almost the occupational maximum exposure limit. Attention should be paid to room's ventilation and indoor air when inflating a new mattress vacuum packed. Exposure of the sensitive groups as children or pregnant women should be avoided [25-30].

EXPERIMENTAL SECTION

Materials

Carbotrap B, containing active charcoal, was obtained from Supelco, Bellefonte, PA. Deuterated benzene 99.5 atom % was purchased from Alfa Aesar GmBH, Germany. BTEX solution of 2000 ng/ml was purchased from Supelco, Switzerland. All other reagents were from Merck, Germany.

Sample preparation

The cartridges for absorbing BTEX were glass cylinders of 40 mm length, packed with 300 mg of activated charcoal with a particle size of 35–50 mesh. A flow rate of 60 mL·min^{-1} was used for the air samples absorption on active charcoal cartridges. Then the volatiles were extracted in dichloromethane for 2 min. After centrifugation, the internal standard, deuterated benzene (99.5 atom %) was added and 2 µL were injected into the GC.

Method validation

Aliquot samples containing 20, 40, 60 and 80 µg BTEX were adsorbed with a pump on 300 mg active coal at a flow rate of 60 mL$\cdot$min^{-1} and then were extracted in 1ml dichloromethane. 1mg of deuterated benzene was added as internal standard at each sample. For comparison reason, BTEX standards with pyridine as internal standard was adsorbed in the range 0-100 µg BTEX, in the already published conditions [24].

Apparatus

The determination of the BTEX in air samples was performed by using GC/MS analyses. A Trace DSQ Thermo Finnigan quadrupole mass spectrometer coupled with a Trace GC was used. BTEX and the internal standard were separated on a Rtx-5MS capillary column, 30m x 0.25 mm, 0.25µm film thickness, using a 7.5 min temperature program from 33°C (2min), 10°C/min to 70°C, then 30°C/min to 200°C in the SIM mode. The following conditions were used: transfer line temperature: 250°C, injector temperature: 200°C; ion source temperature 250°C; Splitter: 10:1. Electron energy was 70eV and emission current, 100µA [24].

The following important ions from the mass spectra of benzene, toluene, ethyl benzene and xylene were used in the SIM mode m/z 78 for benzene, m/z 91 and 92 for toluene, m/z 91 and 106 for ethyl benzene and xylenes [24], and m/z 84 for deuterated benzene. The method was validated in the 0 – 80 µg range and linearity, precision, accuracy and limit of detection parameters were studied.

The regression curves were obtained as a function of the ratio of BTEX standards peaks areas to internal standard (deuterated benzene or pyridine) peak area against the known quantity of the BTEX standards. Quantitation of the BTEX.was performed by adding the same quantity of the internal standards to the unknown samples and using the calculated regression curves. Benzen was possible to be calculated also by matrix calculation in Excel or isotopic calculation.

REFERENCES

[1]. F. Mangani, L. Lattanzi, M. Attaran Rezai, G. Cecchetti, *Chromatographia*, **2000**, *52*, 217.
[2]. J.F. Collins, *Office of Environmental Health Hazard Assessment*, Berkeley, CA. **2014**.
[3]. S. Wilbur, S. Keith, O. Faroon, *Agency for Toxic Substances and Disease Registry (ATSDR)*, U.S. Public Health Service, U.S. Department of Health and Human Services, Atlanta, GA. **2007**.

[4]. D. Bayliss, J. Jinot, B. Sonawane, *U.S. Environmental Protection Agency, National Center for Environmental Assessment, Office of Research and Development*, Washington, DC. **2002**.

[5]. http://www.epa.gov/ttnatw01/hlthef/benzene.html

[6]. A.L. Theis, A.J. Waldack, S.M. Hansen, M.A. Jeannot, *Anal. Chem,* **2001**, *73*(23), 5651.

[7]. B.M. El-Haj, A.M. Al-Amri, M.H. Hassan, R.K. Bin-Khadem, A.A. Al-Hadi, *J. Anal. Toxicol.* **2000**, *24*(6), 390.

[8]. R.A. Wood, M.D. Burchett, R. Alquezar, R.L. Orwell, J. Tarran, F. Torpy, *Water, Air, and Soil Pollution,* **2006**, *175*, 163.

[9]. A. Kumar, I. Víden, *Environ. Monit. Assess,* **2007**, *131*, 301.

[10]. T.J. Ward, H. Underberg, D. Jones, R.F. Jr. Hamilton., E. Adams, *Environ. Monit. Assess*, **2009**, *153*, 119.

[11]. C.S. Guimaraes, D. Custodio, R.C.S.de Oliveira, L.S. Varandas, G. Arbilla, *Bull. Environ. Contam. Toxicol,* **2010**, 84, 180.

[12]. P.B. Lokhande, V.V. Patil, H.A. Mujawar, *Environ. Monit. Assess*, **2009**, *157*, 51.

[13]. S. Tumbiolo, J.F. Gal, P.C. Maria, O. Zerbinati, *Anal. Bioanal. Chem*, **2004**, *380*, 824.

[14]. A.F.L. Godoi, E.Y. Sawada, M.R.R. de Marchi, R. Van Grieken, R.H.M. Godoi, *Water Air Soil Pollut: Focus,* **2009**, *9,* 163.

[15]. K.H. Jung, F. Artigas, J.Y. Shin, *Environ. Monit. Assess*, **2011**, *173*, 555.

[16]. C. Yoon, K. Lee, D. Park, *Environ. Sci. Pollut. Res*, **2011**, *18*, 333.

[17]. P. Iovino, R. Polverino, S. Salvestrini, S. Capasso, *Environ. Monit. Assess* **2009**, *150*, 437.

[18]. A.J. Clark, J.L. Calvillo, M.S. Roosa, D.B. Green, J.A. Ganske, *Anal. Bioanal. Chem.,* **2011**, *399*, 3589.

[19]. Y.J. Hong, H.A. Jeng, Y.Y. Gau, C. Lin, I. L. Lee, *Environ. Monit. Assess,* **2006**, *119*, 43.

[20]. L.A. Smith, T.H. Stock, K.C. Chung, S. Mukerjee, X.L. Liao, C. Stallings, M. Afshar, *Environ. Monit. Assess*, **2007**, *128*, 369.

[21]. V. Tiwari, Y. Hanai, S. Masunaga, *Air Qual. Atmos. Health*, **2010**, *3*, 65.

[22]. M.P. Baya, E.B. Bakeas, P.A. Siskos, *Indoor Built Environ.,* **2004**, *13*, 53.

[23]. J.M. Kokosa, A. Przyjazny, *J. Chromatogr. A*, **2003**, *983*(1-2), 205.

[24]. M. Culea, O. Cozar, C. Melian, D. Ristoiu, *Indoor Built Environ.,* **2005**, *14*, 241.

[25]. C.P. Weisel, S. Park, H. Pyo, K. Mohan, G. Witz, *J. Expo. Anal. Environ. Epidemiol.,* **2003**, *13*(5), 393.

[26]. I. Aguilera, M. Guxens, R. Garcia-Esteban, T. Corbella, M.J. Nieuwenhuijsen, C.M. Foradada, J.Sunyer, *Environ. Health Perspect,* **2009**, *117*, 1322.

[27]. J.T.M. Buters, W. Schober, J. Gutermuth, T. Jakob, A. Aguilar-Pimentel, J. Huss-Marp, C. Traidl-Hoffmann, S. Mair, F. Mayer, K. Breuer, H. Behrendt, *Environ. Sci. Techno.,* **2007**, *41*, 2622*.*

[28]. P.J. Lupo, E. Symanski, D. Kim Waller, W. Chan, P.H. Langlois, M.A. Canfield, L.E. Mitchell, *Environ. Health Perspect*, **2011**, *119*, 397.

[29]. J. Castellsague, J. Sunyer, M. Saez, J.M. Anto, *Thorax*, **1995**, *50*, 1051.

[30]. P.I. Serrano-Trespalacios, L. Ryan, J.D. Spengler, *J. Expo. Anal. Environ. Epidemiol.*, **2004**, *1*, 118.

ECONOMIC IMPLICATIONS OF CARBON CAPTURE OPTIONS FOR POWER GENERATION BASED ON GASIFICATION

ANAMARIA PADUREAN[a], ANA-MARIA CORMOS[a]*

ABSTRACT. The present paper evaluates, from an economical point of view, pre- and post-combustion capture from gasification power plants. The cases of Integrated Gasification Combined Cycle (IGCC) power plant which uses coal mixed with sawdust and generates about 400 MW net electricity with and without CO_2 capture is presented in detail. The comparison is done considering the most important economic indicators e.g. cost of electricity, CO_2 avoided and removed costs etc. Concerning the total investment cost, the calculation results show that the cost of IGCC with Carbon Capture and Storage (CCS) is higher (pre-combustion capture using Selexol® about 23% higher and post-combustion capture using MEA about 36% higher) than the plant without capture. Also, comparing the two main investigated cases for CO_2 capture process, the results show that the electricity production cost for post-combustion capture technology is about 21% higher than the cost for pre-combustion capture technology; CO_2 captured cost for post-combustion capture technology is about 90% higher than for pre-combustion capture technology and CO_2 avoided cost in the post-combustion capture technology case is increased by a factor of 2.15 than in the pre-combustion capture technology case.

Keywords: Power generation, Carbon Capture and Storage (CCS), Economic assessment.

INTRODUCTION

The important technological transformations in the field of energy conversion and utilization have led to major changes in the economic and social operation of the world [1]. The increased energy consumption is no

---

[a] *Universitatea Babeş-Bolyai, Facultatea de Chimie şi Inginerie Chimică, Str. Kogălniceanu, Nr. 1, RO-400084 Cluj-Napoca, Romania. *Corresponding author: cani@chem.ubbcluj.ro*

longer only associated with the conception of progress, but also with a certain number of threats which reflect on our society and environment. For instance energy supplies presently rely mainly on fossil fuels [2]. If consumption continues at the present rates, the proven reserves represent about 52.9 years for oil, 55.7 years for natural gas and almost 109 years for coal [3-4]. Thus the risks of reduction of fossil energy sources and the impact of energy production from fossil fuels on the environment represent a matter of growing concern [2,5]. In addition to the risks for the environment on a local scale, the world is now faced with the danger of global warming caused by CO_2 emissions. A possible way to limit the risks related to climate change caused by CO_2 emissions is to increase the efficiency of power plants and other energy intensive industrial processes or decrease the energy demand in combination with CO_2 capture and long time storage of at least a large proportion of the CO_2 emitted [6]. The only feasible solution for now remains this carbon capture and storage technologies (CCS) [7].

The introduction of carbon capture and storage into large scale industrial processes is expected to have a significant impact on CO_2 emissions. Gasification technology is an energy conversion method having good potential for capturing CO_2 with the low energy and cost penalties [8]. There are various technologic options to fit the carbon capture unit in a IGCC design e.g. gas-liquid absorption or gas-solid (sorbent) pre- and post-combustion capture configurations [9].

The present paper presents an in-depth economic evaluation of a previous work done in our research group [10-12]. An IGCC power plant, based on coal and sawdust co-gasification to generate 360 – 444 MW net electricity with a carbon capture rate higher than 90% (pre-combustion capture is using mixture of dimethyl ethers of polyethylene glycol Selexol[®] as solvent and post-combustion capture is using monoethanolamine-MEA as solvent) was the basis for the study. The technical description of the investigated technologies (see Figure 1) can be found in the previous published articles [10-11]. The whole power plant concepts were modeled and simulated using ChemCAD software.

The key technical performance indicators presented in previous work [10-12] show that the implementation of CO_2 capture technologies into power plants leads to a substantial reduction of the specific CO_2 emissions for both capture technologies investigated and that the pre-combustion capture technology is more energy efficient than post-combustion capture. In order to have a complete picture and to decide which CO_2 capture technology is the best, an in-depth economical evaluation was conducted. Thus, the present work illustrates a comparison of the current costs of CO_2 capture technologies

in order to assess the relative rankings of the different technologies anticipated to meet the most of the future demand for electricity. A detailed economic assessment was done for pre- and post-combustion capture concepts using gas-liquid absorption. The comparison done using the most important economic indicators e.g. cost of electricity (Levelised Cost of Electricity, LCOE), the cost of CO_2 avoided and the cost of CO_2 captured.
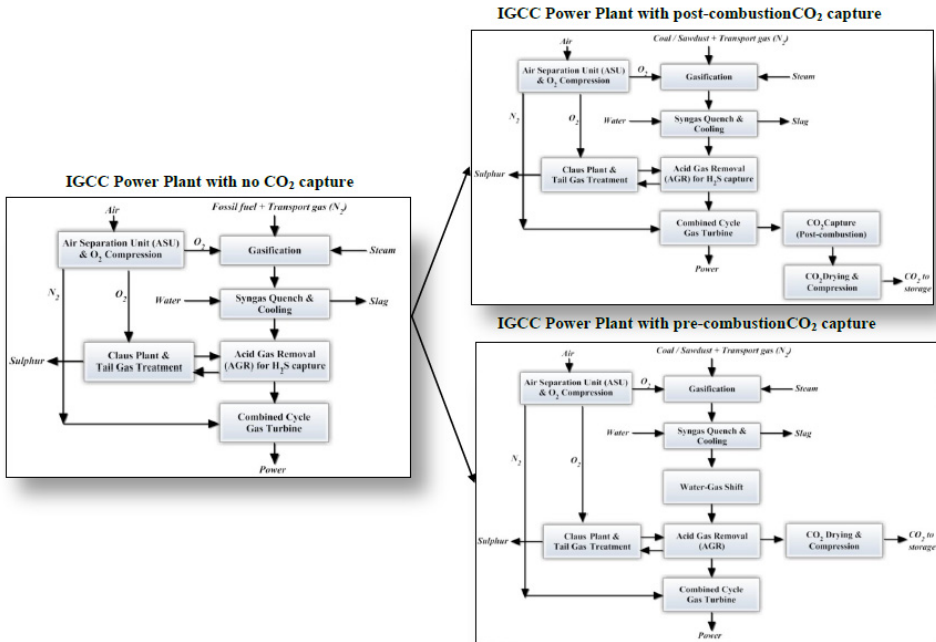

Figure 1. Gasification power plants without and with CO_2 capture
(pre- and post-combustion capture)

RESULTS AND DISCUSSION

1. Capital Costs

Investment cost can be divided into four main parts: on – site investment (which covers process equipment and utility investment), off – site investments, engineering fee and working capital [13]. The cost of a specific item of equipment / plant sub-system can be seen as a function of size, material of construction, design temperature and design pressure. Cost data are often presented as cost versus capacity charts, or expressed as a power

law of capacity (see equation 1), where C_E represents the equipment cost with capacity Q, C_B represents the know the base cost for equipment with capacity Q_B, M is a constant depending on equipment cost and f_M, f_P and f_T are the correction factors for materials of construction, design pressure and design temperature (available in the open literature) [14]. The correction factor values, used for studies, were chosen for carbon steel, design pressure between 0.50 to 7.00 bar and design temperature of 500°C [15-16].

$$C_E = C_B \cdot \left(\frac{Q}{Q_B}\right)^M f_M f_P f_T \tag{1}$$

The technical parameters of various investigated cases (mass and energy balances) were calculated from simulation (for details see [10-11]). Table 1 presents overall plant capital costs estimation of analyzed case studied (Case 1: IGCC without CCS, Case 2: IGCC with Selexol®-based pre-combustion CO_2 capture and Case 3: IGCC with MEA-based post-combustion CO_2 capture.

Table 1. Capital cost estimations for IGCC power plants

Main Plant Data	Unit	Case 1	Case 2	Case 3
Total installed cost	MM €	761.00	932.72	1036.08
Total investment cost	MM €	913.26	1119.26	1243.30
Gross power output	MW_e	519.80	529.79	460.35
Net power output	MW_e	444.72	424.97	359.24
Specific investment cost	€/kW gross	1756.95	2112.65	2700.77
Specific investment cost	€/kW net	2053.57	2633.74	3460.92

As it can be noticed from Table 1, the total investment cost for power plant with pre-combustion capture process using Selexol® (Case 2) is about 22% higher than the cost for the plant without capture (Case 1). The IGCC investment cost scheme with post-combustion process using MEA (Case 3) is about 36% higher than the total investment cost for the plant without capture. The overall capital cost increase for the cases with CO_2 capture is mainly a result of the increase in the overall plant efficiency, which enlarge the gas processing facilities (gasification island, syngas conditioning train etc.) and the ancillary equipment per kW of generated electricity.

116

These results are in accordance with the recent study results of the International Energy Agency [17], Global CCS Institute report [19] and other literature references [19-22]. Comparing these two main cases investigated for CO_2 capture process (pre- and post-combustion capture), the calculation shows that the total investment cost for post-combustion capture is about 11% higher than pre – combustion capture.

2. Operating and maintenance (O&M) costs

Operational and maintenance (O&M) costs cover the cost of fuel (coal and sawdust), auxiliary fuel (natural gas), catalysts, solvents, maintenance costs, manpower costs etc. Usually, the cost of fuel, catalysts and solvents has the largest influence on overall plant economics. These commodities costs are found in trade journals such as Chemical Marketing Reporter and European Chemical News [23].

The operating and maintenance (O&M) costs can be divided in fixed and variable costs (see Table 2). Therefore, for the purpose of this study the fixed O&M costs are estimated to be 0.997 ¢/kWh for the plant without CCS capture, 1.216 ¢/kWh for the plant with pre-combustion CO_2 capture using Selexol® as solvent and 1.419 ¢/kWh for the plant with post-combustion CO_2 capture using MEA as solvent. And the O&M variable costs are assume to be 1.984 ¢/kWh for the plant without CCS capture, 2.369 ¢/kWh for the plant with pre-combustion CO_2 capture using Selexol® as solvent and 2.546 ¢/kWh for the plant with post-combustion CO_2 capture using MEA as solvent.

After the CO_2 has been captured, it must be transported to an appropriate storage site for sequestration (e.g. saline aquifer, depleted oil and gas fields). Pipelines are the primary option for large scale transport, with shipping as a second possibility [24]. According to IPCC 2005 report, generally a range of around $1 – $6/tone of CO_2 stored can be expected [25-26].

Table 2. Operating and Maintenance (O&M) power plants costs estimation

Fixed O&M	Case 1		Case 2		Case 3	
	MM€/y	k€ /kWh	MM€/y	k€/kWh	MM€/y	k€/kWh
Maintenance cost	27.07	8.11	31.47	9.87	32.98	12.24
Direct labor cost	4.76	1.42	5.60	1.75	5.60	2.07
Administrative cost	1.43	0.42	1.68	0.52	1.68	0.62
Total	33.26	9.97	38.75	12.16	40.26	14.94

Variable O&M	Case 1		Case 2		Case 3	
	MM€/y	k€/kWh	MM€/y	k€/kWh	MM€/y	k€/kWh
Fuel	58.60	17.56	65.53	20.56	58.60	21.74
Auxiliary fuel	2.13	0.63	2.13	0.66	2.13	0.79
Make up water	0.17	0.04	0.17	0.05	0.17	0.05
Catalysts	0.50	0.15	1.50	0.47	1.50	0.55
Solvents	0.00	0.00	0.96	0.30	0.99	0.36
Chemicals	1.69	0.51	1.70	0.53	1.73	0.64
Waste disposal	3.09	0.92	3.51	1.10	3.48	1.29
Total	66.17	19.84	75.49	23.69	68.59	25.46

As it can be noticed from Table 2, the total O&M cost (MM€/year) for the IGCC scheme with pre-combustion capture using Selexol® (Case 2) is about 14.89% higher than the cost for the plant without capture (Case 1). The IGCC scheme with post-combustion capture using MEA (Case 3) is about 9.47% higher than the total investment cost for the plant without capture. These results are in accordance with the recent study results of the International Energy Agency [17], Global CCS Institute [18] and NETL [22] reports. Comparing these two main cases investigated for CO_2 capture process (pre- and post-combustion capture options), the calculation shows that the total O&M cost for pre-combustion capture technology is about 4.95% higher than post-combustion capture technology.

3. Plant cash flow, CO_2 emitted – avoided, CO_2 captured costs

After extracting the underlying capital and operating costs that reflect the performance characteristics of each technology, levelised costs of electricity (LCOE) is calculated. The cost of energy from the plant can be evaluated using a discounted cash flow methodology (for more details regarding this method see [14]).

The 25-year LCOE is shown for the evaluated cases in Figure 2.

As it can be seen from Figure 2, the LCOE is largely dominated by capital costs at least 50% of the total in all cases, followed by fuel costs and operating costs. The CO_2 transport and storage LCOE component comprises less than 3% of the total LCOE in both IGCC CO_2 capture cases. The best methods of assessing the profitability of all the investigated cases are based on projections of the cash flows during the plant life. Figure 3 shows the cash flow curves for these investigated processes.
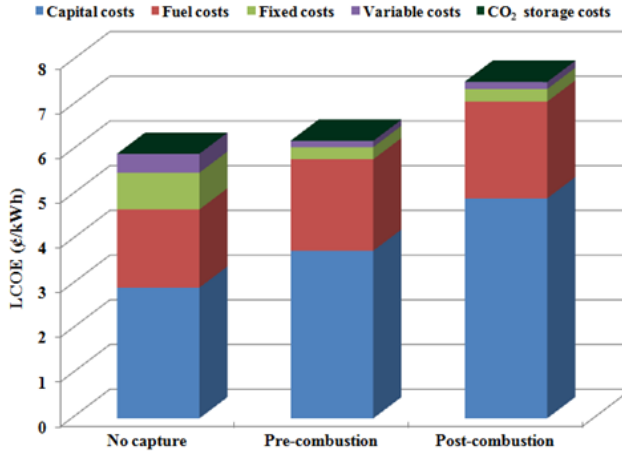
Figure 2. Levelised costs of electricity (LCOE) for investigated power plant cases
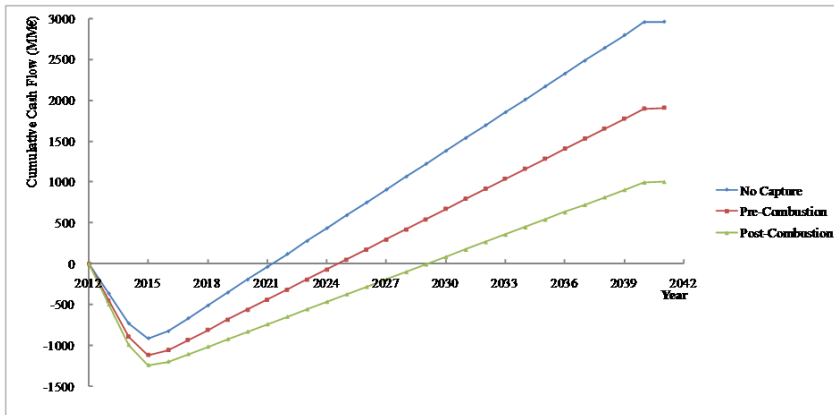

Figure 3. Cash flow curves for power plants without and with CO_2 capture
(pre- and post-combustion capture)

The Figure 3 show the evolution of cumulative cash flow as a function of time in the case of the plant without CCS, the case of pre – combustion capture and the case of post – combustion capture. The payback period is extend over a number of years (7 years for the plant without CCS scenario, 10 years for the plant with pre-combustion capture technology scenario and 15 years for the plant with post-combustion capture technology scenario) leading to a significantly negative initial cash flow, and then as the plant comes online and starts to generate electricity, the cash flow rises according to the amount of power produced and the operational costs of the plant.

119

According to Intergovernmental Panel on Climate Change (IPCC) reports, additional to the levelised cost of electricity, there are other metrics used for comparing CCS technologies such as cost per ton of CO_2 avoided or emitted relative to the plant without CCS and cost of CO_2 captured [25]. As it was already discussed in previous paragraphs, the CO_2 capture and storage purpose is to reduce CO_2 emissions to the atmosphere. According to that view, it is not the amount of CO_2 captured per unit of production (per kWh electricity) that is important, but is the amount of CO_2 emission avoided [26-29]. So, the cost of CO_2 captured was calculated in two different ways, the cost of CO_2 removed and the cost of CO_2 avoided, as illustrated in equations 2 and 3:

$$CO_2 \text{ Removal Cost} = \frac{LCOE_{with\_CCS} - LCOE_{without\_CCS}}{CO_2 \text{ removed}} \left[\frac{Euro}{t_{CO_2}}\right] \qquad (2)$$

$$CO_2 \text{ Avoided Cost} = \frac{LCOE_{with\_CCS} - LCOE_{without\_CCS}}{CO_2 \text{ emissions}_{without\_CCS} - CO_2 \text{ emissions}_{with\_CCS}} \left[\frac{Euro}{t_{CO_2}}\right] \qquad (3)$$

Table 3 shows the electricity production costs, CO_2 avoided and captured costs, for all investigated IGCC cases without and with CO_2 capture.

Table 3. Cost of electricity, CO_2 avoided and removal costs

Description	Units	Case 1	Case 2	Case 3
Solvent	-	-	Selexol®	MEA
LCOE	¢/kWh	5.92	7.61	9.25
CO_2 avoided cost	€/t_{CO_2}	-	21.40	46.11
CO_2 removal cost	€/t_{CO_2}	-	19.58	37.24

As it can be noticed from Table 3, the electricity production cost for the IGCC scheme with pre-combustion process using Selexol® is about 28.54% higher than the electricity production cost for the plant without capture and for the IGCC scheme with post-combustion process using MEA is about 56.25% higher than the electricity production cost for the plant without capture. The results show the advantages of pre-combustion capture for IGCC plants.

Comparing the two main investigated cases for CO_2 capture process (pre – and post – combustion capture technology), the results show that the electricity production cost for post-combustion capture technology is about

21% higher than the electricity production cost for pre-combustion capture technology, CO_2 captured cost for post-combustion capture technology is about 90% higher than CO_2 captured cost pre-combustion capture technology and CO_2 avoided cost in the post – combustion capture technology case is increased by a factor of 2.15 than the CO_2 avoided cost in the pre-combustion capture technology case.

4. Sensitivity analysis

A sensitivity analysis was conducted to determine which model parameters most affect the electricity production cost, CO_2 avoided and removal costs for each CCS investigated option. This sensitivity analysis is of particular importance to give weight and predictability to any economic evaluation. Figure 4 and Figure 5 present the resulting change in electricity, CO_2 avoidance and removal costs when varying capital and O&M cost, fuel cost, discount rate and load factor for previous mentioned cases.
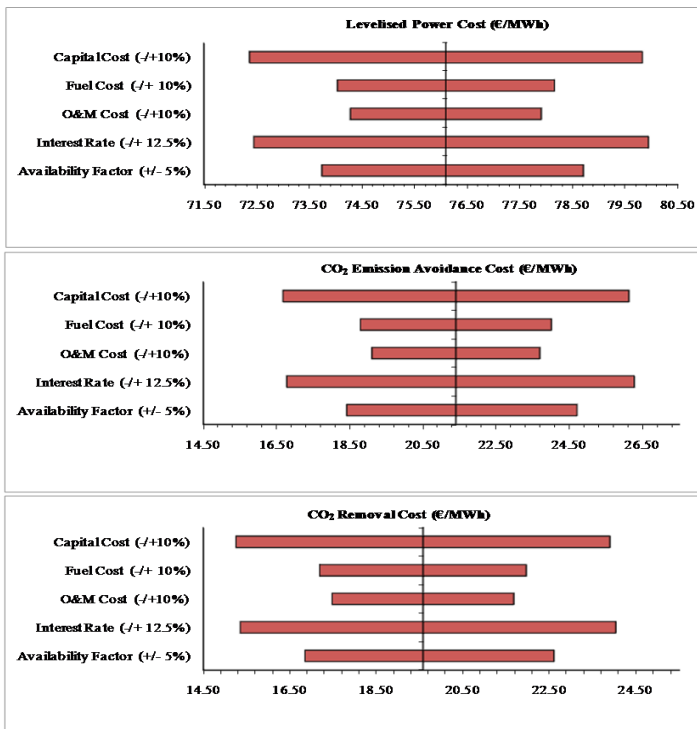

Figure 4. Change in the cost of electricity, CO_2 avoidance and CO_2 removal costs for pre – combustion capture

The vertical axis presents the levelised value of electricity cost, CO_2 avoidance and CO_2 removal costs, and the horizontal bars indicate the percentage modifications of these values caused by a variation in the assumptions for capital and O&M cost (A), fuel cost (B), discount rate (C) and load factor (D).

A) From the sensitivity analysis results illustrated in Figure 4 and Figure 5 it can be observed that the influence of capital cost on electricity production cost, CO_2 avoided and removal costs is more pronounced than the influence on O&M cost in both investigated CCS technologies. This can be easily explained by the significant share of the capital cost in the whole economic assessment.
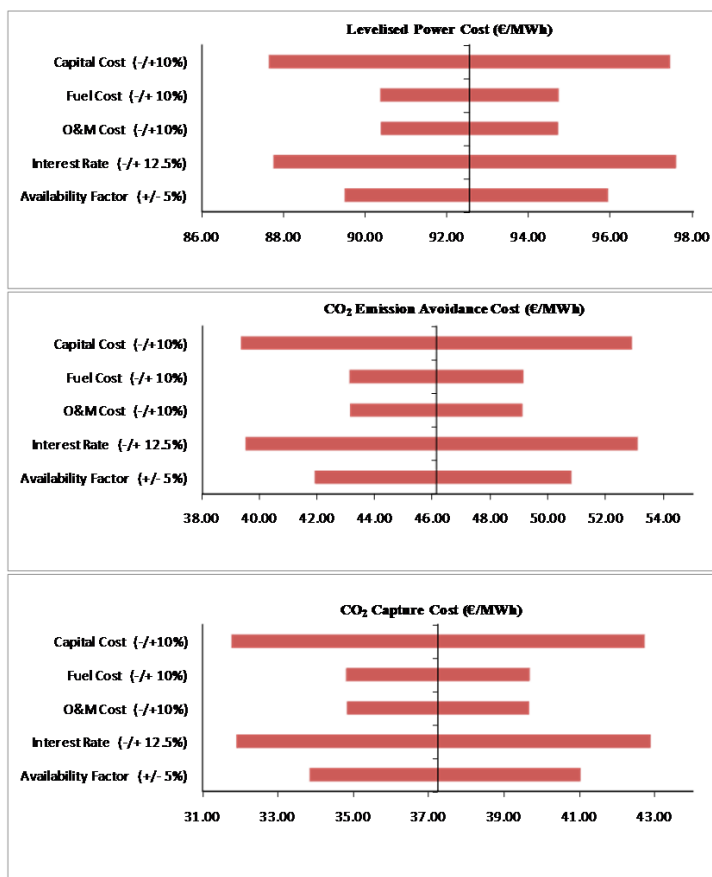

Figure 5. Change in the cost of electricity, CO_2 avoidance and CO_2 removal costs for post – combustion capture

B)   Regarding the fuel price influence it can seen that for the 10% increase of the fuel price, the electricity cost, for Selexol[®] pre – combustion capture plant, increases with 0.21 ¢/kWh, the cost of CO_2 emission avoidance increases with 2.61 €/tCO_2 and the cost of CO_2 removed increases with 2.39 €/tCO_2 For the MEA post – combustion capture plant the electricity cost increases with 0.21 ¢/kWh, the cost of CO_2 emission avoidance increases with 3.01 €/tCO_2 and the cost of CO_2 removed increases with 2.43 €/tCO_2. For the 10% reduction in fuel price the costs decrease with the same factors: for pre-combustion capture case 0.21 ¢/kWh for electricity cost, 2.61 €/tCO_2 for CO_2 avoidance cost and 2.39 €/tCO_2 for CO_2 removal cost and for post-combustion capture case 0.21 ¢/kWh for electricity cost, 3.01€/tCO_2 for CO_2 avoidance cost and 2.43 €/tCO_2 for CO_2 removal cost.

C)   A 8% discount rate, in constant money values was used for the base case. If the discount rate is reduced from 8% to 7%, the cost of electricity from the plant with Selexol[®] pre – combustion capture increases with 0.38 ¢/kWh, the cost of CO_2 emission avoidance increases with 4.88 €/tCO2 and the cost of CO_2 removed increases with 4.46 €/tCO_2. For the MEA post – combustion plant the costs increases with 0.53 ¢/kWh, the cost of CO_2 emission avoidance increases with 6.98 €/tCO_2 and the cost of CO_2 removed increases with 5.64 €/tCO_2.

D)   To illustrate the effects of operation at lower and higher load factors, Figure 4 and Figure 5 show the costs for the plants at 89.25% and 80.75% load factors. As it can be noticed, operation at low load factors increases the costs of electricity, CO_2 avoidance and removal costs in both carbon capture cases. The increase is greater for post-combustion capture plant than for pre-combustion case. This is because the fixed costs of pre-combustion capture plant are lower than those of post-combustion. This aspect is important from operational point of view these power plants being suitable to be operated in base load scenario.

5. Variation of relevant boundary conditions

An overall techno – economical process evaluation reveals that under the base case boundary conditions of this work, Selexol[®] solvent (for pre-combustion capture) and MEA solvent (for post-combustion capture) are best suited for a retrofit integration in the considered IGCC power plant (see previous paragraphs). The present section reports an investigation of how does the plant performance parameters changes if the CO_2 capture performance changes (more specifically the variation of the carbon capture rate). The bellow cases were investigated and compared (using ChemCAD simulations):

- Case A: IGCC with no carbon capture (this case is identical with Case 1 presented in previous sections);
  - Case B: IGCC with 70% CO_2 pre-combustion capture using Selexol[®];
  - Case C: IGCC with 80% CO_2 pre-combustion capture using Selexol[®];
  - Case D: IGCC with 90% CO_2 pre-combustion capture using Selexol[®];
  - Case E: IGCC with 70% CO_2 post-combustion capture using MEA;
  - Case F: IGCC with 80% CO_2 post-combustion capture using MEA;
  - Case G: IGCC with 90% CO_2 post-combustion capture using MEA.

Table 5. Overall gasification power plants performance indicators

Main Plant Data	Units	B	C	D	E	F	G
Gross power	MW$_e$	529.91	529.85	529.79	472.29	462.82	460.35
Net power	MW$_e$	425.56	425.27	424.97	378.84	365.94	359.24
Gross efficiency	%	45.00	44.99	44.98	44.85	43.96	43.72
Net efficiency	%	36.13	36.11	36.08	35.97	34.75	34.11
CO_2 capture rate	%	71.25	80.37	91.43	69.5	79.42	90.88
CO_2 emissions	kg/MWh	240.31	164.08	79.63	181.01	139.20	95.44

Comparing these three post-combustion IGCC capture cases (Case E, Case F and Case G) with the pre-combustion IGCC capture cases (Case B, Case C and Case D) can be concluded that net electrical efficiencies are lower in the case of using post-combustion capture technique (with 0.16% lower for 70% capture, with 1.36% lower for 80% capture and with 1.97% lower for 90% capture). Table 6 presents the capital costs estimations as well as specific investment costs (per kW gross and net) for the evaluated cases.

Table 6. Overall gasification power plants capital cost estimation

Main Plant Data	Units	B	C	D	E	F	G
Total installed cost	MM €	909.85	920.21	932.72	984.27	1006.5	1036.0
Total investment cost	MM €	1091.8	1104.2	1119.2	1181.1	1207.8	1243.3
Specific investment cost	€/kW$_{e\ gross}$	2060.3	2084.0	2112.6	2500.8	2609.7	2700.7
Specific investment cost	€/kW$_{e\ net}$	2565.6	2596.5	2633.7	3117.7	3300.6	3460.9

As it can be noticed from the Table 6, comparing gasification power plant without carbon capture (Case A, see [10-11]) with the same energy conversion technology but with post-combustion capture (Cases E, F and G), the total investment cost per net kWe for the CCS cases are about 51.81% (Case E), 60.72% (Case F) and 68.53% (case G) higher than the total investment cost for the case without capture (Case A).

Comparing the post-combustion capture cases (Cases E, F and G) to the pre-combustion capture cases (Cases B, C and D) it can be observed that capital investment costs are much higher in the case of using post-combustion capture technique (with 21.51% higher for 70% capture, with 27.11% higher for 80% capture and with 31.40% higher for 90% capture). The reason for this fact is related with the fact that a much more gas flow has to be treated in case of post-combustion capture than in case of pre-combustion and the capture unit is bigger. The incremental cost due to CO_2 capture for the CCS IGCC investigated cases can be observed as well in Figure 6.
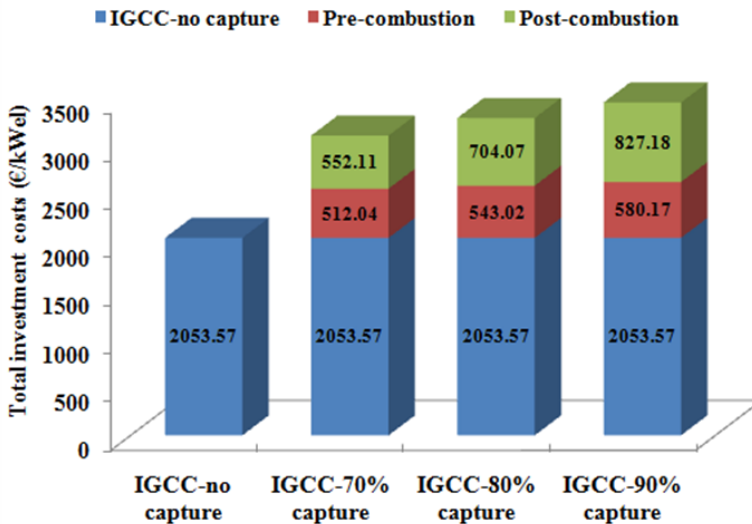

Figure 6. The incremental cost due to pre- and post-combustion CO_2 capture

For the electricity cost evaluation, as in the previously mentioned cases (Cases B C and D), a plant lifetime of 25 years, a load factor of 85%, the coal price of 2.2 €/GJ and sawdust price of 1.12 €/GJ has been assumed.

Table 7. Cost of electricity, CO_2 avoided and removal costs

Description	Units	B	C	D	E	F	G
LCOE	¢/kWh	7.41	7.51	7.61	8.44	8.89	9.25
CO_2 avoided cost	€/t_{CO2}	20.91	20.99	21.40	39.25	43.39	46.11
CO_2 removal cost	€/t_{CO2}	22.31	20.93	19.58	37.55	37.37	37.24

As it can be seen from Table 7 cost of electricity for the IGCC with CCS implemented rises with about 42.56% for Case E, 50.16% for Case F and 56.25% for Case G compared to the Case A. Comparing these three post-combustion capture cases (Cases E, F and G) with the pre – combustion capture cases (Cases B, C and D) it can be observed that the cost of electricity is much higher in the case of using post-combustion capture technique (with 13.90% higher for 70% capture, with 18.37% higher for 80% capture and with 21.55% higher for 90% capture).

CO_2 avoided and removal costs are important and useful metrics for comparing economics of a specific CO_2 capture process against alternative capture technologies. Comparing investigated technologies: post-combustion IGCC capture cases (Cases E, F and G) with the pre-combustion IGCC capture cases (Cases B, C and D) can be observed that both CO_2 captured and CO_2 avoided costs are much higher in the case of using post – combustion capture technique (by a factor of 1.87 higher for 70% capture, by a factor of 2.06 higher for 80% capture and by a factor of 2.15 higher for 90% capture for avoided costs and by a factor of 1.68 higher for 70% capture, by a factor of 1.83 for 80% capture and by a factor of 1.90 for 90% capture for captured costs).

The reported results in this paper could be of significant importance for the case that a demo project on carbon capture and storage technology will be implemented in Romania [30].

CONCLUSIONS

CCS technologies are aiming to mitigate the CO_2 emissions from power generation as well as from other energy-intensive industrial sectors (e.g. oil refineries, chemicals, metallurgy, construction materials etc.). This paper is evaluating from economic side two carbon capture technologies suitable for IGCC power plants. The assessment targeted pre-combustion and post-combustion CO_2 capture technologies because these two are the most common and commercially mature technologies today.

Concerning the total investment cost, the calculation results show that the total investment cost for the gasification power plants with CO_2 capture process is higher (pre-combustion process using Selexol® about 22% higher and post-combustion process using MEA about 36% higher) than the total investment cost for the plant without capture. Also, comparing the two main investigated cases for CO_2 capture process, the results show that the electricity production cost for post-combustion capture technology is about 21% higher than the electricity production cost for pre-combustion capture technology, CO_2 captured cost for post-combustion capture technology is about 90% higher than CO_2 captured cost pre-combustion capture technology and CO_2 avoided cost in the post-combustion capture technology case is increased by a factor of 2.15 than the CO_2 avoided cost in the pre-combustion capture technology case. As an overall conclusion of the present economic evaluation is that the pre-combustion capture using physical solvents is more suitable for capturing CO_2 from the gasification-based power plants than the post-combustion capture using chemical solvents.

ACKNOWLEDGMENTS

REFERENCES

[1]. H. Spliethoff, "Power Generation from Solid Fuels", Springer, **2010**.
[2]. A. Rejoy, "Energy and Climate. How to achieve a successful energy transition", Wiley, **2009**.
[3]. IEA, International Energy Agency, "CO_2 Capture and Storage. Energy Technology Analysis. A key carbon abatement option", **2008**.
[4]. BP Global, Statistical Review of World Energy, www.bp.com (June **2013**).
[5]. G.A. Marrero, *Energy Economics*, **2010**, *32*, 1356.
[6]. M. Abu-Zahra, L. Schneiders, J. Niederer, P. Feron, G. Versteeg, *International Journal of Greenhouse Gas Control*, **2007**, *1*, 37.

[7]. J.K. Eccles, L. Pratson, R.G. Newell, R.B. Jackson, *Energy Economics*, **2012**, *34*, 1569.

[8]. A. Skorek-Osikowska, K. Janusz-Szymańska, J. Kotowicz, *Energy*, **2012**, *45*, 92.

[9]. C. Kunze, H. Spliethoff, *Fuel Processing Technology,* **2010**, *91*, 934.

[10]. A. Padurean, C.C. Cormos, A.M. Cormos, P.S. Agachi, *International Journal of Greenhouse Gas Control*, **2011**, *5*, 676.

[11]. A. Padurean, C.C. Cormos, P.S. Agachi, *International Journal of Greenhouse Gas Control*, **2012***, 7*, 1.

[12]. C.C. Cormos, *Energy*, **2012**, *42*, 434.

[13]. G. Towler, R.K. Sinnott, "Chemical engineering design: Principles, practice and economics of plant and process design", Butterworth-Heinemann, **2007**.

[14]. R. Smith, "Chemical processes: Design and integration", West Sussex, England: Wiley; **2005**.

[15]. L.M. Abadie, J.M. Chamorro, *Energy Economics*, **2008**, *30*, 2992.

[16]. P. Mores, N. Rodríguez, N. Scenna, S. Mussati, *International Journal of Greenhouse Gas Control*, **2012**, 10, 148.

[17]. IEA, International Energy Agency, "Cost and Performance of Carbon Dioxide Capture from Power Generation", **2011**.

[18]. Global CCS Institute, "Economic assessment of carbon capture and storage technologies", WorleyParsons, **2011**.

[19]. C.C. Cormos, K. Vatopoulos, E. Tzimas, *Energy*, **2013**, *51*, 37.

[20]. A. Pettinau, F. Ferrara, C. Amorino, *Energy*, **2013**, *50*, 160.

[21]. N. Smith, G. Miller, I. Aandi, R. Gadsden, J. Davison, *Energy Procedia*, **2013**, 37, 2443.

[22]. NETL, Department of Energy, Cost and performance baseline for fossil energy plants. Vol. 1: Bituminous coal and natural gas to electricity. DOE/NETL-2007/1281, **2007**.

[23]. ICIS Pricing, www.icispricing.com, (August **2013**).

[24]. T. Naucler, W. Campbell, J. Ruijs, "Carbon Capture and Storage: Assessing the Economics", McKinsey & Company Inc., 2008.

[25]. B. Metz, O. Davidson, H. de Coninck, M. Loos, L. Meyer (eds.), "IPCC Special Report on Carbon Dioxide Capture and Storage", Prepared by Working Group III of the Intergovernmental Panel on Climate Change, Cambridge University Press, Cambridge, NY, USA, **2005**.

[26]. Zero Emission Platform (ZEP) Report, "The cost of CO_2 storage. Post-demonstration CCS in the UE", **2011**.

[27]. E.S. Rubin, C. Chen, A.B. Rao, *Energy Policy*, **2007**, *35*, 4444.

[28]. C.C. Cormos, "Conceptual design of typical power plant configurations for the estimation of reference capital costs including material", Report IE/2010/07/23 107058, **2010**.

[29]. J. Davison, *Energy*, **2007**, *32*, 1163.

[30]. Getica CCS Demo Project, www.getica-ccs.ro (August **2013**).